University of Nevada, Reno

Elucidating the regulation and function of circRNAs

A dissertation submitted in partial fulfillment of the requirements for the degree of Doctor of Philosophy in Cellular and Molecular Biology

By

David Knupp

Dr. Pedro Miura/Advisor

December, 2021

THE GRADUATE SCHOOL

We recommend that the dissertation
prepared under our supervision by

DAVID KNUPP

entitled

Elucidating the regulation and function of circRNAs

be accepted in partial fulfillment of the
requirements for the degree of

Doctor of Philosophy

Pedro Miura, Ph.D.
Advisor

Alexander van der Linden, Ph.D.
Committee Member

Thomas Kidd, Ph.D.
Committee Member

Simon Pieraut, Ph.D.
Committee Member

Tong Zhou, Ph.D.
Graduate School Representative

David W. Zeh, Ph.D., Dean
Graduate School

December, 2021

Abstract

Circular RNAs (circRNAs) are a newly appreciated class of RNAs that are expressed in a wide range of organisms, tissues, and disease states. The factors regulating circRNA biogenesis are poorly understood. CircRNAs are typically produced from exons of protein-coding genes through a process termed backsplicing. CircRNAs are enriched in the brain compared to other tissues in humans, and increase globally in expression during neuronal differentiation. In Chapter 2, we discovered that the neural-enriched splicing factor NOVA2 positively regulates hundreds of circRNAs in the developing mouse brain. We found that this regulation occurs through NOVA2 binding within introns flanking circRNA loci. This work identified the first RNA binding protein that facilitates circRNA enrichment in the mammalian brain.

CircRNAs accumulate during aging across various organisms, especially in the brain. What functions, if any, do these age-related circRNAs have? A considerable roadblock to studying circRNA function has been the difficulty to establish circRNA-specific mutants. In Chapter 3 we identified sequences in introns that were important for circularization of two age-regulated circRNAs expressed from the *crh-1* gene in the nematode *C. elegans*. Using CRISPR-Cas9, we generated intronic deletions that completely abolished *crh-1* circRNAs without interrupting linear *crh-1* mRNA expression. Remarkably, we found that elimination of these circRNAs increased mean lifespan in *C. elegans*, suggesting that they contribute to age-related decline.

Dedication

I would like to thank my family and all of the friends I have made at UNR for providing the support essential to completing my graduate studies.

Table of Contents

List of Figures

CHAPTER 1: REGULATION AND FUNCTION OF CIRCULAR RNAS

INTRODUCTION

Normal cell function depends on the accurate, timed expression of both protein-coding RNAs (mRNAs) and non-coding RNAs (ncRNAs). ncRNAs participate in a diverse array of functions ranging from transcriptional regulation, to RNA processing and translation. Circular RNAs (circRNAs) represent one of the many unique subcategories of ncRNAs with largely uncharacterized functions. Recent advancements in RNA-sequencing (RNA-seq) have uncovered the true propensity of circRNA expression in vertebrate and invertebrate species (Ivanov et al., 2015; Jeck et al., 2013; Memczak et al., 2013; Rybak-Wolf et al., 2015; Salzman et al., 2012; Westholm et al., 2014). Tens of thousands of distinct circRNAs have been discovered in humans (Jeck et al., 2013; Memczak et al., 2013; Rybak-Wolf et al., 2015; Salzman et al., 2012), exhibiting remarkable stability compared to their protein-coding counterparts (Jeck et al., 2013), and featuring unique secondary structures allowing them to participate in a wide-range of cellular functions (Liu et al., 2019; Xia et al., 2018). Notably, circRNAs are enriched in the brains of several mammals (Rybak-Wolf et al., 2015; You et al., 2015; Zhou et al., 2018), including humans (Rybak-Wolf et al., 2015) and dramatically accumulate during development and aging (Cortes-Lopez et al., 2018; Gruner et al., 2016; Westholm et al., 2014; Xu et al., 2018; Zhou et al.,

2018). Novel roles for circRNAs are continuing to emerge and suggest that they are integral to maintaining normal cellular homeostasis.

Formation of circular RNAs through backsplicing

Alternative splicing is an essential mechanism to regulate eukaryotic gene expression, resulting in the generation of multiple mRNA species from a single gene. Alternative splicing is pervasive, occurring in approximately 95% of human genes (Pan et al., 2008; Wang et al., 2008). The splicing reaction is catalyzed by the spliceosome, a large RNA-protein complex [reviewed in (Matera and Wang, 2014; Will and Luhrmann, 2011). Here, small nuclear ribonucleoprotein particles (snRNPs), and non-snRNP components recognize short, conserved motifs at the junctions between exons and intervening introns to inform the final sequence content of a mature RNA. These motifs include the 5' splice site (5'ss) at the beginning of an intron (most frequently a GT dinucleotide), the 3' splice site (3'ss) at the end of an intron (AG dinucleotide), the branch point adenosine, and the polypyrimidine tract (Matera and Wang, 2014; Will and Luhrmann, 2011). Additional *cis*-acting elements recruit *trans*-acting factors to further regulate final sequence content (Matera and Wang, 2014; Will and Luhrmann, 2011).

Alternative splicing is typically carried out through one of four modalities– cassette exons (exon skipping or mutually exclusive exons), intron retention, alternative 5' splice site usage and alternative 3' splice site usage (Wang et al., 2008) (**Figure 1A**). However, circRNAs are formed via a newly recognized type of alternative splicing termed backsplicing. Here, the 3'ss (splice donor) of a

circularizing transcript covalently bonds an upstream 5'ss (splice acceptor) to form a closed loop (Li et al., 2018) (**Figure 1B**)**.** Circularizing exons are almost always flanked by the canonical AG/GT splice signals suggesting circRNAs are produced by the *U2* spliceosome (Panda et al., 2017; Starke et al., 2015; Vo et al., 2019). Supporting this hypothesis, Cef1-purified spliceosome in yeast was shown recently to contain circRNA transcripts catalyzed by exon-definition complexes (Li et al., 2019). In addition, isoginkgetin treatment which blocks U4/U5/U6-tri-snRNP spliceosome assembly dramatically reduced nascent circRNA production in HeLa cells (Starke et al., 2015). The efficiency of backsplicing is low compared to canonical splicing (Zhang et al., 2016). Thus, most circRNAs are typically lowly expressed compared to linearly spliced mRNAs from the same gene (Guo et al., 2014; Salzman et al., 2013). However, due to their circular nature circRNAs are relatively resistant to exoribonuclease degradation and thus exhibit remarkably long half-lives in cells (Enuka et al., 2016; Jeck et al., 2013). CircRNAs are not polyadenylated (polyA) and as a consequence were often excluded from traditional polyA-selected RNA-seq libraries. Advancements in RNA-seq technologies, such as total RNA-seq, which depletes ribosomal RNA but leaves polyA and non-polyA RNA transcripts behind have facilitated the detection of circRNAs in numerous organisms.

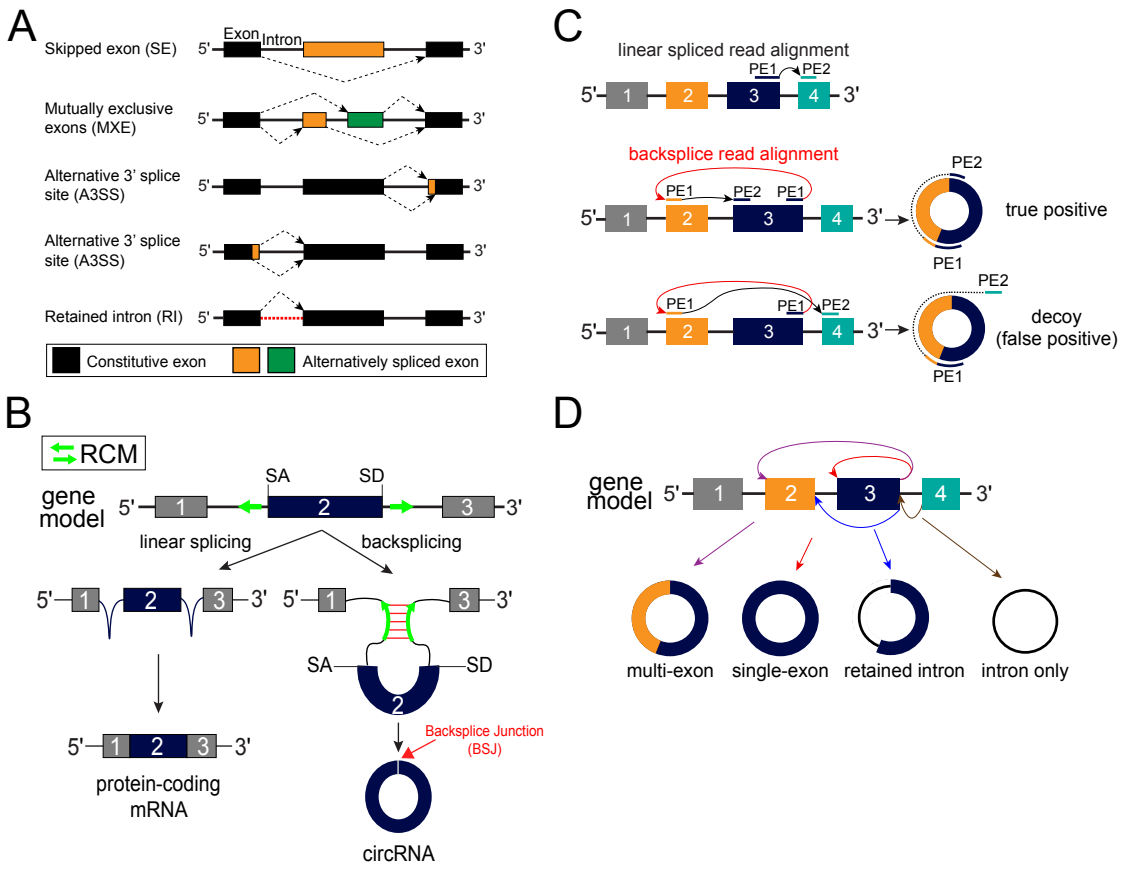

Figure 1. Alternative splicing produces distinct linear and circular transcripts. (A) Schematic of the four basic types of alternative splicing. Dotted black lines indicate splice site usage. Dotted red line indicates retained intron event. **(B)** CircRNAs are produced via backsplicing. In linear splicing (*left*), an upstream splice donor (SD) is joined to a downstream splice acceptor (SA). In backsplicing (*right*) the splice donor of exon 2 is covalently bonded to the upstream splice acceptor to form a circular transcript. This reaction may be facilitated by reverse complementary matches (RCM) present in the flanking introns of the circularizing locus. **(C)** Schematic of a paired-end (PE) read mapping to a linear spliced or backspliced transcript. In the linear spliced

transcript, read pair one (PE1) maps to exon 3 while read pair two (PE2) maps downstream to exon 4. In backsplice read alignment, PE1 is split between exon 3 and exon 2 representative of a backsplice junction (BSJ). *Upper panel*, PE2 maps to internal circRNA sequence predicted by PE1, signifying a true positive circRNA. *Lower panel*, PE2 maps outside of the predicted circRNA sequence, signifying a decoy read or false positive. **(D)** Alternative backsplicing can result in multiple unique circRNA isoforms.

Identification of CircRNAs by RNA-seq

In the last decade, several circRNA prediction programs have been developed (Chen et al., 2021). CircRNA detection by RNA-seq relies on split read alignments to the unique backsplice junction (BSJ) sequence (**Figure 1C**). For example, in a multi-exon circRNA, the downstream exon would appear to precede the upstream exon. These so-called “out-of-order exons” led to the original identification of circRNAs in mammalian cells in the early 1990’s (Cocquerelle et al., 1992; Nigro et al., 1991). When designing a total RNA-seq experiment to identify circRNAs, there are some aspects that can help improve circRNA detection outcomes. For instance, the use of paired-end reads, which arise from sequencing a cDNA fragment from both ends, can improve sensitivity by identifying decoy read pairs that align outside the predicted circRNA sequence, and thus reduce potential false-positives (**Figure 1C**). In addition, high sequencing depth (e.g., the total number of RNA-seq reads that can be allocated to individual samples) can further bolster circRNA detection and quantification by increasing the number of reads that can potentially align to the circRNA BSJ sequence. After circRNAs have been identified and quantitated, additional reduction of false positives can be achieved by applying minimum BSJ read thresholds across individual samples and requiring that a circRNA is detected in a minimum number of replicates. Lastly, as a result of their low expression, it is important to validate circRNA expression trends from RNA-seq analyses. RNase-R, a 3’ to 5’ exoribonuclease which degrades most linear RNAs in the cell, is typically used in conjunction with RT-qPCR to validate the circularity of a putative

circRNA, as circRNAs are relatively resistant to RNase-R mediated degradation (Jeck et al., 2013). Although not widely adopted, RNase-R may also be used prior to RNA-seq to enrich for BSJ aligning reads, leading to more robust quantification and improved sensitivity.

Due to the many total RNA-seq experiments that have been performed and/or analyzed in search of circRNAs, we now know many features regarding their sequence content, expression patterns, and biogenesis. For instance, circRNAs can contain exonic, intronic or both sequences originating from their parental gene (**Figure 1D**) and can undergo any of the four splicing modalities common to linear AS (Gao et al., 2016; Xin et al., 2021). CircRNAs display tissue-specific expression patterns (Barrett and Salzman, 2016; Ji et al., 2019; Xin et al., 2021) and are enriched in the brains of several vertebrates including rats (Mahmoudi and Cairns, 2019), mice (Ji et al., 2019; Rybak-Wolf et al., 2015; You et al., 2015), rhesus macaques (Ji et al., 2019), and humans (Ji et al., 2019; Rybak-Wolf et al., 2015). In a recent metanalysis of transcriptomic data from several mammals, Ji et al. investigated orthologous genes between species that produce circRNAs with 1) the same BSJ sequence and 2) share at least 90% of circularized primary sequence. Here, 19% of circRNAs were found to be conserved between humans and macaque, whereas only 4% of human expressed circRNAs were also expressed in mice (Ji et al., 2019). This could suggest that circRNAs are actively evolving and circRNAs conserved between species might have essential physiological functions. Along these lines, less than 0.1% of circRNAs have been individually characterized. Leveraging

transcriptomic data to identify abundant, conserved circRNAs, enriched in specific tissues such as brain will likely aid in identifying additional functional circRNAs.

Intronic elements facilitate backsplicing

Exons that generate circRNAs are often flanked by relatively long introns compared to non-circularizing exon controls (Ivanov et al., 2015; Jeck et al., 2013; Salzman et al., 2012; Westholm et al., 2014). Perhaps one of the earliest examples of this arises from *circSry*, a single-exon circRNA expressed from the mouse *Sry* gene discovered in 1993 (Capel et al., 1993; Dubin et al., 1995). This abundant circRNA is flanked by long introns containing several complementary sequences or reverse complementary matches (RCMs) that facilitate its expression (Capel et al., 1993; Dubin et al., 1995). Fast-forward twenty years later, and *in vivo* transcriptomic data generated by total RNA-seq from human fibroblasts demonstrated that genome-wide, circRNAs have significantly longer flanking introns (Jeck et al., 2013). Furthermore, flanking introns were 6-fold more likely to contain complementary *Alu* sequences, a type of RCM, relative to non-circularizing exons (Jeck et al., 2013). Similar results were obtained for circRNAs expressed in human embryonic stem cells and pig cortex samples (Veno et al., 2015; Zhang et al., 2014). In the nematode *C. elegans,* circRNAs were also significantly more likely to be flanked by long introns (Ivanov et al., 2015). *C. elegans* lacks *Alus* and repetitive elements in general (Consortium, 1998; Sijen and Plasterk, 2003; Stein et al., 2003) and yet, circRNA flanking

introns were also found to be enriched for RCMs compared to control exons that don't circularize (Cortes-Lopez et al., 2018; Ivanov et al., 2015). Together, these data suggest that RCMs are a conserved feature for generating circRNAs.

It has been hypothesized that RCMs, including inverted repeats such as *Alus* (IR*Alus*) facilitate backsplicing by bringing participating splice sites into closer proximity. To provide direct experimental evidence for RCM-mediated circRNA biogenesis*, in vitro* minigenes have been designed to express endogenous circRNAs (Kramer et al., 2015; Liang and Wilusz, 2014). In short, to generate a circRNA from an expression vector, the circularizing exon(s) and their flanking introns (typically 500-1000 nucleotides (nt) upstream and downstream of the terminal circularizing exons) are cloned into a plasmid backbone. Transfection of such minigenes expressing *circPOLR2A* which harbors IR*Alus* in its flanking introns, demonstrated that they were required for *circPOLR2A* biogenesis, as IR*Alu* deletion resulted in complete loss of *circPOLR2A* expression (Zhang et al., 2014). Furthermore, insertion of other RCMs (non-IR*Alus*) into *circPOLR2A* flanking introns could also promote its circularization. Similar results have been obtained for other circRNA expressing vectors (Kramer et al., 2015; Liang and Wilusz, 2014; Liu et al., 2018). Recently, deletion of intronic RCMs flanking the endogenous *cia-cGAS* locus was able to abolish its expression *in vivo* (Xia et al., 2018), further supporting a model for RCM-mediated backsplicing.

Since distal genomic regions within a circRNA-producing gene must be transcribed before RCM secondary structure can form, this would suggest that

circRNA-producing genes must be transcribed to full or near completion before backsplicing can occur. In agreement with this supposition, Zhang et al. demonstrated that the majority of human expressed circRNAs are generated post-transcriptionally (Zhang et al., 2016). In PA1 cells, most circRNAs were undetectable until 2-14 hours after their host gene were fully transcribed (Zhang et al., 2016). In support, a separate analysis demonstrated that inhibition of the co-transcriptional 3'-end processing factor Cpsf73 led to increased circRNA expression (Liang et al., 2017). Yet there are always exceptions to the rule. A small subset of human circRNAs in PA1 cells were co-transcriptionally produced (Zhang et al., 2016), and numerous chromatin-bound circRNAs were discovered in *Drosophila* head and mouse liver samples (Ashwal-Fluss et al., 2014). Together, these data suggest that the majority of circRNAs in human are produced post-transcriptionally. The relative proportion of co- versus post-transcriptional processing in other organisms enriched with RCMs such as *C. elegans*, has not been evaluated. It would be interesting to uncover sequence characteristics that might predict whether or not a circRNA will be co- or post-transcriptionally processed, and would aid in understanding the backsplicing mechanism.

Backsplicing is regulated by RNA binding proteins

In contrast to circRNAs expressed in humans or *C. elegans*, the flanking introns of *Drosophila* expressed circRNAs are not enriched for RCMs (Westholm et al., 2014). Although this is not to say that RCM-mediated circRNA biogenesis

does not occur in *Drosophila*. Expression of a circRNA produced from the *laccase2* gene was shown to require intronic RCMs (Kramer et al., 2015). Thus, while RCM-mediated circRNA biogenesis is not absent in *Drosophila*, it appeared likely that a separate mechanism might be responsible for the majority of circRNAs.

The absence of *cis*-elements that could facilitate circRNA biogenesis in *Drosophila* led to the search for regulatory *trans*-acting factors. The most notable case investigated the biogenesis of *circMbl*. *circMbl*, which lacks RCMs in its flanking introns, is generated from the second exon of the *muscleblind* (*mbl*/*MBNL1*) gene and is the predominant *mbl* transcript in *Drosophila* heads (Ashwal-Fluss et al., 2014). Instead, several intronic MBL binding sites were identified, suggesting that MBL might promote production of *circMbl*. To test this hypothesis researchers overexpressed MBL in *Drosophila* S2 cells co-transfected with a *circMbl* expression vector containing the putative MBL binding sites. A concomitant increase in *circMbl* expression was observed (Ashwal-Fluss et al., 2014). Mutation of MBL binding sites within the flanking introns of *circMbl* abrogated most of this effect. In fact, insertion of MBL binding sites into introns flanking an unrelated circ-exon led to the generation of a circRNA responsive to MBL expression (Ashwal-Fluss et al., 2014). Thus, MBL was identified as the first *trans*-acting factor to regulate circRNA expression.

Around the same time, the splicing factor Quaking (QKI) was found to promote circRNA biogenesis transcriptome-wide during epithelial-mesenchymal transition in human cells (Conn et al., 2015). Similar to the regulation of *circMbl*,

circRNAs regulated by QKI were also found to contain QKI binding sites within their flanking introns. The deletion of either the upstream or downstream QKI binding sites alone in an artificial circRNA reporter construct dramatically reduced the amount of expressed circRNA. Remarkably, insertion of QKI binding sites around exons that do not typically circularize, resulted in efficient circRNA expression (Conn et al., 2015). Given that QKI can form dimerize with itself (Teplova et al., 2013), it has been proposed that QKI might facilitate circRNA biogenesis by dimerizing across an exon. Although direct evidence for this is still lacking, it remains an intriguing possibility.

It is apparent that splicing factors and other various RNA-binding proteins (RBPs) have the ability to regulate circRNA expression in cases when intronic RCMs are lacking. Yet RCMs and regulation by RBPs need not be independent. Analyses performed in *Drosophila* found that multiple hnRNPs and SR proteins, which direct pre-mRNA splicing patterns, can positively or negatively regulate circRNA biogenesis even when RCMs are present (Kramer et al., 2015). This suggested that some factors might act to strengthen or weaken existing intronic base-pairing. Indeed, the double-stranded RNA (dsRNA) binding proteins ADAR1 and ADAR2 which deaminates adenosines to inosines (A-to-I) (Kim et al., 1994; O'Connell et al., 1995) were found to largely inhibit circRNA expression in *C. elegans* and in mammalian cell culture (Ivanov et al., 2015; Rybak-Wolf et al., 2015). It was hypothesized that ADAR binding and subsequent A-to-I editing within RCMs weakens overall base-pairing interactions. Accordingly, RCMs within the flanking introns of circRNA loci expressed in *C. elegans* were found to

be highly enriched for A-to-I editing events (Ivanov et al., 2015). Analysis of ADAR editing in human datasets also found a greater frequency of editing in circRNA flanking introns relative to length-matched introns or other introns from the same host gene, and these edits typically occurred within 200-600 nt of the circularized exons (Ivanov et al., 2015).

What other RBPs might regulate circRNA expression through binding intronic complementary regions? To address this, Li et al. performed a screen of RBPs in PA1 cells using biotin-labeled RNA pull-down assays with *in vitro* transcribed RNA containing inverted repeats (Li et al., 2017a). Perhaps unsurprisingly ADAR1 was among the top associated proteins (Li et al., 2017a). In addition, the nuclear factors NF90 and NF110 were also among the most enriched. Depletion of either factor in HeLa cells resulted in a global trend towards reduced circRNA expression (Li et al., 2017a). Thus, similar to what has been found in *C. elegans* (Ivanov et al., 2015), dsRNA binding proteins in human cells can also interact with RCMs to either enhance or reduce their stability.

Given that circRNAs are regulated by *trans*-acting factors, it is likely that naturally occurring mutations within these proteins would impact endogenous circRNA expression patterns. A prime example is the splicing factor FUS. C-terminal mutations in FUS result in its mislocalization to the cytoplasm where it forms protein aggregates linked to amyotrophic lateral sclerosis (ALS) (Kwiatkowski et al., 2009; Lenzi et al., 2015; Vance et al., 2009). ALS-causative mutations in FUS also alter its splicing patterns (Groen et al., 2013; Sun et al., 2015). In mouse-derived induced pluripotent stem cell (iPSC) motor neurons

(MNs) loss of FUS resulted in downregulation of over 100 circRNAs (Errichelli et al., 2017). Attempts to rescue downregulated circRNAs by overexpressing wild-type FUS (FUS^{WT}) or with FUS variants carrying ALS-linked mutations demonstrated that only FUS^{WT} was able to rescue circRNA expression. This observation is likely due to reduced nuclear localization of FUS carrying ALS-linked mutations (Kwiatkowski et al., 2009; Lenzi et al., 2015; Vance et al., 2009). How well these results are reflected in human tissues is unknown. Regardless, changes in alternative splicing underlie many neurological diseases (Vuong et al., 2016), and some phenotypes might be attributable in part to dysregulated backsplicing. These data leads one to ask what the functional consequences of aberrant backsplicing are and what roles do circRNAs play within the cell?

CircRNA functions

A significant obstacle to addressing the question of circRNA function relates to the difficulty in selectively disrupting backsplicing without affecting linearly spliced transcripts from the same host gene. Knockdown of circRNAs by shRNAs that target the unique BSJ sequence (**Figure 2A**) of circularizing exons have been used extensively (Du et al., 2017; Pamudurti et al., 2020; Stoll et al., 2018; Zheng et al., 2016). Interestingly, lentivirus-mediated expression of shRNAs for *in vivo* knockdown of circRNAs expressed in mammalian tissues have had limited success (Huang et al., 2017; Zimmerman et al., 2020). In contrast, adeno-associated virus (AAV) expression constructs demonstrate

efficient knockdown over long periods of time (Liu et al., 2017; Shan et al., 2017). Thus, AAV constructs might have more utility for *in vivo* experiments. Nonetheless, the BSJ sequence is not always amenable to unique siRNA/shRNA design without off-targeting risks.

More recently, CRISPR-Cas9 editing has been used effectively to disrupt backsplicing by deleting intronic *cis*-elements that facilitate circularization (Xia et al., 2018; Zhu et al., 2019) (**Figure 2A**). In one instance, CRISPR was used to delete an entire circRNA loci in mice (discussed below), when linearly spliced transcripts from the circRNA locus were not detected (Piwecka et al., 2017). Given the prevalence of intronic RCMs, the former strategy will likely become more common moving forward.

CircRNAs were initially believed to act primarily as decoys for microRNAs (miRNAs) (**Figure 2B**). This idea stemmed from the observation that two of the earliest identified circRNAs, circ*Sry* and CDR1as (also known as ciRS-7) harbored numerous binding sites for miR-138 and miR-7, respectively (Hansen et al., 2013). In several instances circRNAs have been shown to act as decoys or "sponges" for miRNAs, resulting in changes in cell proliferation (Zheng et al., 2016), insulin secretion (Stoll et al., 2018), pluripotency (Yu et al., 2017), and astrocyte activation (Huang et al., 2017) *in vitro*. However, it is unknown if these aforementioned phenotypes persist in an *in vivo* context. Analysis of AGO2-CLIP data to identify circRNA-miRNA interactions in HEK293 cells demonstrated that no circRNAs stood out as having convincing sponge potential besides CDR1as

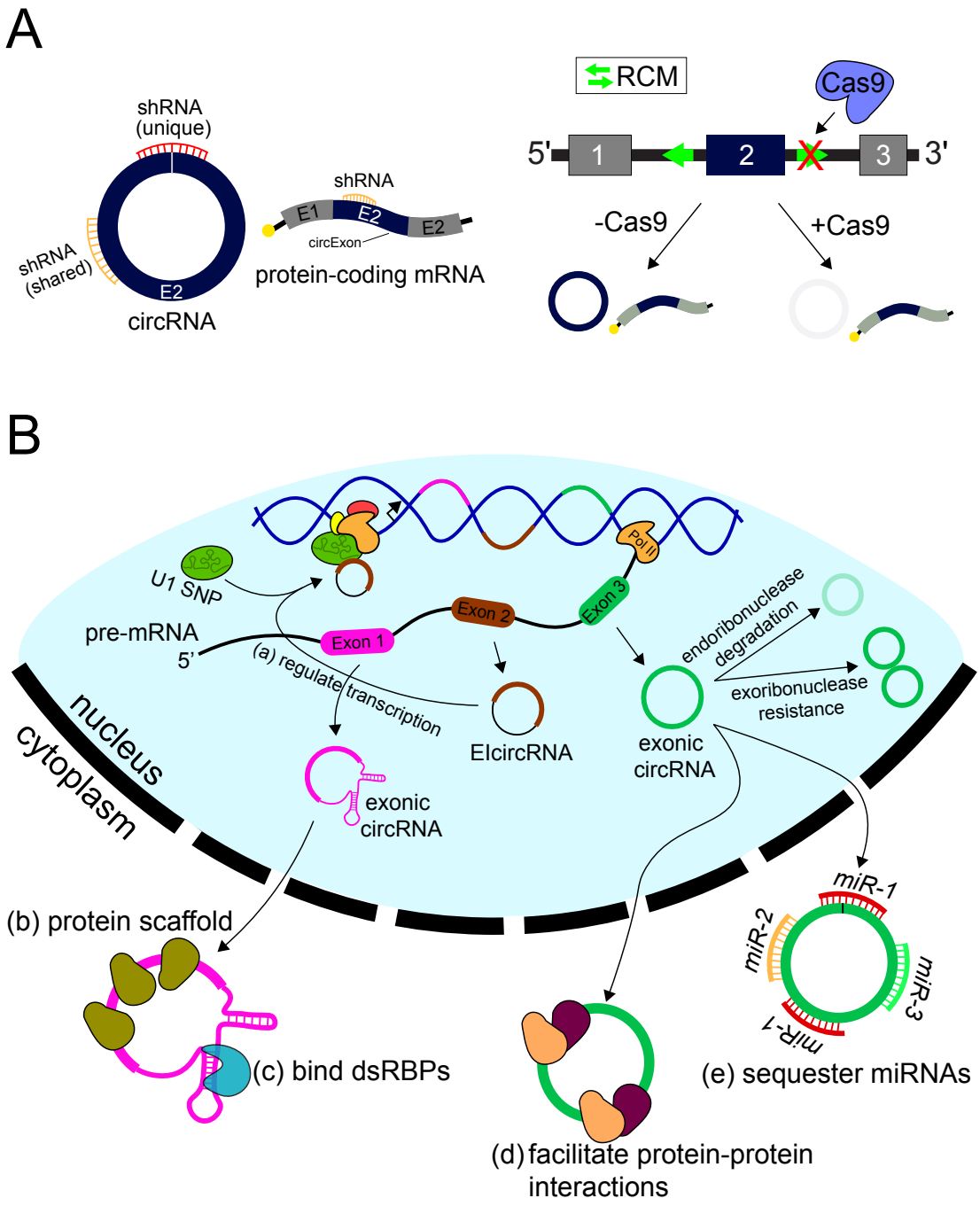

Figure 2. CircRNA loss-of-function approaches and *in vivo* functions. (A) (*left*) CircRNAs may be targeted for knockdown by shRNAs. Knockdown of the circRNA transcript only, requires the design of shRNA (red) specific to the unique

BSJ sequence. shRNA (orange) targeting the shared mRNA and circRNA sequence will reduce expression of both transcripts simultaneously. (*right*) CRISPR-Cas9 targeting of intronic *cis*-elements, such as RCMs (green arrows) flanking the circularizing exon (blue rectangle) can specifically reduce or abolish circRNA expression without affecting the linear spliced transcript from the same host gene. **(B)** CircRNAs possess diverse cellular functions including (a) regulation of host gene transcription by exon-intron circRNAs (EIcircRNA), (b) protein scaffolding, (c) formation of unique secondary structures to bind double-stranded RNA-binding proteins (dsRBPs), (d) facilitate protein-protein interactions and (e) sequester micro-RNAs (miRNAs) away from intended targets.

(Guo et al., 2014). Coupled with the low expression of most circRNAs, these data suggest that miRNA sponging is not a general function of circRNAs. As stated, one notable exception is CDR1as, which contains 73 conserved binding sites for miR-7 and one conserved binding site for miR-671 in humans and is highly abundant in the mammalian brain (Hansen et al., 2013; Piwecka et al., 2017). Notably, the miR-7 sites are only partially complementary to CDR1as such that miR-7:AGO2 complexes cannot degrade the circRNA. However, CDR1as can be degraded by miR-671 (Hansen et al., 2011; Kleaveland et al., 2018). Interestingly, genetic knockout of CDR1as in mice resulted in neuropsychiatric disorders and reduced excitatory synaptic transmission (Piwecka et al., 2017). This phenotype shown in CDR1as null mice was initially believed to result from sponging of miR-7 away from its targets (Piwecka et al., 2017). However, more recently it has been proposed that CDR1as acts as a vehicle to deliver miR-7:AGO2 complexes to targets within neuronal processes, a complex mechanism regulated at least in part by the long non-coding RNA, *Cyrano* (Kleaveland et al., 2018). *Cyrano* is suspected to enhance miR-671 mediated degradation of CDR1as through modulation of miR-7 expression. In *Cyrano* deficient mice, miR-7 levels increase 40-fold (Kleaveland et al., 2018), which might facilitate degradation of CDR1as by localizing more AGO2 to the circRNA for enhanced miR-671 mediated degradation. Upon degradation by miR-671, it is hypothesized that bound miR-7:AGO2 complexes would then be released to downregulate target genes in neurons (Kleaveland et al., 2018). While experimental evidence for miRNA delivery by CDR1as is incomplete, these data nonetheless indicate

that circRNAs might be important for normal brain function and might interact with other ncRNAs in complex regulatory networks.

In addition to interacting with miRNAs, circRNAs can also function as protein scaffolds with diverse outcomes [for detailed review see (Huang et al., 2020)] (**Figure 2B**). For instance, *circFoxo3* forms a tertiary complex with cell cycle proteins cyclin-dependent kinase 2 (CDK2) and cyclin-dependent kinase inhibitor 1 (p21) to reduce cell cycle progression by inhibiting CDK2 (Huang et al., 2020). *circMbl*, which is regulated by MBL protein, can also bind and sequester MBL to negatively regulate the expression of *mbl* mRNA (Ashwal-Fluss et al., 2014). Similarly, *circPABPN1* can regulate the expression of PABPN1 by sequestering the RBP HuR (Abdelmohsen et al., 2017). Together, these data suggest that circRNAs might act as post-transcriptional regulators of gene expression.

A noteworthy subtype of circRNAs which contain both exon and intron sequence (known as EIcircRNAs) further supports this hypothesis. Interestingly, unlike most circRNAs which are localized to the cytoplasm (Li et al., 2015), EIcircRNAs are enriched in the nucleus and can act to regulate transcription of their host gene via interactions with RNA pol II and U1 SNP (Li et al., 2015) (**Figure 2B**). Recently, long-read sequencing from human tissues found hundreds of putative EIcircRNAs (Panda et al., 2017). What fraction of these EIcircRNAs are localized to the nucleus and/or regulate transcription? Unlike miRNA sequestration, which likely requires multiple binding sites and relatively high expression from the circRNA to achieve a measurable effect, transcriptional

regulation does not necessarily require high expression. For instance, EIcircRNAs, circEIF3J and circPAIP2 have estimated copy numbers around 20-30 in HeLa cells (Li et al., 2015). There is also evidence that post-transcriptional regulation of gene expression by circRNAs might have some protective effects. In an analysis of samples obtained from patients with coronary artery disease (CAD), patients with high expression of *circANRIL* were associated with reduced CAD burden (Holdt et al., 2016). *circANRIL* sequesters pre-ribosomal assembly factor PES1 which in turn increases pre-rRNA abundance and impairs ribosome biogenesis, resulting in apoptosis (Holdt et al., 2016). Atherosclerotic plaques from human samples found significant correlations between *circANRIL* levels and pre-rRNA abundance (Holdt et al., 2016). This might suggest that *circANRIL* is a protective factor against atherosclerosis by inducing apoptosis.

The majority of circRNA are lowly expressed relative to protein-coding mRNAs from the same gene (Guo et al., 2014; Memczak et al., 2013; Salzman et al., 2012; Szabo et al., 2015). Thus, how can transcripts present at only a few copies per cell exert a measurable effect? Moreover, the primary sequence of most circRNAs are shared with their more abundant mRNA counterparts. This would suggest that the same circRNA:RNA or circRNA:protein interactions would exist for the parental mRNA as well. To overcome low expression, circRNAs might act in cooperation to exert their function. In addition, circRNAs might also form unique secondary structures to mediate distinct RNA or protein interactions that do not occur in the linear mRNA (**Figure 2B**). Recently, this was found to be the case many circRNAs expressed in PA1 cells (Liu et al., 2019). Upon viral

infection or poly(I:C) stimulation circRNA expression is dramatically reduced (Li et al., 2017a; Liu et al., 2019). This is largely a result of RNase L activation, an endoribonuclease capable of degrading circRNAs (Liu et al., 2019). NF90/NF110 regulate circRNA biogenesis in the nucleus (Li et al., 2017a), but shuttle to the cytoplasm to perform antiviral activities (Harashima et al., 2010; Pfeifer et al., 2008), and their export relies on phosphorylated protein kinase R (PKR). PKR can bind both short (<33 bp) and long (>33 bp) dsRNAs, with only the latter leading to its activation (Nallagatla et al., 2011; Zheng and Bevilacqua, 2004). Many circRNAs were found to possess unique, short dsRNA duplexes able to bind PKR without leading to its activation. Thus, under normal conditions circRNAs act as endogenous PKR inhibitors, but upon viral infection and RNase-L mediated degradation, allow PKR to bind viral dsRNAs and shuttle NF90/NF110 to the cytoplasm (Liu et al., 2019). Intriguingly, overexpression of circRNAs with short dsRNA duplexes in primary cells obtained from patients with systemic lupus was able to suppress interferon gene expression (Liu et al., 2019), suggesting they have therapeutic utility in autoimmune diseases.

To what extent circRNAs can act individually to modulate the innate immune response is ongoing. Recently, the circRNA, *cia-cGAS* was shown to protect long term hematopoietic stem cells from inflammatory-mediated exhaustion (Xia et al., 2018). Similar to dsRNA-mediated PKR inhibition, *cia-cGAS* forms a distinct dsRNA duplex that can bind cGAS protein, a cytosolic sensor of foreign DNA that activates type I interferons, without leading to its activation (Xia et al., 2018). In mouse intestinal cells, *circPAN3* was shown to be

required for maintenance of intestinal stem cells, through stabilization of IL-13 receptor subunit-α1 (Zhu et al., 2019). Together these results suggest circRNAs are intimately involved in innate immune system function.

CircRNAs are upregulated during neural differentiation and accumulate during aging.

Note, portions of the following text have been adapted from (Knupp and Miura, 2018).

A fundamental hallmark of circRNA biology is their enrichment in the mammalian brain relative to non-neural tissues (Rybak-Wolf et al., 2015; Szabo et al., 2015; You et al., 2015). During neural differentiation and synapse maturation, the expression of hundreds to thousands of circRNAs dramatically increase (Rybak-Wolf et al., 2015; Veno et al., 2015; You et al., 2015) and they are often derived from genes with synapse or neuron-related functions (Rybak-Wolf et al., 2015; You et al., 2015). Interestingly, many of these circRNAs are enriched at synapses (Rybak-Wolf et al., 2015; You et al., 2015). For instance, in mice *circHomer1A* was significantly upregulated in the dendrites of neurons following their activation (You et al., 2015), suggesting *circHomer1A* might have neural function. In some instances, the circRNA is primarily localized to the synapse whereas the linear transcript from the same host gene is remains cytoplasmic, as is the case for *circStau2a* (Rybak-Wolf et al., 2015). How circRNAs are trafficked to synapses is unknown. It is possible that similar to

circRNAs involved in immune function, distinct secondary structures form and allow the binding of dsRBPs which mediate their independent transportation long distances to synapses. Interestingly, circRNA accumulation in neurons is not limited to development.

Compelling evidence has amassed in various animals showing that circRNAs globally accumulate during aging (Cortes-Lopez et al., 2018; Gruner et al., 2016; Hall et al., 2017; Westholm et al., 2014; Xu et al., 2018; Zhou et al., 2018). In *Drosophila*, circRNAs in aging head samples (1, 4, and 20 days post-eclosion) showed that 262 circRNAs were significantly upregulated >2-fold in 20-day vs 1-day old samples (Westholm et al., 2014) thus uncovering a global age-increase in circRNAs during aging. Moreover, the observed increases were independent of general transcription of the circRNA hosting genes. These findings have since been expanded to a study of aging *Drosophila* photoreceptor neurons (Hall et al., 2017). Here, Hall et al. sought to identify gene expression changes contributing to visual senescence in photoreceptor neurons at a comprehensive set of ages—10, 20, 25, 30, and 40 days post-eclosion. CircRNA profiling revealed an age-accumulation trend from 10-days to 40-days, extending the findings from Westholm et al, and providing evidence that global circRNA levels continue to increase from 20 days to 40 days of age in *Drosophila*. Since nuclei of photoreceptor neurons were profiled in this study, this suggests that age-accumulation trends found from whole *Drosophila* heads (Westholm et al., 2014) might be largely attributed to accumulation in neurons.

To determine if age-accumulation of circRNAs also occurs in mammals, Gruner et al. profiled circRNAs in aging male C57Bl/6 mice (Gruner et al., 2016). Using total RNA-Seq, circRNAs were identified in the cortex, hippocampus, and heart of 1-month old and 22-month old mice. Comparing the old and young time points, a highly significant increase in circRNA expression was observed for hippocampus and cortex samples. Similar to findings in fly, expression of the host genes of the circRNAs was not biased toward upregulation, meaning that the increase in circRNA expression was likely not due to increased transcription from the host genes. In contrast to the findings in brain tissues, global circRNA levels were unchanged in the hearts of young versus old mice—instead, relatively equal numbers of circRNAs were found to increase or decrease with age (Gruner et al., 2016). These results are in agreement with independent studies conducted in rats and Rhesus monkeys which found that circRNAs accumulated in aging brain tissue but not in other tissues such as muscle (Abdelmohsen et al., 2015; Xu et al., 2018; Zhou et al., 2018).

Recently, circRNA profiling was performed in aging *C. elegans* (Cortes-Lopez et al., 2018), a model organism which has had incredible utility with respect to the study of aging (*see below*, *C. elegans* as a model for aging). In contrast to previous studies, whole worms were profiled instead of brain tissue or isolated neurons. Total RNA-seq profiling at larval stage 4 (L4), day 1, day 7, and day 10 adults uncovered the strongest circRNA age-accumulation trend to-date (Cortes-Lopez et al., 2018). Over 90% of circRNAs detected increased at least 1.5-fold between L4 and day 10.

Together, these studies in *C. elegans*, *Drosophila,* mice, rats and Rhesus monkey demonstrate that age-accumulation of brain-expressed circRNAs is a phenomenon conserved across phyla. Importantly, all these studies provide various levels of evidence that age-related circRNA increases were independent from host gene expression. This means that most circRNA increases were not due to transcriptional upregulation of the host genes.

What mechanisms might account for the increased levels of circRNAs during development and aging? Due to their lack of free ends, circRNAs are resistant to degradation from exoribonucleases (Jeck et al., 2013). This, coupled with the post-mitotic nature of neurons, implies that the increased levels of circRNAs reported in multiple animals could be a result of accumulation as opposed to specific gene regulation. Following this logic, linear RNAs from the circRNA host genes would be synthesized in post-mitotic cells, and degraded, whereas the turnover of circRNAs in the same cells would be much slower. When cells divide or die, the stable circRNAs are lost, which would imply that post-mitotic cells would have more circRNAs than proliferative cells. Supporting this line of reasoning, circRNAs are less abundant in proliferative cells (Bachmayr-Heyda et al., 2015; Song et al., 2016) and are negatively correlated with increasing numbers of proliferative, glial subpopulations in cultured cells (Rybak-Wolf et al., 2015). The strong age-accumulation circRNA trends found in whole *C. elegans* samples also supports this explanation as the majority of cells in adult *C. elegans* are post-mitotic (Sulston and Horvitz, 1977).

Aging is associated with global changes in splicing patterns in multiple organisms, including humans (Harries et al., 2011; Mazin et al., 2013; Rodriguez et al., 2016). Since circRNAs are products of alternative splicing, it is reasonable to assume age-related changes in back-splicing might contribute to the progressive age-accumulation of circRNAs. As discussed, several RBPs and splicing factors have been found to regulate circRNAs in both invertebrate and vertebrate systems, and several are expressed in neurons (*see section*, 'Backsplicing is regulated by RNA binding proteins'). However, until recently (Knupp et al., 2021), no RBPs had been identified that could explain the *in vivo* accumulation of neural expressed circRNAs in mammals (also *see Chapter 2*). This coupled with the fact that 1) not all circRNAs are upregulated during aging and 2) that some circRNAs increase or decrease in expression during brain development (Veno et al., 2015) signifies that their accumulation cannot be solely attributed to enhanced stability.

Future work is needed to understand the cellular and subcellular expression patterns of circRNAs in aging animals. Fluorescence-activated cell sorting (FACS) of brain cell populations including endothelial cells, neurons, and glia followed by circRNA profiling by bulk RNA-seq or by single-cell RNA-seq should elucidate cell-type specific differences in circRNA accumulation trends.

C. elegans utility for identifying functional age-related circRNAs

Research using *C. elegans* has contributed significantly to our understanding of aging as a process regulated by distinct cellular pathways

(reviewed in (Denzel et al., 2019)). *C. elegans* has several convenient features that make them suitable as a system for basic aging research. 1) *C. elegans* is easy and inexpensive to culture and handle. 2) exhibit a relatively short (~3 days at 20°C) generation time and lifespan (~3 weeks at 20°C). 3) Possess distinct tissues including a well-characterized nervous system of reasonable complexity. 4) Multiple quantitative phenotypes (ex. egg-laying, chemotaxis, foraging, lifespan) amenable to forward and reverse genetic screens.

As discussed, circRNAs are dynamically expressed throughout *C. elegans* lifespan and display the most robust accumulation trends of any organism to-date (Cortes-Lopez et al., 2018). What functions, if any, do these age-related circRNAs have? Can circRNAs act individually or collectively to extend lifespan or are they are detrimental consequence of aging? Similar to mammals, circRNAs expressed in *C. elegans* show significant enrichment for RCMs in their flanking introns (Cortes-Lopez et al., 2018; Ivanov et al., 2015), which can be targeted for deletion by techniques such as CRISPR-Cas9 to diminish their expression. Given that genetic manipulation in *C. elegans* relatively faster than in mammals, *C. elegans* is positioned as a premier model for assessing circRNA function on a large scale at speed. Indeed, several circRNAs have already been disrupted successfully in *C. elegans* through such an approach (Cao, 2021). Thus, *C. elegans* is a relatively untapped resource suitable for the screening of functional circRNAs.

Concluding remarks

The circRNA field has progressed significantly in the last decade. Previously regarded as transcriptional noise, circRNAs are now well established as transcripts with tissue-specific expression patterns and diverse functional potential. Past work on understanding the regulation of circRNA expression has identified several *cis*- and *trans*-acting factors integral to circRNA biogenesis. Hundreds of circRNAs are enriched in brain tissues and accumulate with age, yet the mechanism underlying this neural enrichment or age-accumulation is largely uncharacterized. Moreover, the function of nearly all neural expressed or age-related circRNAs are unknown. Model organisms such as *C. elegans* are powerful resources that will be instrumental in addressing these knowledge gaps. To what extent circRNAs are involved in immunity and diseases is also emerging and suggest that they might serve as future therapeutic agents or disease targets or biomarkers.

Overview

My dissertation research investigates two key aspects regarding circRNA biology, 1) circRNA enrichment in the developing mammalian brain and 2) the function of age-related circRNAs. To address point 1, I sought out to identify a neural-expressed, *trans*-acting factor that could at least in part underlie the high expression of circRNAs in the mammalian brain. To address point 2, I leveraged the model organism *C. elegans* as a tool to investigate the function of age-accumulating circRNAs.

Chapter 2: To identify a regulator of circRNA biogenesis in the brain we initially reanalyzed publicly available total RNA-seq datasets from wild-type (WT), NOVA1 and NOVA2 knockout embryonic whole cortex tissues. We found that global circRNA expression was significantly reduced in NOVA2-KO but not NOVA1-KO mouse cortex samples. Investigating NOVA2 datasets more closely, we found a modest bias toward downregulation of circRNAs in the absence of NOVA2. This suggests that NOVA2 is a positive regulator of circRNA biogenesis in the developing mouse brain. We next analyzed published RNA-seq datasets from FAC-sorted mouse embryonic cortical neurons from WT and conditional NOVA2-KO mutants (NOVA2-cKO). Given that NOVA2 is a neuron-enriched splicing factor, and that circRNAs are expressed in multiple brain tissues apart from neurons, we expected more robust circRNA expression changes in sorted neuron populations relative to whole cortex. We observed striking downregulation of circRNAs in NOVA2-cKO sorted cortical neurons relative to the whole cortex

dataset. We constructed backsplicing minigenes for an endogenous NOVA2-regulated circRNA, *circEfnb2* and found that intronic NOVA2-binding sites were important for its regulation. We investigated NOVA2-regulation more generally using artificial backsplicing minigenes and found that NOVA2 binding in both flanking introns of the circularizing exon was important for NOVA2 regulation. Lastly, we analyzed published NOVA2-CLIP data obtained from embryonic cortical neurons and found that both introns flanking a NOVA2-regulated circRNA were bound by NOVA2 at a significantly greater frequency than non-regulated control circRNAs. In sum, we describe a novel role for NOVA2 in the regulation of backsplicing and identified the first RBP to regulate circRNAs in the developing mammalian brain and neurons.

Chapter3: We previously identified hundreds of circRNAs that accumulated during *C. elegans* lifespan. Two of the most abundant, age-accumulating circRNAs in this analysis are spliced from exon 4 of the *crh-1* gene, the CREB homolog in worms. We found that long intronic RCMs flanked the *crh-1* circRNA locus. We show that *crh-1* circRNA biogenesis is regulated by the dsRNA binding protein ADAR1. We hypothesized that the intronic RCMs flanking the *crh-1* circRNA loci likely mediated their expression. Thus, to disrupt circRNA expression we deleted the downstream RCM using CRISPR-Cas9. We examined two independent mutant alleles and found that *circ-crh-1* expression was abolished, without interrupting linear *crh-1* expression or active CREB expression. We found that both mutant lines had significantly longer mean lifespans compared to WT worms. Rescue of *crh-1* circRNA expression in

neurons was able to partially reduce lifespan extension. RNA-seq of WT and mutant worms identified hundreds of gene expression changes, implicating involvement of the innate immune system and transcription factor *hlh-11*. Our work identified the first circRNAs with a lifespan related phenotype in a loss-of-function scenario and suggests that *crh-1* circRNAs are detrimental to *C. elegans* longevity.

Chapter 2: NOVA2 regulates neural circRNA biogenesis

David Knupp[1], Daphne A. Cooper[1], Yuhki Saito[2], Robert B. Darnell[2] and Pedro Miura[1*]

[1]Department of Biology, University of Nevada, Reno, Reno, NV 89557, USA

[2]Laboratory of Molecular Neuro-oncology and Howard Hughes Medical Institute, The Rockefeller University, New York, NY 10065, USA

This chapter was published in Nucleic Acids Research. Volume 49, Issue 12, 9 July 2021, Pages 6849-6862, doi: https://doi.org/10.1093/nar/gkab523 (Knupp et al., 2021)

AUTHOR CONTRIBUTIONS

D. Knupp performed all *in vitro* experiments and RNA-seq analyses of *in vivo* NOVA1 or NOVA2 datasets, generated all figures and helped write the manuscript.

D. Cooper provided helpful guidance for CIRI2-based circRNA read alignments and wrote a subset of custom scripts used in the CIRI2 pipeline.

Y. Saito provided output data files from published NOVA2-CLIP experiments used in **Figure 6** and **Figure S6**. Y. Saito also provided RNA isolated from WT and *Nova2*-KO E18.5 mouse cortex used in RT-qPCR validations (related to **Figure 3F**). Y. Saito is a Research Assistant Professor in Robert B. Darnell's lab.

Chapter 2 was performed under the guidance and supervision of Dr. Pedro Miura. P. Miura also helped write the manuscript.

ABSTRACT

Circular RNAs (circRNAs) are highly expressed in the brain and their expression increases during neuronal differentiation. The factors regulating circRNAs in the developing mouse brain are unknown. NOVA1 and NOVA2 are neural-enriched RNA-binding proteins with well-characterized roles in alternative splicing. Profiling of circRNAs from RNA-seq data revealed that global circRNA levels were reduced in embryonic cortex of *Nova2* but not *Nova1* knockout mice. Analysis of isolated inhibitory and excitatory cortical neurons lacking NOVA2 revealed an even more dramatic reduction of circRNAs and establishes a widespread role for NOVA2 in enhancing circRNA biogenesis. To investigate the *cis*-elements controlling NOVA2-regulation of circRNA biogenesis, we generated a backsplicing reporter based on the *Efnb2* gene. We found that NOVA2-mediated backsplicing of circ*Efnb2* was impaired when YCAY clusters located in flanking introns were removed. CLIP (cross-linking and immunoprecipitation) and additional reporter analyses demonstrated the importance of NOVA2 binding sites located in both flanking introns of circRNA loci. NOVA2 is the first RNA-binding protein identified to globally promote circRNA biogenesis in the developing brain.

INTRODUCTION

Alternative splicing (AS) affects approximately 95% of human multi-exon genes (Pan et al., 2008). Through AS, hundreds of thousands of RNA isoforms with distinct structural properties, localization patterns, and translation efficiencies can be expressed as protein isoforms with diverse functions (Kelemen et al., 2013). In the mammalian nervous system, AS is especially pervasive and highly conserved (Barbosa-Morais et al., 2012; Merkin et al., 2012). During brain development, AS is responsible for establishing neuron-specific splicing patterns at defined stages, and developmentally regulated alternative exons have essential roles in synapse formation, neuronal migration and axon guidance (Dillman et al., 2013; Mazin et al., 2013; Molyneaux et al., 2015; Vuong et al., 2016). Stage-specific AS patterns during development are controlled by RNA binding proteins (RBPs) enriched or specifically expressed in neurons and are critical for proper development as their dysregulation underlies many neurological disorders (Gehman et al., 2011; Licatalosi and Darnell, 2006; Ruggiu et al., 2009; Saito et al., 2016; Shibayama et al., 2009).

Circular RNAs (circRNAs) are generated through backsplicing, a type of AS (Li et al., 2018). During backsplicing, the downstream 5' splice site (SS) covalently bonds the upstream 3' SS of a circularizing exon creating a closed loop “circle” that is resistant to exoribonuclease digestion (Li et al., 2018). Most characterized circRNAs are derived from annotated exons of protein-coding genes, and many are independently regulated from their host genes and exhibit

unique expression patterns over various time-points (Veno et al., 2015). Thus far, ascribed circRNA functions include sequestration of microRNAs, translation of small peptides, modulation of the immune response, and transportation and scaffolding of RBPs (Abdelmohsen et al., 2017; Du et al., 2016; Hansen et al., 2013; Holdt et al., 2011; Huang et al., 2015; Legnini et al., 2017; Li et al., 2017a; Li et al., 2017b; Liu et al., 2019; Pamudurti et al., 2017; Yang et al., 2017). CircRNAs are enriched in brain tissues on a genome-wide level (Memczak et al., 2013; Rybak-Wolf et al., 2015; Westholm et al., 2014; You et al., 2015) and are dramatically upregulated during neural differentiation and maturation (Rybak-Wolf et al., 2015; Veno et al., 2015; You et al., 2015). CircRNAs are also found to accumulate during aging and this trend appears to be specific to brain tissues and neurons (Gruner et al., 2016; Hall et al., 2017; Knupp and Miura, 2018).The functional significance of brain-expressed circRNAs is emerging, with only a handful of circRNAs found to have roles in the nervous system (Piwecka et al., 2017; Suenkel et al., 2020; Zimmerman et al., 2020).

Several, RBPs have been identified to regulate circRNA biogenesis, including Muscleblind, Quaking (QKI), ADAR, FUS, and several hnRNPs and SR proteins (Ashwal-Fluss et al., 2014; Conn et al., 2015; Errichelli et al., 2017; Ivanov et al., 2015; Kramer et al., 2015). However, investigation of circRNA regulation by RBPs from *in vivo* brain or neuron datasets is lacking. There are several well-characterized splicing factors with roles in the nervous system including RBFOX1/2/3, PTPBP1/2, nrSR100/Srrm4, Hu proteins, and NOVA1/2 (Vuong et al., 2016). Deletion or dysregulation of any of these splicing factors

results in serious and often lethal neurological defects (Vuong et al., 2016). Among the best characterized neural-enriched splicing factors are the NOVA proteins, which were originally discovered as autoantigens in patients with paraneoplastic opsoclonus-myoclonus ataxia, a neurological condition characterized by motor and cognitive defects (Buckanovich et al., 1993; Luque et al., 1991; Yang et al., 1998). NOVA1 and NOVA2 are paralogues that bind clusters of YCAY motifs to regulate alternative splicing (Buckanovich and Darnell, 1997; Buckanovich et al., 1996; Lewis et al., 2000). Knockout (KO) of either paralogue in mice results in early lethality. This has been attributed to death of motor neurons in the case of NOVA1 deficiency, and aberrant migration of cortical and Purkinje neurons in the case of NOVA2 (Jensen et al., 2000a; Saito et al., 2016; Saito et al., 2019; Yano et al., 2010). Although both proteins recognize the same RNA binding motif, their expression is largely reciprocal. For instance, immunohistochemical and *in situ* hybridization data indicate NOVA2 is lowly expressed in midbrain and spinal cord, whereas high expression is observed in the cortex and hippocampus. In contrast, NOVA1 is highly expressed in the midbrain and spinal cord and is relatively low expressed in the cortex (Saito et al., 2016; Yang et al., 1998). Furthermore, NOVA1 and NOVA2 appear to have different splicing regulatory networks in the developing cortex itself (Saito et al., 2016). More recently, conditional knockout (cKO) of NOVA2 in either excitatory (Emx1+) or inhibitory (Gad2+) neurons led to thousands of AS events that were largely unique to each cell-type (Saito et al., 2019). In addition, loss of NOVA2 in excitatory neurons resulted in disorganization of cortical and

hippocampal laminar structures, whereas this was not observed in NOVA2-KO inhibitory neurons. These findings showcase the importance of examining AS outcomes among different neuron subtypes.

Here, we examined circRNA expression in RNA-Seq data from mouse cortex samples lacking NOVA1 or NOVA2. We found that the absence of NOVA2 caused a reduction in global circRNA levels. In sorted excitatory and inhibitory neurons, NOVA2 loss was found to dramatically reduce circRNA expression. These changes in circRNA levels were largely independent from transcriptional changes or changes in linear alternative splicing. Using CLIP data and backsplicing reporter analysis, we found that NOVA2 binding sites in the introns flanking circRNA exons are important for NOVA-2 mediated circRNA biogenesis.

MATERIALS AND METHODS

Accession numbers

Wild-Type (WT), *Nova1-KO* and *Nova2-KO* whole cortex RNA-seq data were obtained from Gene Expression Omnibus (GEO) under accession number GSE69711. Fluorescence-activated cell sorted (FACS) sorted *Nova2*-KO neuron RNA-seq datasets were obtained from GEO under accession number GSE103316. For individual Sequence Read Archive (SRA) accession numbers see **Supplementary File S1**.

Mouse tissue preparation, RNA extraction, RNaseR Treatment, and RT-qPCR

All procedures in mice were performed in compliance with protocols approved by the Institutional Animal Care and Use Committee (IACUC) of the Rockefeller University or the University of Nevada, Reno. Mouse tissue samples were pulverized using a mortar and pestle on dry ice, and RNA was extracted using Trizol (ThermoFisher Scientific). For harvesting cultured cells PBS washes were performed followed by Trizol extraction. For RNase R treatment, 100µg total RNA from cortex or cultured HEK293 cells was treated with or without 1µL of RNaseR [20 U/µl] (Lucigen), plus 1.9µL RNaseOUT [40 U/µL] (ThermoFisher Scientific) and 1µL Turbo-DNase [2 U/µL] (Invitrogen) in a 60µL reaction volume for 30 minutes at 37°C. RNase R reactions were terminated and RNA was purified as previously described (Cortes-Lopez et al., 2018). Equal amounts of RNase R or mock treated RNA served as input for cDNA preparation. PolyA+ RNA and polyA- RNA was obtained using previously described methods (Cortes-Lopez et al., 2018). Briefly, the NucleoTrap mRNA column-based kit (Machery-Nagel) was used according to the manufacturers protocol. RNA present in the flow-through (not bound to oligo(dT) beads) was precipitated to isolate the polyA- fraction. For RT-qPCR experiments, Turbo-DNase (Invitrogen) treated RNA was reverse transcribed using random hexamers (Invitrogen) and Maxima reverse transcriptase (ThermoFisher Scientific) according to the manufacturer's specifications. RT-qPCR was performed on a BioRad CFX96 real time PCR

machine using SYBR select mastermix for CFX (Applied Biosystems). The delta delta Ct method was used for quantification. Target gene expression for both circRNA and host-mRNA expression was normalized to *Gapdh*. Experiments were performed using biological triplicates. Student's t-test (two-tailed and unpaired) was used to test for statistical significance.

Cell Culture

HEK293 cells (ATCC) were cultured in DMEM (ThermoFisher Scientific) with 10% FBS (Atlanta Biologicals). HEK293 cells were transfected with NOVA2 expression plasmid or empty vector control (Gifts from Dr. Zhe Chen at University of Minnesota) in addition to the circ*Efnb2* or circ*Min*i backsplicing reporters, using PEI transfection reagent (Polysciences), and reduced serum medium Opti-MEM (ThermoFisher Scientific). The cells were cultured for 24 hours prior to RNA extraction.

Northern Blotting

RNA samples were denatured by mixing with 3 volumes NorthernMax Formaldehyde loading dye (ThermoFisher Scientific) and ethidium bromide (10 µg/mL) for 15min at 65°C. Denatured samples were loaded onto a 1% MOPS gel with 1x Denaturing Gel Buffer (ThermoFisher Scientific) and ran at 102V for 60 min. RNA samples were transferred to a Cytiva Whatman Nytran SuperCharge membrane (ThermoFisher Scientific) for 1.5 hours using a Whatman TurboBlotter

transfer system (ThermoFisher Scientific) and NorthernMax Transfer Buffer. Samples were then UV cross-linked with a Stratagene linker to the nylon membrane prior to probe hybridization. Double-stranded DNA probes were prepared by end-point PCR and labeled with dCTP [□-32P] (PerkinElmer) using the Cytvia Amersham Megaprimer labeling kit (Thermo Fisher Scientific) according to manufacturer's instructions. Blots were hybridized overnight in ULTRAhyb™ Ultrasensitive Hybridization buffer (ThermoFisher Scientific) at 42°C. Following hybridization, blots were washed at room temperature 2x5 min in a low-stringency buffer followed by 2x15 min in a high-stringency buffer at 42°C. Blots were then exposed for 4-5 days to a GE Storage Phosphor screen (Millipore Sigma) before imaging on a Typhoon™ FLA 7000 imager (GE). Probe sequences are listed in **Supplementary File S9**.

RNA-Seq Analysis for CircRNA prediction, mapping and differential expression.

For de novo identification of circRNAs raw FASTQ files were aligned to the mm9 genome using HISAT2 v2.1.0 (Love et al., 2014) (parameters: --no-mixed –no-discordant). Unmapped reads were aligned using BWA v0.7.8-r455 mem and CIRI2 v2.0.4 (Gao et al., 2018) was used to obtain a set of predicted circRNA loci using default parameters. For alignment to circRNA junction spanning FASTA sequence templates of 220 nt we used Bowtie2 v2.2.5 (Langmead and Salzberg, 2012) (parameters: -score-min=C,-15,0). After mapping, Picard

(http://broadinstitute.github.io/picard) (parameters: MarkDuplicates ASSUME_SORTED=true REMOVE_DUPLICATES=true) was used to remove duplicates from our mapping data. To quantify the number of mapped reads for each junction we used featurecounts v1.5.0 (Liao et al., 2014) (parameters: -C -t circle_junction). mm9 circRNA coordinates were converted to mm10 genome-build using UCSC liftover tool. All supplementary data tables are reported in mm10 coordinates.

For each dataset (*Nova1*-KO vs. WT, *Nova2*-KO vs. WT, *Nova2*-cKO$^{tdTomato;Emx1\text{-}Cre}$ vs. WT, *Nova2*-cKO$^{tdTomato;Gad2\text{-}Cre}$ vs. WT) a cutoff of 6 reads across the 6 libraries for each condition (3 biological replicates per condition) was set. To account for difference in library depth among samples, scaling by circRNA Counts Per Million of reads (CPM) in each library was performed. Fold-change CPM values were generated between KO and WT conditions. A cutoff of 2.0-fold-change difference and significance threshold of $P<0.05$ via t-test was used across the normalized CPM values to identify differentially expressed circRNAs. Correction for multiple hypothesis testing was not performed.

The CircTest pipeline was performed to quantify host gene independent circRNA expression patterns. DCC/CircTest v0.4.7 was used to quantify host gene read counts. In accordance with DCC pipeline (Cheng et al., 2016), FASTQ files were mapped with STAR 2.6.0b using the recommended parameters and aligned to the GRCm38 genome. The circRNA and linear RNA counts obtained from DCC

were used as input for the Circ.test module (parameters: Nreplcates=3 filter.sample=4 filter.count =3 percentage = 0.1 circle_description=c(1:3)). To define a circRNA as host gene independently expressed, we used the default parameter, adj. *P*<0.05 (Benjamini-Hochberg correction). ggplot2 (Wickham, 2016) R packages and custom scripts were used to generate all plots.

Mapping and quantification of linear RNA expression

Reads were aligned to the NCBI37 reference genome using HISAT2 v2.1.0 (GENCODE annotations M1 release, NCBIM37, Ensembl 65). FeatureCounts v1.5.0 (parameters -t exon -g gene_id) was used to obtain a counts table as input for differential expression analysis. For differential expression analysis, DESeq2 v1.26.0 was performed using Benjamini-Hochberg correction and apeglm Bayesian shrinkage estimators with a 2.0-fold-change and adj. *P*<0.05 required to consider a linear RNA as differentially expressed**.** For alternative splicing analysis, the rMATS pipeline (Shen et al., 2014) was used to calculate significant exon skipping events in *Nova2*-cKO$^{tdTomato;Emx1\text{-}Cre}$ versus WT and *Nova2*-cKO$^{tdTomato;Gad2\text{-}Cre}$ versus WT datasets. FASTQ files were mapped using STAR 2.6.0b using default parameters (parameters: --chimSegmentMin 2 --outFilterMismatchNmax 3 –alignEndsType EndToEnd –runThreadN 4 –outSAMstrandField intronMotif –outSAMtype BAM SortedByCoordinate –alignSJDBoverhang 6 –alignIntronMax 30000) and aligned to the GRCm38/mm10 genome (GENCODE annotations vM22 release). rMATs-v.3.2.5 was used to discover significant alternative splice events under the default

parameters. For post processing, we filtered the output file, SE.MATS.ReadsOnTargetAndJunctionCounts.txt to contain skipping events with FDR<0.01. Mapped circRNA BED files were converted to mm10 coordinates using UCSC genome browser liftover tool. Then bedtools suite was used to find overlap with significant exon skipping events. Overlaps were manually checked using Integrative Genomics Viewer (IGV) (Qu et al., 2016).

NOVA2-CLIP analysis

cTag-CLIP data from excitatory (Emx1+) and inhibitory (Gad2+) neurons (Saito et al., 2019) were used to examine overlap with NOVA2-regulated circRNAs. Emx1+ and Gad2+ circRNAs that were NOVA2-regulated in both the CIRI2 and DCC/CircTest analyses were chosen for comparison against non-differentially expressed circRNAs (FC<1 and P>0.50) identified by CIRI2 (minimum average 3 BSJ counts per condition). First, we extracted intron coordinates from the UCSC table browser. Next, Bedtools suite was used to extract upstream and downstream introns flanking the circRNA loci. Finally, Bedtools suite was used to identify the presence or absence of intronic NOVA2-CLIP peaks (upstream/downstream or both flanking introns).

Backsplicing Reporter Assays

All plasmids are available upon request. The pUC19 plasmid backbone was used to generate circ*Efnb2* and circ*Mini* backsplicing reporters with modifications.

Briefly, the CMV enhancer/promoter region was amplified from the pcDNA3.0 backbone using Phusion High-Fidelity Polymerase (NEB) and subcloned into the pUC19 vector upstream of the circ*Efnb2* or circ*Mini* backsplicing cassettes. In addition, BGH and rB-Globin poly(A) sequences were subcloned downstream of the backsplicing cassettes using synthetic gene fragments (gBlocks, IDT) for transcription termination. All fragments used to generate the backbone vector and subsequent backsplicing cassettes were cloned using the NEB Hifi assembly kit (NEB) following the manufacturers protocols.

For circ*Efnb2* reporter three genomic fragments were amplified by PCR using Phusion High-Fidelity Polymerase. The three genomic fragments (mm10 coordinates) are as follows: 1) Truncated upstream *Efnb2* exon1 (81 bp) plus downstream flanking intron (134 bp) (chr8:8660350-8660564); 2) circularizing *Efnb2* exon 2 (284 bp) plus partial upstream (448 bp) and downstream (475 bp) flanking introns (chr8:8638731-8639937) and 3) truncated *Efnb2* exon 3 (72 bp) plus partial intronic upstream sequence (197 bp) (chr8:8623169-8623437); (chr8:8660350-8660564). Initial transfection experiments with circ*Efnb2*-WT demonstrated two unintended backspliced products originating from the AmpR cassette and non-coding sequence immediately downstream of the CMV promoter when examined by RT-PCR. As a result, we introduced two silent mutations into the AmpR coding sequence and deleted 115 bp of non-essential sequence between the CMV promoter and circ*Efnb2* cassette. Follow-up experiments showed all unintended backspliced products were abolished.

Mutations located in the circ*Efnb2* introns were introduced by PCR amplification of the pWT backbone using Phusion High-Fidelity polymerase and ligation with gBlock donor DNA carrying point mutations targeting YCAY motifs. Mutations were confirmed by Sanger sequencing.

To generate the artificial circMini-WT vector, two gBlocks consisting of full-length GFP coding sequence, partial human *ZKscan1* intron sequence and partial *Mboat2* intron sequence were cloned into the modified pUC19 vector described above. We used the Berkeley Drosophila Genome Project splice prediction tool (https://www.fruitfly.org/seq_tools/splice.html) with default settings to guide GFP and intron sequence modifications that would improve splicing efficiency and prevent unintended splice products from being generated. In addition, existing YCAY motifs were mutated to prevent NOVA2 binding. Artificial 10x YCAY sequence was produced via gBlocks and were cloned 50 bp upstream (pMini-UP), 49 bp downstream (pMini-Down) or in both locations (pMini-Both) in relation to the circRNA loci.

RESULTS

Global circRNA levels are reduced in *Nova2*-KO whole cortex

To investigate potential factors that might contribute to regulation of circRNAs in the murine brain, we analyzed paired-end total RNA-seq data from embryonic *Nova1-KO* and *Nova2*-KO mouse cortex samples for changes in circRNA expression (Saito et al., 2016) (**Supplementary File S1**). These RNA-seq libraries were generated using random hexamer-based priming as opposed to oligo(dT) priming for cDNA synthesis, thus enabling detection of circRNAs which are not-polyadenylated. CircRNAs were identified by back-splice junction (BSJ) reads using the CIRI2 algorithm (**Figure 3A**). We set a minimum expression threshold of 6 BSJ reads across the 6 libraries (minimum average of 1 read per biological replicate) for each dataset, resulting in 1565 and 3708 exonic circRNAs identified for the *Nova1* and *Nova2* datasets, respectively (**Supplementary File S2 and File S3**). BSJ read counts were normalized to library size to obtain Counts Per Million mapped reads (CPM). Global circRNA CPM values were found to be significantly reduced in *Nova2*-KO samples compared to controls ($P<2.48\text{x}10^{-11}$, Wilcoxon-rank sum test with continuity correction) (**Figure 3B**). In contrast, global circRNA levels were not altered in *Nova1*-KO mice compared to controls (**Figure 3B**).

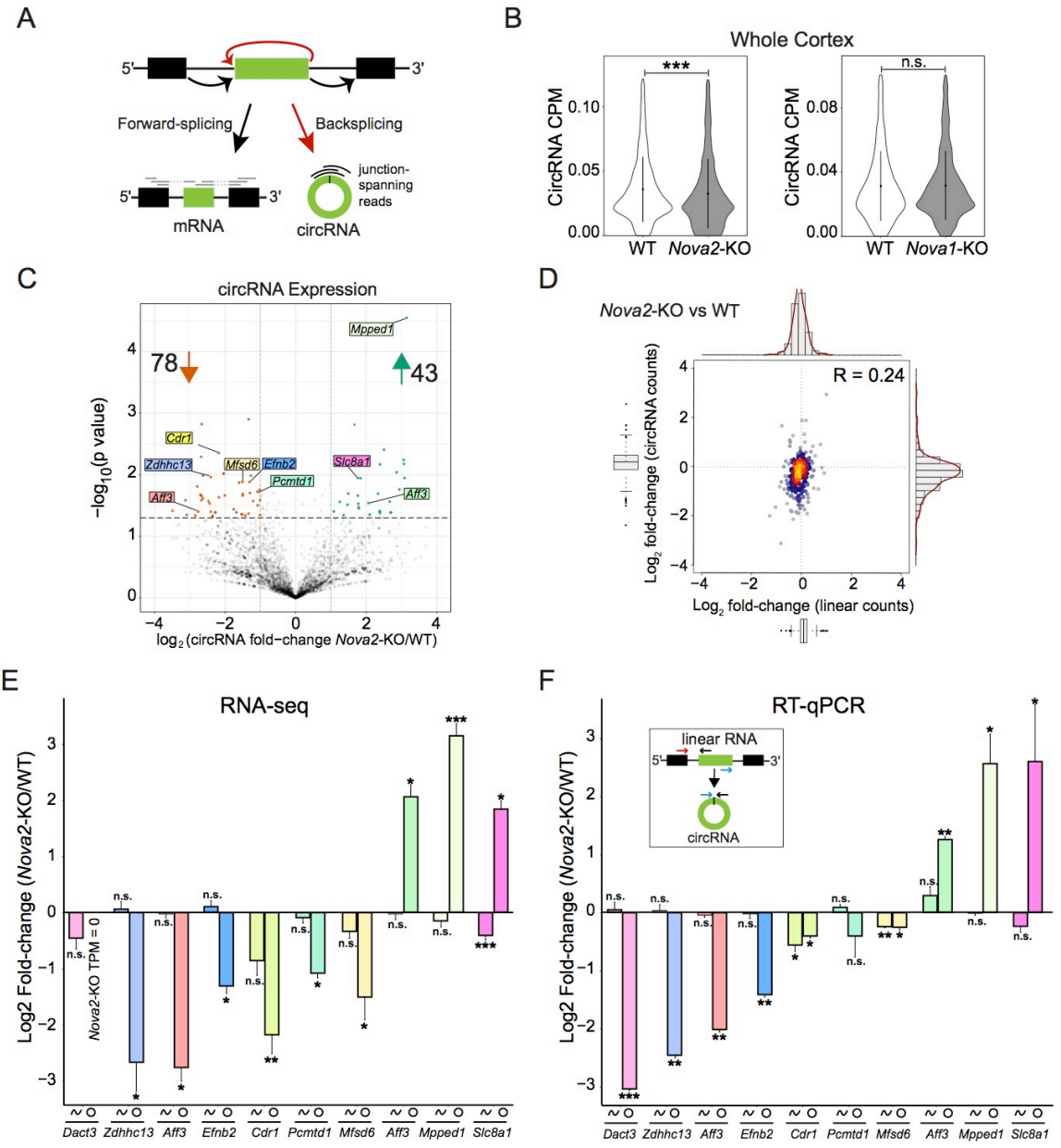

Figure 3. NOVA2 regulation of circRNA biogenesis in mouse cortex.

(**A**) Schematic of forward-spliced and backspliced read alignments for detection of linear RNA and circRNA expression, respectively. The circularizing exon is shown in green. (**B**) CircRNA CPM is significantly reduced in *Nova2*-KO (*left*) but not *Nova1*-KO (*right*) whole cortex. Significance reflects non-parametrical

Wilcoxon rank-sum test with continuity correction. n = 3 biological replicates for each condition. (**C**) Volcano plot of circRNAs in *Nova2*-KO vs. WT showing circRNAs downregulated (orange dots) and upregulated (green dots) in the knockout condition (log_2FC>1, P<0.05). (**D**) High density scatterplot of 311 circRNAs (minimum 3 BSJ read counts in 4 out of 6 replicates). Y-axis reflects log_2 fold-change of circRNA counts. X-axis reflects log_2 fold-change of linear counts from host genes. (**E**) RNA-seq quantification of 10 circRNAs (7 downregulated, 3 upregulated) in *Nova2*-KO vs WT and their corresponding host gene mRNA expression. (**F**) RT-qPCR quantification of the same 10 regulated circRNAs and their host gene mRNAs normalized to *Gapdh*. Inset diagram depicts primer locations used for circRNA and host gene linear mRNA quantification. *P<0.05; **P<0.01; ***P<0.001; n.s., not significant. Student's t-test was used for statistical significance (two-tailed, unpaired). CPM, Counts Per Million. See also **Figure S1** and **Figure S3**.

In order to capture expression of individual circRNAs in *Nova2*-KO cortex we generated volcano plots using *P*-value and fold-change, as previously reported (Gruner et al., 2016). We observed a slight trend for downregulation in *Nova2*-KO mouse cortex compared to WT samples. From the volcano plot, it is evident that more circRNAs were downregulated than upregulated in the KO condition ($P<0.05$, $Log_2FC>1$) (**Figure 3C**). In contrast, the *Nova1*-KO dataset lacked any biased expression trend (**Figure S1A**). The reduced circRNA levels in *Nova2*-KO samples could have been a consequence of reduced transcriptional activity from the host genes that the circRNAs are derived from. Thus, we performed differential expression analysis for the mRNAs generated from the host genes of the regulated circRNAs (**Figure S1B**). Alignment was performed using HISAT2 (Kim et al., 2015), and DESeq2 (Love et al., 2014) was used to perform differential expression analysis of mRNAs. No significant changes in host gene mRNA expression were detected. In addition, density plots were generated to contrast total read counts from circRNAs versus their linear RNA counterpart from the same host gene, read counts were obtained using DCC (see Materials and Methods) (Cheng et al., 2016). We observed a clear downward shift along the y-axis, reflecting reduced circRNA expression, while linear RNA expression along the x-axis centered near zero indicating only minor expression changes (**Figure 3D**). Together, these data suggest that NOVA2-mediated regulation of circRNA biogenesis is largely independent of host gene transcription changes.

In order to provide experimental support for the circRNA expression trends, we performed RT-qPCR confirmation for 10 circRNAs that were either reduced (7 loci) or increased (3 loci) in the *Nova2*-KO condition (**Figure 3F**). For circRNA quantification, outward facing primers that only detect the circularized exons were used (**Figure 3F**). For quantification of the cognate mRNA, we employed primer sets with one primer located in an exon that is circularized and the other is located in the flanking upstream or downstream exon (**Figure 3F and Supplementary File S9**). Overall, we observed a good correlation between RNA-seq expression trends and our RT-qPCR results, confirming expression trends for 9/10 circRNAs and 8/10 host gene linear RNAs. In addition, we validated the circularity of these targets with RNase R, a 3' to 5' exoribonuclease that degrades linear RNAs while circRNAs are relatively more resistant (Jeck et al., 2013). We found all 10 to be resistant to RNase R treatment, whereas the linear control gene, *Psmd4*, was degraded (**Figure S1C**). These experiments indicate that our sequencing analysis pipeline can detect bonafide circRNA expression changes.

Loss of NOVA2 dramatically reduces global circRNA levels in isolated neuron subpopulations

NOVA2 expression is mostly limited to neurons (Yang et al., 1998). In contrast, circRNAs are expressed in various brain cell-types such as astrocytes, neurons, glia and oligodendrocytes (Rybak-Wolf et al., 2015; Sekar et al., 2018).

We reasoned that our analysis in whole cortex might obscure the specific regulation of circRNAs in neurons by NOVA2. Thus, we analyzed circRNAs in NOVA2 deficient neuron subpopulation datasets. Total RNA-seq data from fluorescence-activated cell sorted (FACS) embryonic inhibitory and excitatory cortical neurons deficient in NOVA2 (Saito et al., 2019) were analyzed using the CIRI2 pipeline. We identified 4123 and 2440 exonic circRNAs in Gad2+ and Emx1+ datasets, respectively, that passed our minimum BSJ read threshold (**Supplementary File S4 and S5**). Global circRNA levels were significantly decreased in both *Nova2*-KO datasets ($P<2.2x10^{-16}$, Wilcoxon-rank sum test with continuity correction) (**Figure 4A, B**; inset violin plots). Similar to results from whole cortex, linear expression from the host gene of the differentially expressed circRNAs did not show any significant changes (**Figure S2A, B**). Volcano plots demonstrated a striking downregulation trend for hundreds of circRNAs in both inhibitory and excitatory neurons in the absence of NOVA2, with only a handful of upregulated circRNAs (**Figure 4A, B**). At least 9-fold more circRNAs were downregulated in either dataset compared to the number of circRNAs upregulated. Reduced circRNA expression in the knockouts remained when the analysis was performed with increased minimum thresholds of 10, 20, and 30 backspliced reads per condition (**Figure S3A-C**). Our results indicate that NOVA2 generally promotes circRNA biogenesis in cortical neurons.

We next analyzed the same datasets using DCC/CircTest, an independent circRNA analysis pipeline (Cheng et al., 2016). DCC computes forward and backspliced read counts, whereas the CircTest module calculates the ratio of

BSJ reads to linear, forward spliced reads and robustly tests for their independence. Applying a stringent filtering method (minimum 3 BSJ counts in 4 out of 6 biological replicates), we identified 519 and 750 circRNAs from excitatory and inhibitory cortical neuron populations, respectively (**Supplementary File S6**). In agreement with our CIRI2 analysis (**Figure 4A, B**), in the absence of NOVA2, we found a significant reduction of circRNA expression when normalized to the linear reads arising from the same host-gene ($P<2.2x10^{-16}$, Wilcoxon-rank sum test with continuity correction; **Figure 4C**). Density plots showed a pronounced reduction in circRNA expression in both *Nova2*-KO neuron populations (vertical axis, **Figure 4D, E**). In contrast, linear RNAs from the same host gene showed only a minor shift to the right along the x-axis. Overall, we observed a weak correlation (Emx1+; R=0.36 and Gad2+; R=0.23) between circular and linear expression changes. We found that 456/519 Emx1+ expressed circRNAs (87%) and 495/750 of Gad2+ circRNAs (66%) passed CircTest significance testing for independence of circRNA and linear RNA expression (**Supplementary File S6**). Taken together, these results demonstrate that NOVA2-regulation of backsplicing is independent of linear host gene expression.

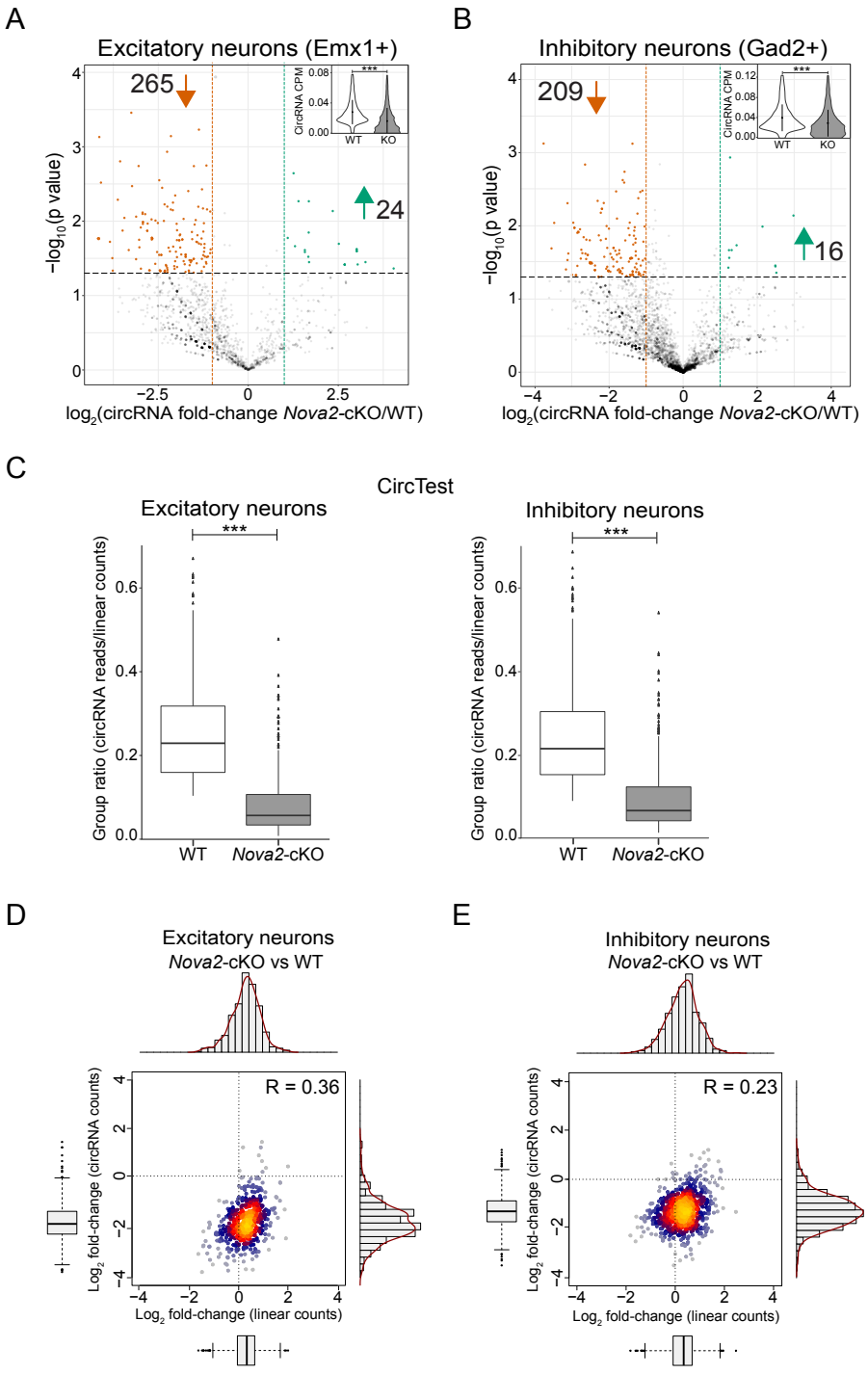

Figure 4. NOVA2 regulation of circRNA biogenesis in cortical excitatory and inhibitory neurons.

(**A**) Volcano plot of circRNAs detected using CIRI2 in excitatory cortical neurons (Emx1) and (**B**) inhibitory cortical neurons (Gad2) deficient in NOVA2. In both datasets, more circRNAs were significantly downregulated compared to upregulated in *Nova2*-cKO cells relative to WT ($log_2FC>1$, $P<0.05$). Inset violin plots show significant reduction in total circRNA CPM. Statistical analyses were carried out as in **Figure 3B**. (**C**) CircTest group ratio is significantly reduced in *Nova2-c*KO condition. Significance reflects non-parametrical Wilcoxon rank-sum test with continuity correction. n = 3 biological replicates for each condition. Group ratio is defined as the number of BSJ reads divided by the number linear-spliced reads (y-axis). (**D**) High density scatterplot of 456 DCC/CircTest identified high confidence circRNAs (minimum 3 BSJ read counts in 4 out of 6 biological replicates) from excitatory neurons deficient in NOVA2. Y-axis reflects log_2 fold-change of circRNA counts. X-axis reflects log_2 fold-change of linear counts from host genes. Pearson correlation coefficient is shown in the upper right corner, indicating weak correlation between circRNA and linear RNA counts in *Nova2*-null excitatory neurons. (**E**) Same analysis repeated for *Nova2*-cKO inhibitory neurons with 495 high confidence circRNAs represented. ***$P<0.001$. CPM,

NOVA2-regulated circRNAs and exon skipping events show little overlap

There are some reported instances of circRNA loci overlapping with exon skipping events (reviewed in (Ebbesen et al., 2017)). We thus determined to what degree NOVA2 regulated exon skipping events (SE) overlapped with NOVA2 regulated circRNAs. We applied replicate Multivariate Analysis of Transcript Splicing (rMATS) (Shen et al., 2014) to probe for statistically significant SE events in the excitatory and inhibitory neuron datasets (**Supplementary File S7**). Returning to our CIRI2 generated list of differentially expressed circRNAs, we found that in excitatory neurons, only 3/24 upregulated circRNAs and 10/265 downregulated circRNAs overlapped with at least one significant SE event. Likewise, in inhibitory neurons only 1/16 upregulated circRNAs and 7/209 downregulated circRNAs overlapped with at least one significant SE event. Of note, all the circRNAs that overlapped with at least one SE event were multi-exonic, and in all instances only some of the exons within the circRNA loci were skipped. i.e., none of the regulated skipping events skipped an entire NOVA2-regulated circRNA. Given these results, we conclude that NOVA2-regulation of circRNAs is unrelated to NOVA2-mediated exon skipping.

NOVA2-regulated circRNAs display cell-type specific regulation

We examined the overlap of NOVA2-regulated circRNAs between excitatory and inhibitory cell populations. We found that 247/293 and 120/225 of the NOVA2-regulated circRNAs in excitatory and inhibitory neurons, respectively, were expressed in both neuronal subtypes. Despite this broad overlap, we found that the identity of NOVA2-regulated circRNAs were largely distinct between the two cell-types (**Figure S4A**). Only 18 circRNAs were found to be NOVA2-regulated in both excitatory and inhibitory neurons. This is in line with what was previously found with the same datasets for linear alternative splicing (Saito et al., 2019). Thus, it appears that NOVA2 circRNA regulation exhibits neuronal sub-type specificity.

Circ*Efnb2* is an abundant, conserved circRNA regulated by NOVA2

Having uncovered a genome-wide role for NOVA2 in circRNA regulation, we next turned to a single circRNAs locus for investigation into the mechanism. To choose a candidate for further study, we identified the circRNAs found to be differentially expressed in both pipelines (CIRI2 or CircTest) and found 74 in the Emx1 dataset and 36 in the Gad2 dataset (**Supplementary File S8**). Of these, only 7 circRNAs (all reduced in the *Nova2*-KO condition) were common to both Emx1 and Gad2 datasets (**Supplementary File S8**). This included circ*0015034* (referred to from here on as circ*Efnb2*). Circ*Efnb2* is a 284 nt long circRNA

generated from the 2nd exon of the *Efnb2* gene. *Efnb2* encodes ephrin-B2, a transmembrane ligand which mediates cell-to-cell communication via contact with adjacent Eph receptor (Niethamer and Bush, 2019). The same locus also produces a circRNA in humans (circBaseID; hsa_circ_0029247) with identical primary sequence. Finally, circ*Efnb2* is abundant, ranking in the top 15% of high confidence circRNAs with respect to circRNA to mRNA ratio (**Figure 5B**).

To confirm the circularity of circ*Efnb2*, we performed Northern analysis of mouse cortex samples. We observed clear bands of the expected sizes for both the linear and circular products. Treatment with RNase R enriched circ*Efnb2* and depleted the linear transcript, confirming the circular and linear nature of the two major bands (**Figure 5C**). In addition, we captured polyA+ RNA from mouse cortex samples using oligo(dT) beads, as well as unbound RNAs (polyA- fraction) for Northern blot analysis. As expected, the polyA+ fraction enriched for polyadenylated, linear *Efnb2* mRNA and depleted the polyA tail-lacking circRNA (**Figure 5D**).

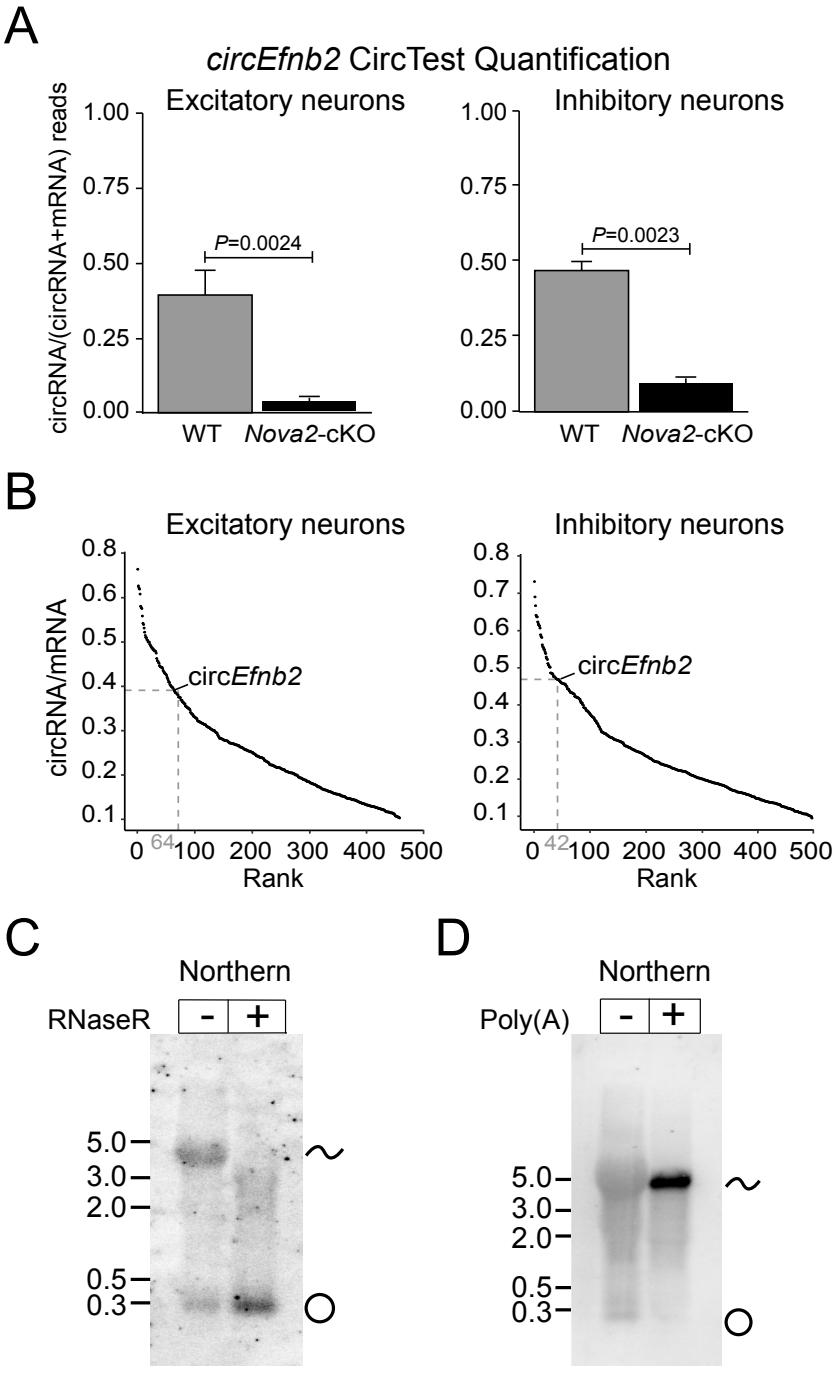

Figure 5. Circ*Efnb2* is an abundant, highly-conserved circRNA regulated by NOVA2.

(**A**) CircRNA to mRNA ratio plot generated by CircTest. Ratio of circular junction read counts from circ*Efnb2* to average total counts at exon borders are shown.

P-values were generated from CircTest module. (**B**) CircRNA/mRNA expression rank of *circEfnb2* in embryonic excitatory (64th) or inhibitory (42nd) neuron datasets (top 15%; both datasets). (**C**) Northern blot using probe overlapping circularized exon of *Efnb2* detects bands corresponding to the circRNA and mRNA from embryonic whole cortex RNA with or without RNase R treatment. (**D**) Northern blot performed for poly(A)- and poly(A)+ samples. RNA samples for Northern were obtained from E18 whole cortex.

Generation of a circEfnb2 backsplicing reporter

NOVA2 has a well-characterized YCAY binding motif (Zhang and Darnell, 2011). In order to determine which binding sites help facilitate NOVA2 regulation of *circEfnb2* we constructed a backsplicing reporter. To guide the design of the backsplicing reporter, we analyzed CLIP tags identified in NOVA2 cTag-CLIP Emx1 and Gad2 neuron datasets (Saito et al., 2019) (**Figure 6A**). Due to the extended lengths of the 5′ and 3′ flanking introns (20.9kb and 15.5kb, respectively), the circularizing exon combined with its full-length flanking introns is not amenable to plasmid subcloning and transfection. We thus opted to subclone truncated upstream and downstream flanking intronic regions that included major NOVA2-CLIP peaks (**Figure 6A**; “fragment 2”). In addition, we included partial sequences from exons 1 and 3 and ~150 bp of intron sequence to retain linear splicing from the reporter (**Figure 6A**; “fragment 1 and 3”). Fragment 3 also included prominent NOVA2-CLIP peaks. In the intronic sequences, we noted the presence of multiple YCAY motifs that were not associated with CLIP tags.

Consistent with previous NOVA2 splicing reporter studies, we examined regulation of circ*Efnb2* in HEK293 cells which express very low levels of *Nova2* (**Figure S5A**) (Dredge and Darnell, 2003; Dredge et al., 2005; Heinzen et al., 2007; Leggere et al., 2016; Saito et al., 2016). Initial analysis of the RNAs generated from the reporter revealed the spurious usage of cryptic splice acceptor and donor sites in the plasmid backbone, which were subsequently mutated (see Materials and Methods). With the corrected plasmid we performed

transient transfections and confirmed the expression and circularity of the reporter generated circRNA by RT-PCR (**Figure S5B**). In addition, we validated the expression and circularity of the reporter circRNA by RNase R treatment followed by Northern blot (**Figure S5C**), and quantified RNase R resistance by RT-qPCR (**Figure S5D**).

We examined the response of our *Efnb2* backsplicing reporter (pWT, **Figure 6B**) to NOVA2 overexpression. Co-transfection of the reporter with NOVA2 led to a ~3.5-fold increase in backsplicing, whereas expression of the linear reporter RNA was unchanged (**Figure 6C**). Co-transfection of another neural-enriched splicing factor, HuD, did not alter backsplicing of circ*Efnb2* (**Figure S5E**), providing evidence of NOVA2 regulatory specificity. Together, these data demonstrate that the *Efnb2* backsplicing reporter recapitulates NOVA2 regulation of *Efnb2* circRNA biogenesis.

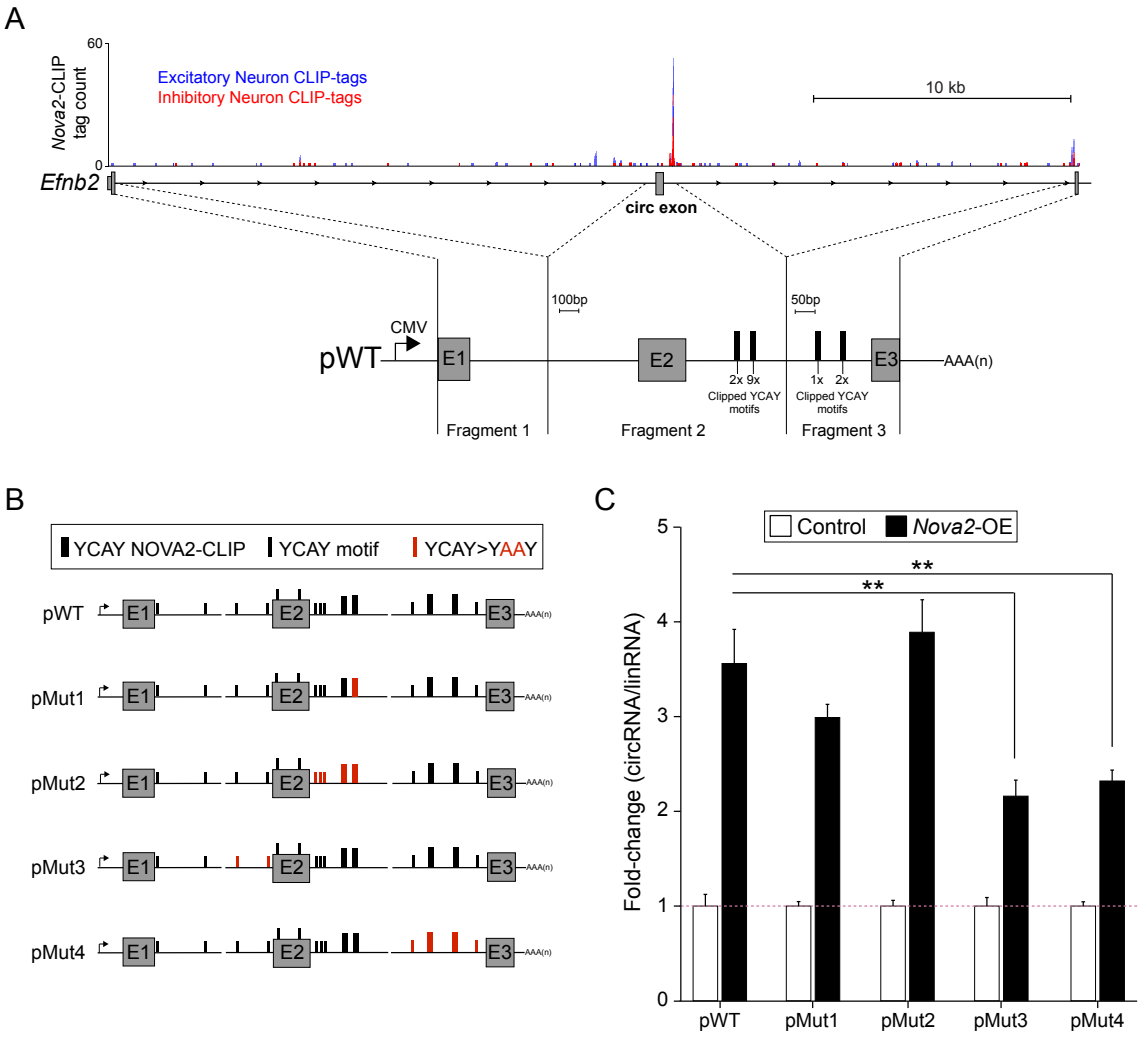

Figure 6. Role of intronic NOVA2 binding sites in Circ-*Efnb2* backsplicing. (**A**) Schematic of *Efnb2* locus shown in antisense (mm10, chr8:8623077-8660773). NOVA2 cTag-CLIP tags from excitatory cortical neurons (blue) or inhibitory neurons (red) visualized using UCSC genome browser. Three genomic fragments used to construct the backsplicing reporter (pWT) are shown below, and the number of individual YCAY motifs present within each NOVA2-CLIP peak (thick black bar) are reported. Note, *Efnb2* Exon 1 (E1) and Exon 3 (E3) in the pWT backsplicing reporter are truncated, whereas circularizing Exon 2 (E2) is

full length. (**B**) Reporter schematics for circEfnb2. NOVA2-CLIP peaks are represented by thick black bars as in panel A. YCAY motifs not associated with NOVA2-CLIP peaks are represented as thin black bars. Mutated YCAY motifs or peaks are shown in red. (**C**) RT-qPCR of circ*Efnb2* expression from reporters co-transfected with NOVA2 expression plasmid (*Nova2*-OE) or empty expression vector in HEK293 cells. For expression data, target genes were normalized to linear-spliced transcript (lin*Efnb2)* generated by the reporter. n=3 biological replicates. Error bars are represented as mean ± SEM. ***P*<0.01, compared to pWT circ*Efnb2* expression. (Students t-test, two-tailed and unpaired). See also **Figure S5**.

NOVA2 regulates backsplicing of circEfnb2 via intronic YCAY motifs

To understand how NOVA2 might regulate circ*Efnb2* backsplicing, we introduced point mutations at putative NOVA2 binding sites (**Figure 6B**). Within our reporter, there were four NOVA2 CLIP peaks, all found within intronic regions. Two peaks were located just downstream of exon 2 (E2), and the other two were located just upstream of exon 3 (E3) (**Figure 6A**). To assess the relevance of YCAY motifs, we mutated them to YAAY, since the CA dinucleotide is essential for NOVA2 recognition (Jensen et al., 2000b). For RT-qPCR quantification, we normalized circRNA expression to linear-spliced transcript expression in order to observe any relative changes in backsplicing. Circular and linear products normalized to *Gapdh* are shown in **Figure S5F**. First, we targeted the CLIP peak consisting of 9 YCAY motifs (**Figure 6A,B**). Surprisingly, we did not observe a significant difference from pWT (**Figure 6C,** pMut1). Next, we mutated the adjacent CLIP peak (2x YCAY), along with three additional YCAY motifs not identified by CLIP (pMut2). However, we still did not observe a reduction in NOVA2-mediated backsplicing of circ*Efnb2* (**Figure 6C**).

We proceeded to mutate two non-clipped YCAY motifs immediately upstream of exon 2 (pMut3). Even though these motifs lacked NOVA2-CLIP support, mutating them caused a significant reduction in NOVA2-regulated backsplicing (**Figure 6C**). Finally, we turned our attention to the intronic region just upstream of exon 3 and mutated both remaining CLIP peaks as well as two

adjacent YCAY motifs not identified by CLIP (pMut4). In this case, we also found significant reduction in NOVA2-mediated backsplicing compared to the WT reporter (**Figure 6C**). Together these data suggest that NOVA2 intronic binding on either side of the *Efnb2* circRNA locus impacts its regulation.

NOVA2 binding sites in circRNA flanking introns promote backsplicing

Given these reporter analysis results, we next turned to genome-wide cTag-CLIP data to investigate whether NOVA2 binding to both flanking introns is a general feature of NOVA2-regulated circRNA loci. For this analysis, we used the subset of high confidence, NOVA2-regulated circRNAs from the excitatory and inhibitory datasets (36 circRNAs for inhibitory neurons and 74 for excitatory neurons). For a non-regulated control comparison group, we used circRNAs unchanged by NOVA2 loss (P>0.50, FC<1) (**Supplementary File S8**). We hypothesized that this robust subset would provide the best chance to identify relevant NOVA2 positional binding information. Using NOVA2-CLIP data obtained from each sorted neuron dataset we checked for the presence of CLIP peaks in the upstream and downstream introns flanking each circRNA. We discovered that in excitatory neurons, NOVA2 bound both flanking introns of a regulated circRNA at a significantly higher frequency than non-differentially expressed controls (P=0.02, Pearson's Chi-squared test with Yates' continuity correction) (**Figure S6A**). In contrast, the presence of CLIP sites in just one

intron (either upstream or downstream) was not significantly different between regulated circRNAs and controls. This suggests that NOVA2 intronic binding on both sides of a circRNA locus plays a role in backsplicing regulation. However, when we investigated inhibitory neurons, which had a lower sample size of regulated circRNAs, statistical significance for the same trend was not observed (**Figure S6B**).

The *Efnb2* backsplicing reporter analysis and CLIP analysis suggested that NOVA2 binding in the introns upstream and downstream of a circularizing locus promote NOVA2 regulated circRNA biogenesis. To further investigate the generality of this observation, we generated an artificial backsplicing minigene reporter, pMini, which was devoid of *Efnb2* sequences. This plasmid contains full length GFP coding sequence in the same vector backbone as our circ*Efnb2* reporter. GFP was fragmented into three artificial exons flanked by intronic sequences consisting of human *ZKscan1* reverse complementary matches (RCMs) to facilitate enhanced circRNA expression (**Figure 7A**). Existing YCAY motifs that might impact circRNA regulation were mutagenized. We confirmed that all of our pMini variants produced a single circRNA products by RT-PCR in control or NOVA2 overexpression conditions using outward facing primers (**Figure S7A**). We also confirmed the expression of the 497 nt circRNA product by Northern blot and RT-qPCR (**Figure 7B,C**), under RNase R or mock treatment conditions. As expected, RNaseR degraded the plasmid generated linear transcript (**Figure 7B,C**).

In the WT pMini reporter, lacking any YCAY motifs (pMini-WT) we did not observe a significant increase in backsplicing in response to NOVA2 overexpression (**Figure 7D**). We next introduced YCAY repeats into various intronic locations on the reporter. We introduced a 10x YCAY repeat into the WT vector (pMini-WT) ~50 bp upstream of the circRNA exon (pMini-Up) or ~50 bp downstream of the circRNA exon (pMini-Down), and in both locations (pMini-Both). For RT-qPCR quantification, we normalized circRNA expression to linear-spliced transcript expression. Circular and linear products normalized to *Gapdh* are shown in **Figure S7B**. Similar to pWT, introduction of YCAY repeats into the upstream intron only did not increase the circular/linear RNA ratio (pMini-Up, **Figure 7D**). A similar result was observed when YCAY repeats were inserted into the downstream intron only (pMini-Down, **Figure 7D**). Finally, we tested the impact of placing NOVA2 binding sites both upstream and downstream of the circularizing exon (pMini-Both). Remarkably, we found that for this reporter, NOVA2 co-transfection led to a nearly 3-fold increase in circular/linear RNA ratio (**Figure 7D**). Thus, similar to our circ*Efnb2* reporter, and in accordance with CLIP data from excitatory neurons, our results show that the presence of NOVA2 binding sites in both introns impacts backsplicing.

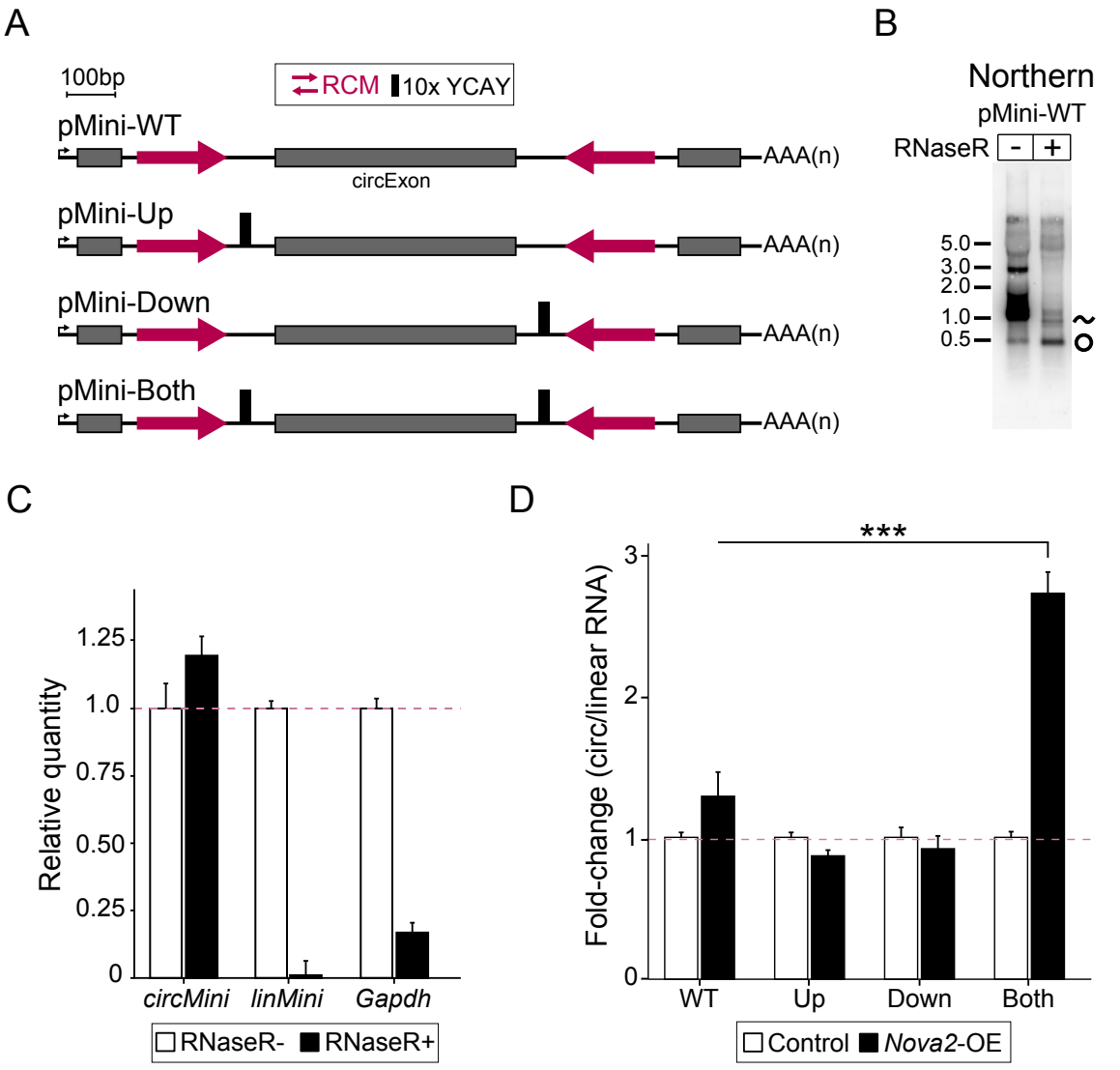

Figure 7. NOVA2 binding sites in both flanking introns mediate NOVA2 backsplicing.

(**A**) Schematics of artificial backsplicing reporters. Exonic sequences (gray) were derived from GFP open reading frame. Reverse complementary matches (RCMs) are shown as red opposing arrows. A repeat region of 10 tandem YCAY motifs (thick black bar) was inserted into the intronic locations shown. (**B**) Northern blot using probe overlapping circularized exon of pMini reporter to

detect circRNA and mRNA from transfected HEK293 cells. RNA was treated with RNase R to deplete linear transcript and enrich for circ*Mini*. (**C**) RT-qPCR expression analysis of Rnase R treated RNA shown in panel B. Expression is relative to the mock Rnase R condition. (**D**) RT-qPCR analysis of circ*Mini* transcript derived from pMini reporter constructs in HEK293 cells cotransfected with NOVA2 expressing plasmid (*Nova2*-OE) or empty vector control. For expression data, circ*Mini* is normalized to the linear-spliced transcript (lin*Mini*) generated by the reporter. N=3 biological replicates. Error bars are represented as mean ± SEM. ***$P<0.001$, compared to pMini-WT circ*Mini* expression. Students t-test, two-tailed and unpaired. See also **Figure S6** and **Figure S7**.

DISCUSSION

Here we identify NOVA2 as a regulator of circRNA biogenesis in neurons. We found that within the mouse embryonic cortex, loss of NOVA2 globally reduced circRNA expression, and that this reduction was largely independent from mRNA expression changes of the host gene. This effect of global circRNA reduction upon NOVA2 loss was even more pronounced when a sorted neuron population was analyzed. We found that NOVA2-regulated circRNAs within each cell-type were largely distinct, despite overlapping expression patterns. To investigate the *cis*-elements involved in circRNA regulation by NOVA2, we focused on a conserved and abundant circRNA from the *Efnb2* gene. Using backsplicing reporter analysis we demonstrated that intronic YCAY sequences both upstream and downstream of the circRNA locus was important for NOVA2-regulation. CLIP analysis in excitatory neurons provided support for this finding.

CircRNAs are typically expressed at a low level compared to their linear counterparts. For most accepted analysis pipelines, only BSJ reads are used for quantification, making differential expression analysis problematic. Thus, we applied multiple validated pipelines to quantify circRNA expression genome-wide (Cheng et al., 2016; Gao et al., 2018), and performed extensive validation of differential expression trends using RT-qPCR (**Figure 3E,F**). Investigating the sorted neuron datasets more closely, we found that NOVA2 appeared to regulate circRNAs in a cell-type specific manner (**Figure S4A**), similar to what has been previously shown for linear alternative splicing (Saito et al., 2019). Additional

genome-wide analyses using library preparation methods that enhance read depth specifically for circRNAs are warranted to provide more conclusive support for this finding. On a similar front, our global analysis of how NOVA2 CLIP peaks correlated with NOVA2 regulated circRNAs could be improved by having more accurate circRNA expression quantification. There was a very low number of high-confidence NOVA2-regulated circRNAs in the Gad2 dataset (only 36)– it is possible that with greater read depth we would identify more regulated circRNAs and obtain better insight into the genome-wide features of circRNA regulation by NOVA2.

We chose circ*Efnb2*, a single-exon circRNA conserved from mouse to human, to investigate what *cis*-elements control NOVA2-regulation of circRNAs biogenesis. Using backsplicing reporter analysis we found that YCAY motifs on either side of the circularizing locus were important for regulating circ*Efnb2* (**Figure 6C**). One of the important motifs identified was located in the intronic region preceding the 3' splice-acceptor of the exon downstream of the circRNAs locus. This suggests that NOVA2 binding in this region far downstream from the circRNA promotes backsplicing. A caveat of this interpretation is that several kb of the intron could not be included in our backsplicing reporter (**Figure 6A**). We discovered that two YCAY motifs upstream of circ*Efnb2* were important for regulation of backsplicing, even though they lacked NOVA2-CLIP support (**Figure 6C**). This was somewhat surprising and suggests that the CLIP datasets might have limited utility in predicting binding sites important for backsplicing. On the other hand, this result could reflect an inherent limitation of cell culture

systems for recapitulating neuronal circRNA regulation patterns. Performing mutagenesis of the intronic YCAY motifs at the endogenous *Efnb2* locus in ES-derived neurons or in mice with CRISPR genome-editing could provide more conclusive support.

To investigate NOVA2 regulation more generally, we constructed an artificial backsplicing vector, pMini, which was devoid of NOVA2 binding sites (**Figure 7A**). We introduced YCAY clusters into intronic regions upstream and downstream of the circularizing exon based on findings from the circ*Efnb2* reporter. We found that NOVA2-induced backsplicing in the pMini reporter required the presence of YCAY clusters in both flanking introns. This result is analogous to what was previously observed for the RBP *quaking* (QKI) (Ashwal-Fluss et al., 2014; Conn et al., 2015). In that study, QKI-regulated backsplicing from a reporter was found to be dependent on QKI binding sites in both upstream and downstream introns (Conn et al., 2015). QKI has been shown to self-dimerize (Teplova et al., 2013), thus it was hypothesized that QKI dimerization could be involved in the backsplicing mechanism. Interestingly, NOVA proteins can also self-dimerize (Teplova et al., 2011), thus similar backsplicing regulatory mechanisms might be at play for both QKI and NOVA2.

Nova2-KO mice display a host of degenerative brain phenotypes which have been attributed to deregulation of linear alternative splicing (Saito et al., 2016; Saito et al., 2019; Yano et al., 2010). Hundreds of circRNAs were found here to be differentially regulated by *Nova2*. Could reduced levels of circRNAs such as circ*Efnb2* contribute to the neurodevelopmental defects of *Nova2*-KO

mice? There are many possible ways NOVA2-regulated circRNAs could impact neural development, given the different ways circRNAs impact gene regulation. For example, some circRNAs travel to synapses and act as scaffolds for various RBPs, whereas others regulate the transcriptional activity of genes in the nucleus (Li et al., 2015; Xia et al., 2018; You et al., 2015). Some circRNAs have been recently associated with neurological defects in mice and humans (Dube et al., 2019; Zimmerman et al., 2020). Despite technical challenges, several recent studies have demonstrated the feasibility of both targeting circRNAs using RNAi (Pamudurti et al., 2020; Suenkel et al., 2020; Zimmerman et al., 2020) and deleting intronic RCMs using CRISPR to reduce or eliminate circRNA expression (Xia et al., 2018). Moving forward, it will be interesting to assess the role of NOVA2-regulated circRNAs such as circ*Efnb2* in neural development using such approaches.

SOFTWARE AVAILABILITY

CIRI2 is an open source, freely available tool for access at Source Forge (https://sourceforge.net/projects/ciri/files/CIRI2/)

HISAT2 is an open source, freely available tool for access at Johns Hopkins University (https://ccb.jhu.edu/software/hisat2/manual.shtml)

STAR is an open source, freely available tool in the GitHub repository (https://github.com/alexdobin/STAR)

DCC/CircTest is an open source, freely available tool in the GitHub repository (https://github.com/dieterich-lab/DCC) and (https://github.com/dieterich-lab/CircTest)

rMATS is an open source, freely available tool at Source Forge (http://rnaseq-mats.sourceforge.net)

SUPPLEMENTARY DATA

Supplementary File S1: RNA-seq datasets used in this study

Supplementary File S2: CIRI2 circRNA expression *Nova1*-KO vs WT E18.5 cortex

Supplementary File S3: CIRI2 circRNA expression *Nova2*-KO vs WT E18.5 cortex

Supplementary File S4: CIRI2 circRNA expression *Nova2*-KO vs WT E18.5 Emx1+ neurons

Supplementary File S5: CIRI2 circRNA expression *Nova2*-KO vs WT E18.5 Gad2+ neurons

Supplementary File S6: DCC/CircTest host-mRNA and circRNA expression *Nova2*-KO vs WT E18.5 Emx1/Gad2 neurons

Supplementary File S7: rMATS AS events and DE-circRNA overlap *Nova2*-KO vs WT E18.5 Emx1+/Gad2+ neurons

Supplementary File S8: Overlap between CIRI2/CircTest results *Nova2*-KO vs WT E18.5 Emx1/Gad2 neurons

Supplementary File S9: Oligonucleotides primers/probes used for RT-qPCR, RT-PCR, and Northern blot

ACKNOWLEDGEMENT

We thank Dr. Zhe Chen (University of Minnesota) for sharing plasmids. We thank Nora Perrone-Bizzozero (University of New Mexico) for sharing the HuD plasmid. We thank A. van der Linden, Z. Chen, Z. Zhang, and B. Bae for helpful feedback and discussion on the manuscript.

FUNDING

This work was supported by National Institute on Aging grant R15 AG052931 and National Institute of General Medical Sciences grant R35 GM138319. D.K. is supported by the National Science Foundation Graduate Research Fellowship Program. Core facilities at the University of Nevada, Reno campus were supported by NIGMS COBRE P30 GM103650.

CONFLICT OF INTEREST

The authors report no conflict of interest.

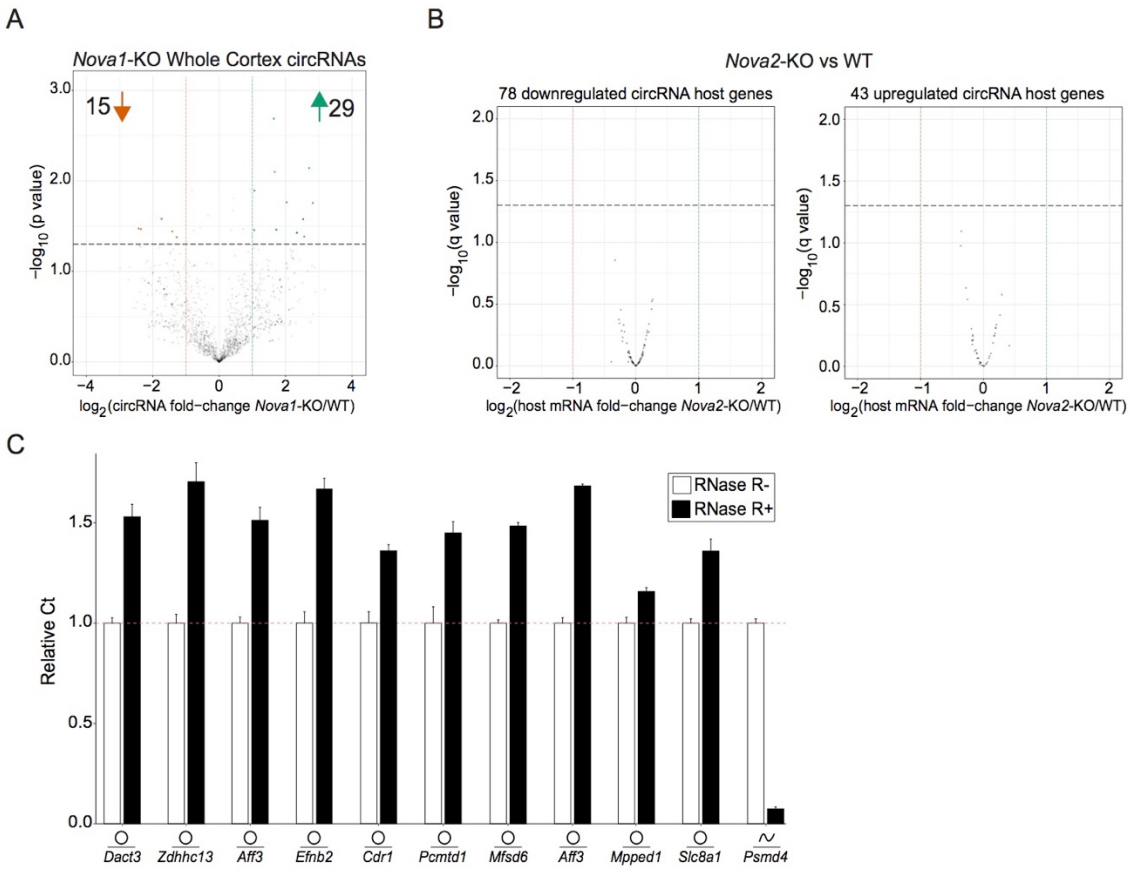

Supplementary Figure 1. NOVA1 circRNA regulation, NOVA2-regulated circRNA host gene mRNA expression, and RNase R resistance of circRNAs.

(**A**) Volcano plot of circRNA expression in *Nova1*-KO vs. WT mouse cortex ($log_2FC>1$, $P<0.05$). (**B**) Host-gene linear RNA expression of downregulated circRNAs (*left panel*) and upregulated circRNAs (*right panel*) identified by CIRI2 are not differentially expressed in *Nova2*-KO cortex. *P* values were obtained by the Wald test and corrected for multiple hypothesis testing using the Benjamini and Hochberg method (DESeq2 default settings). (**C**) RT-qPCR relative expression analysis of 10 circRNAs (shown in **Figure 3E-F**) and one linear RNA

control (*Psmd4*). Total RNA was treated with RNase R or mock control prior to cDNA synthesis. Expression is relative to the mock RNase R condition (RNase R-). Error bars are represented as the mean ± SEM.

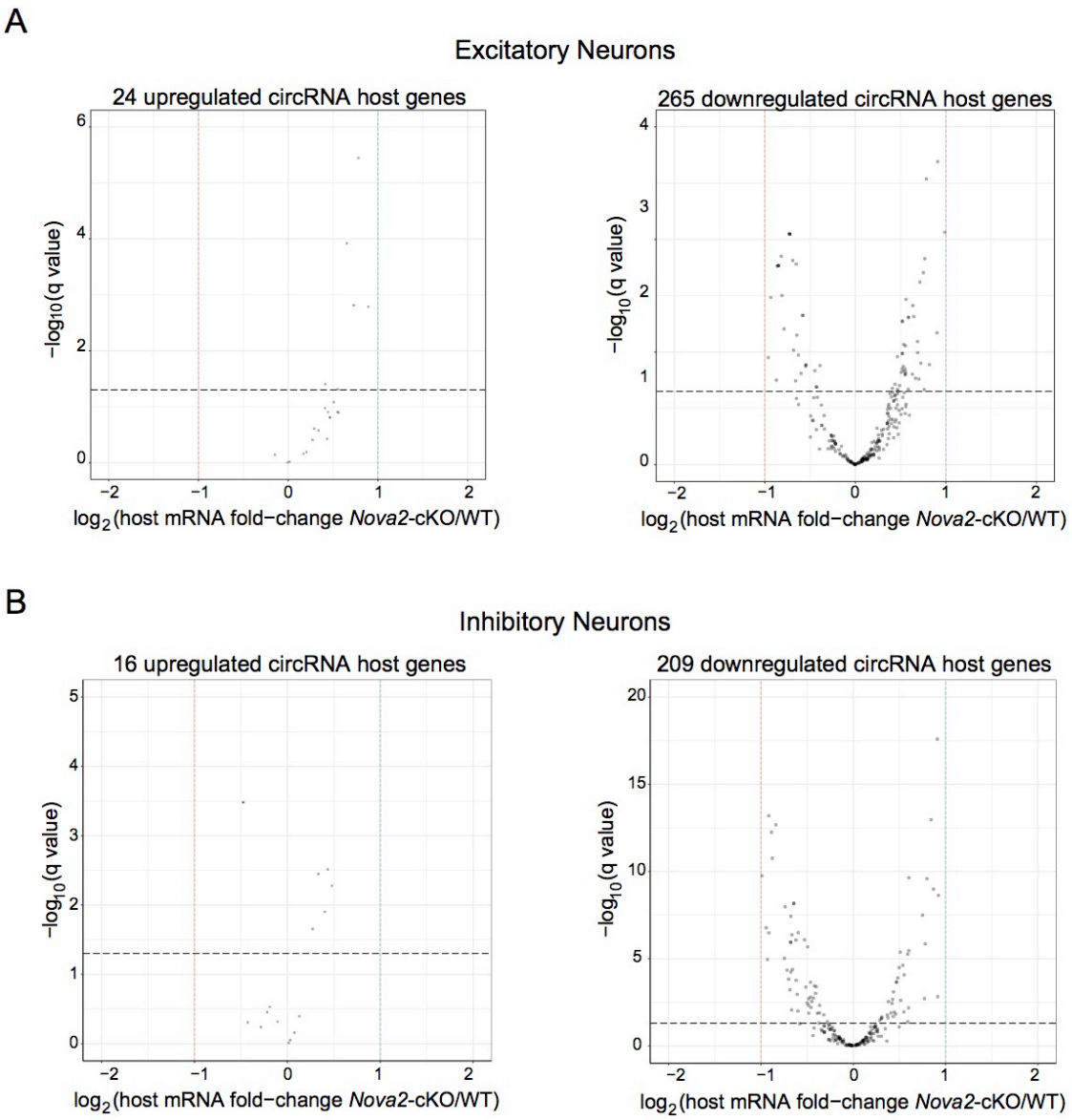

Supplementary Figure 2. NOVA2-regulated circRNA host gene mRNAs are not differentially expressed in excitatory or inhibitory neuron datasets.

(**A**) Host gene mRNA expression of upregulated circRNAs (*left panel*) and downregulated circRNAs (*right panel)* from *Nova2*-KO excitatory neurons are not significantly differentially expressed compared to WT samples ($Log_2FC>1$,

q<0.05). (**B**) The same analysis performed for inhibitory neurons. *P* values for each dataset were obtained using the same approach as in **Figure S1B**.

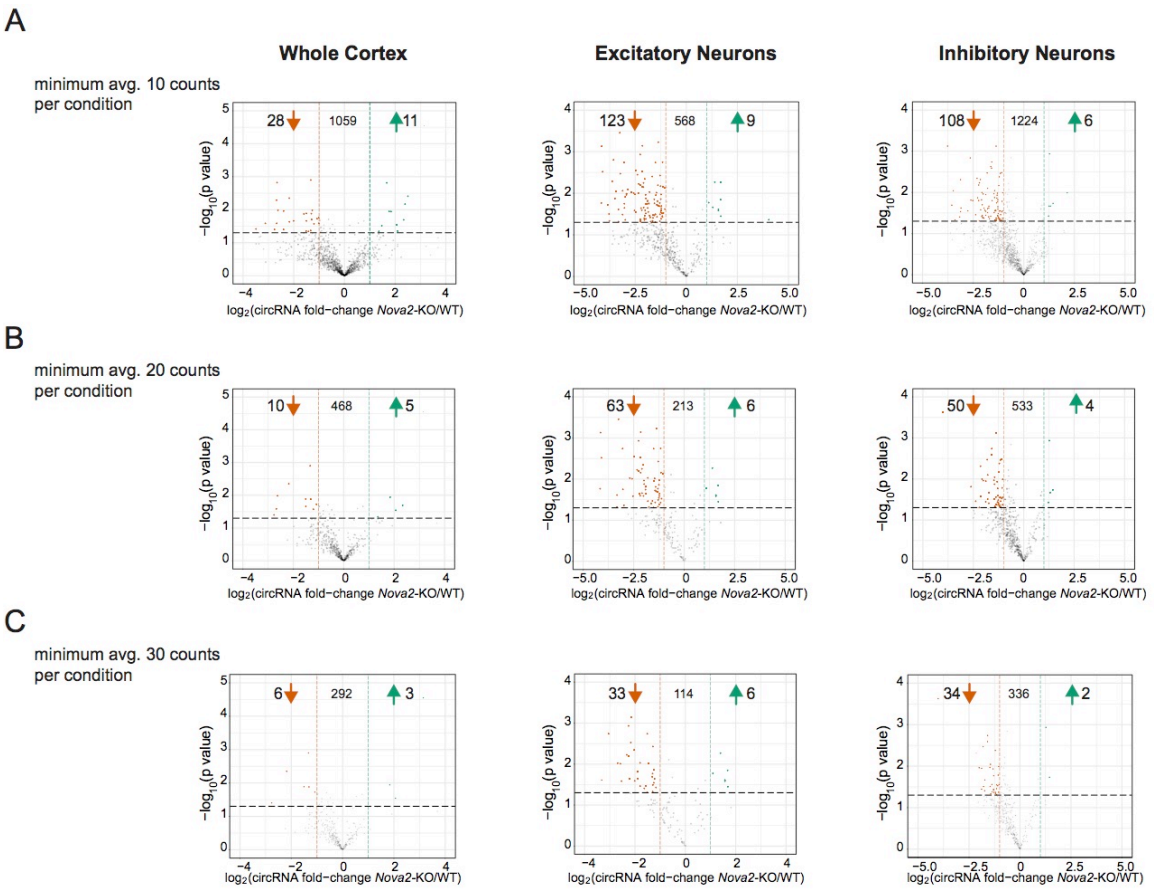

Supplementary Figure 3. Reduced circRNA expression by NOVA2 is consistent among increasing minimum BSJ count thresholds.

Volcano plots of circRNAs identified by CIRI2 are regulated among WT vs *Nova2*-KO whole cortex, excitatory neuron, and inhibitory neuron RNA-seq datasets with minimum averages of (**A**) 10, (**B**) 20, and (**C**) 30 BSJ read count thresholds applied. The number of circRNAs passing each read count threshold are shown in the center of each plot. Significance reflects a $\log_2$FC>1 and *P*<0.05.

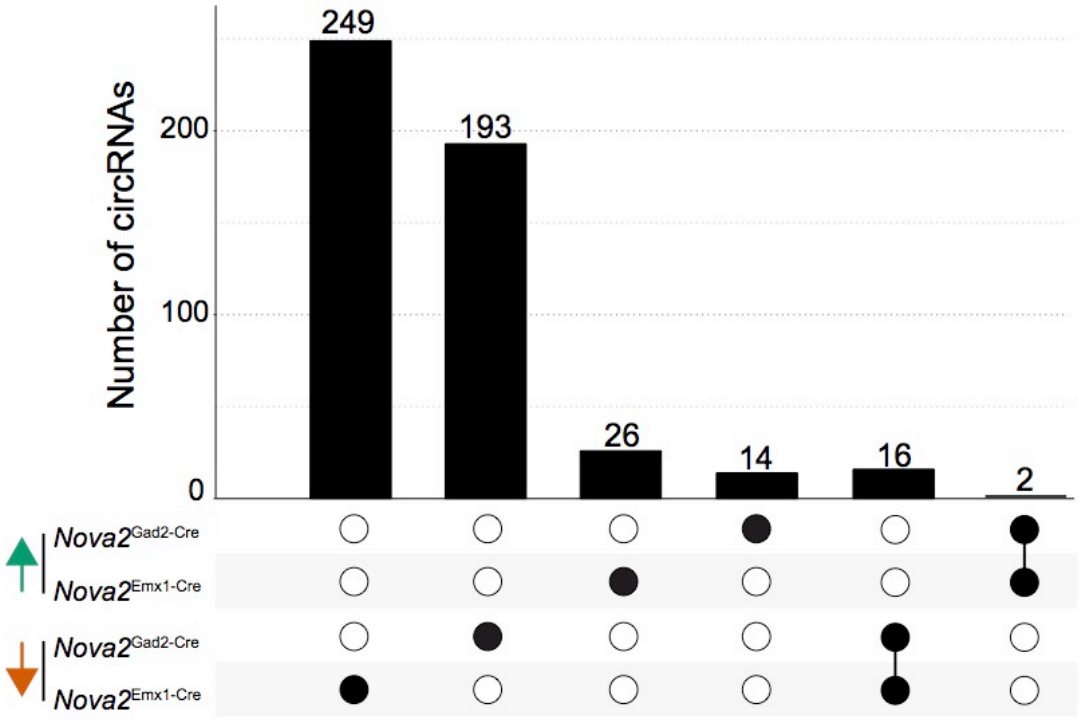

Supplementary Figure 4. NOVA2-regulated circRNAs in neurons exhibit cell-type specificity.

(**A**) Number of differentially expressed circRNAs unique or overlapping in excitatory and inhibitory neuron datasets. Green up arrow represents *Nova2*-cKO upregulated circRNAs. Orange down arrow represents *Nova2*-cKO downregulated circRNAs. CircRNAs were identified using CIRI2.

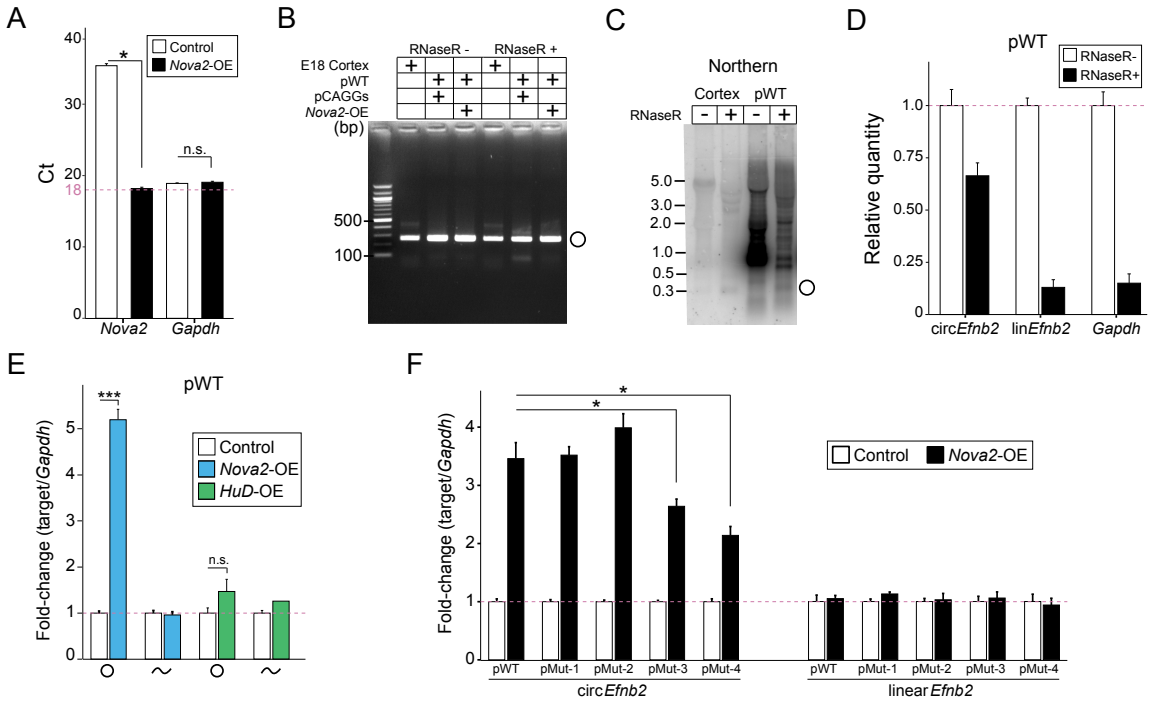

Supplementary Figure 5. Circ*Efnb2* backsplicing reporter generates a single, RNase R resistant, circ*Efnb2* transcript responsive to NOVA2.

(**A**) RT-qPCR relative expression of *Nova2* and *Gapdh* transcripts in HEK293 cells pre- and post-transfection with NOVA2 expression (*Nova2*-OE) plasmid (n=3). (**B**) RT-PCR analysis of circ*Efnb2* transcript from pWT backsplicing reporter with or without RNase R treatment and pre- and post-transfection with NOVA2 expression plasmid in HEK293 cells. Outward facing primers were used to capture a 267 bp product. (**C**) Northern blot analysis utilizing a dsDNA probe targeting the circular and linear transcripts of *Efnb2* gene extracted from mouse cortex or HEK293 cells transfected with the pWT reporter. Circ*Efnb2* signal was enriched post-RNase R treatment while linear transcripts were diminished. (**D**) RT-qPCR relative expression analysis of circ*Efnb2* and linear *Efnb2* transcripts

generated from pWT vector. RNA used to generate cDNA for plot is the same RNA used for Northern blot in panel B. The circ*Efnb2* transcript is more resistant to RNase R treatment relative to the linear *Efnb2* transcript and endogenous *Gapdh* control gene. (**E**) RT-qPCR expression analysis of circ*Efnb2* and lin*Efnb2* generated from pWT reporter pre- and post-transfection with either NOVA2 or HuD expression (*HuD*-OE) vectors. Expression is normalized to *Gapdh* (n=3). (**F**) RT-qPCR expression analysis for circ*Efnb2* (*left*) or linear *Efnb2* (*right*) transcripts generated from pWT and mutated reporter variants pre- and post-transfection with NOVA2 expression vector. Data is related to **Figure 6C**. Expression is normalized to *Gapdh* (n=3). For expression analyses in panel A, E, and F, Student's t-test was used for statistical significance (two-tailed, unpaired) **P*<0.05, ****P*<0.001, n.s., not significant.

A

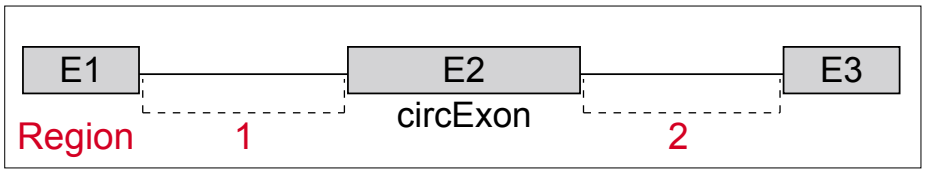

Excitatory neurons

Nova2-CLIP Region	1	2	1 or 2	1 and 2
# of Circs (Control*)	270	253	378	145
# of Circs (Regulated**)	42	43	55	30
Percent (Control)	50%	47%	70%	26%
Percent (Regulated)	57%	58%	74%	41%
P value	0.33	0.09	0.53	0.02

*540 circRNAs **74 circRNAs

B

Inhibitory neurons

Nova2-CLIP Region	1	2	1 or 2	1 and 2
# of Circs (Control*)	640	591	881	350
# of Circs (Regulated**)	18	18	23	13
Percent (Control)	46%	42%	63%	25%
Percent (Regulated)	50%	50%	64%	36%
P value	0.75	0.46	1.00	0.19

*1393 circRNAs **36 circRNAs

Supplementary Figure 6. NOVA2-CLIP peak analysis of NOVA2-regulated circRNAs overlapping between CIRI2 and DCC/CircTest analyses.

(**A**) (*Top*) Schematic of two intronic regions flanking NOVA2-regulated circRNA loci examined for significant NOVA2-CLIP peak presence. The number of NOVA2-regulated (74) or control (540, FC<1, *P*>0.50) circRNAs overlapping an intronic NOVA2-CLIP peak within each defined region from the excitatory neuron

dataset is shown below. (**B**) The same analysis was performed for 36 NOVA2-regulated circRNAs and 1393 control circRNAs from the inhibitory neuron dataset. *P* values were generated by Pearson's Chi-squared test with Yates' continuity correction.

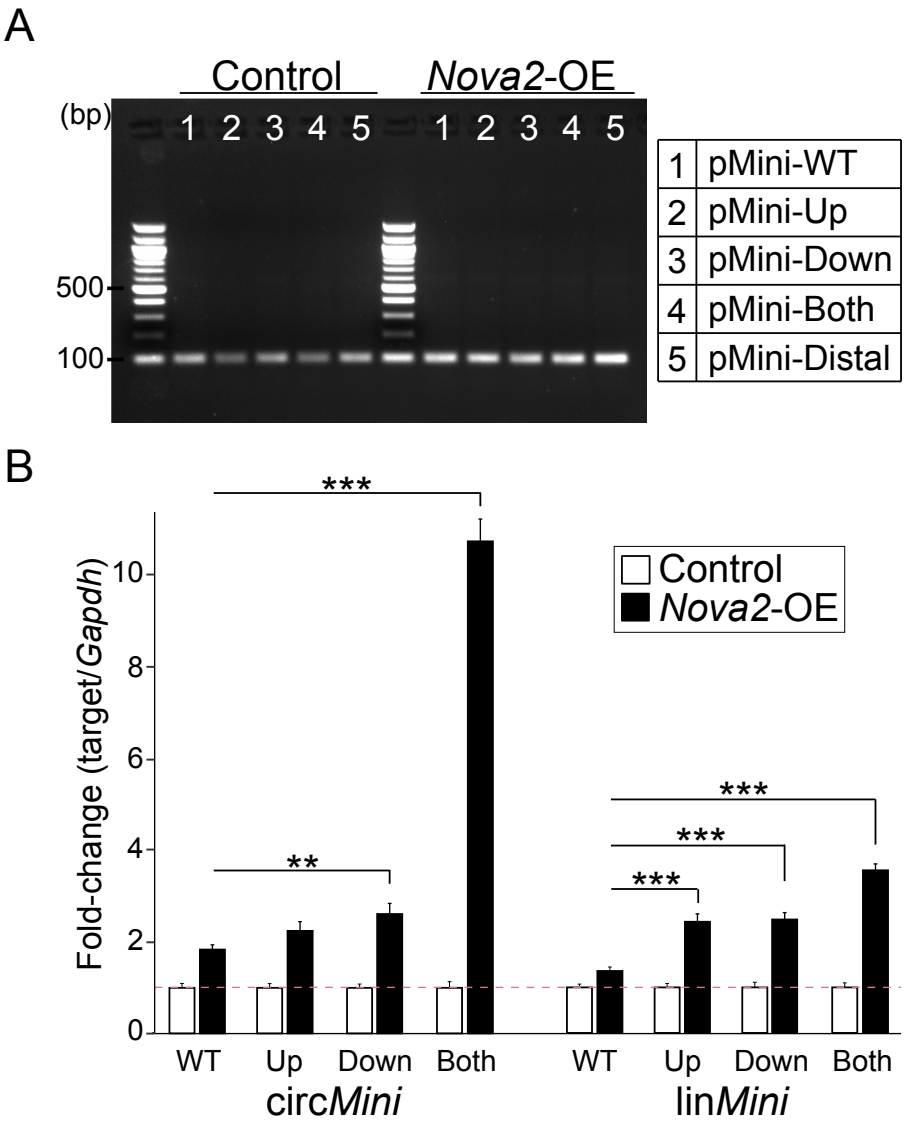

Supplementary Figure 7. pMini backsplicing reporter circular transcript validation and quantitative expression analysis.

(A) RT-PCR analysis of circ*Mini* transcript generated from the five pMini backsplicing reporters pre- and post-transfection with NOVA2 expression (*Nova2*-OE) plasmid in HEK293 cells. Outward facing primers were used to capture a 101 bp product. (**B**) RT-qPCR expression analysis of circular (circ*Mini*)

and linear (lin*Mini*) transcripts generated from the pMini backsplicing reporters in the presence or absence of NOVA2 related to **Figure 7D**. Expression is normalized to *Gapdh* (n=3). Student's t-test was used for statistical significance (two-tailed, unpaired) $^{**}P<0.01$, $^{***}P<0.001$.

Chapter 3: Loss of circRNAs from the *crh-1* gene extends mean lifespan in *C. elegans*

David Knupp*, Brian G. Jorgensen*, Jaffar M. Bhat, Hussam Alshareef, Jeremy J. Grubbs, Pedro Miura, and Alexander M. van der Linden

University of Nevada, Reno, Department of Biology, 1664 N. Virginia St, Reno, NV, 89557, USA

*, these authors should be considered co-first authors

AUTHOR CONTRIBUTIONS

Note: D. Knupp is a graduate student in P. Miura's lab. All other authors are graduate students or post-doctoral scholars in A. van der Linden's lab.

D. Knupp performed RT-qPCR and Northern blot experiments, generated the circ-*crh-1* overexpression backbone (related to **Figure 9B**), analyzed RNA-seq datasets from WT and *crh-1* mutant lines for changes in mRNA expression (related to **Figure 9C**), and helped write and generate figures used in the manuscript. RNA used for RT-qPCR, Northern blot and RNA-seq experiments performed by D. Knupp were extracted by members in A. van der Linden's lab.

B. Jorgensen performed RT-qPCR experiments, lifespan experiments contrasting WT and *circ-crh-1* mutant lines (related to **Figure 9A** and **Figure S8**), extracted

RNA for RNA-seq libraries (related to **Figure 9C**), and helped generate figures used in the manuscript.

J. Bhat performed lifespan experiments contrasting WT and *circ-crh-1* mutant lines (related to **Figure 9A**) and lifespan experiments contrasting WT, *crh-1*(*syb385*) and *circ-crh-1* rescue lines (related to **Figure 9B**).

J. Grubbs performed preliminary RT-qPCR and lifespan experiments contrasting WT and *circ-crh-1* mutant lines (data not shown), performed injections of *circ-crh-1* rescue constructs into WT or *crh-1*(*syb385*) backgrounds followed by selection of transgenic progeny (related to **Figure 9B**) and extracted RNA used in Northern blot (related to **Figure 8E**).

H. Alshareef extracted RNA for RT-qPCR validation of RNA-seq trends (related to **Figure 9D**).

Chapter 3 was performed under the guidance and supervision of Dr. Pedro Miura and Dr. Alexander van der Linden. P. Miura and A. van der Linden helped write the manuscript and generate figures.

Abstract

Accumulation of Circular RNAs (circRNAs) during aging occurs has been shown to occur on a genome-wide level across multiple animals but its significance is unknown. Generating circRNA loss of function mutants is difficult because the vast majority of these RNAs are comprised of exons shared with protein-coding mRNAs. In *C. elegans*, most expressed circRNAs were previously found to accumulate during aging. These included two circRNAs generated from exon 4 of the *crh-1* gene (circ-*crh-1*). Here, we found that biogenesis of circ-*crh-1* was regulated by the double stranded RNA binding protein ADR-1. We identified the presence Reverse Complementary Matches (RCMs) between introns flanking circ-*crh-1*, which are putative ADR-1 target sites. Using CRISPR-Cas9 gene editing we deleted the downstream *circ-crh-1* RCM and found that this eliminated expression of the circRNA. Importantly, linear mRNA expression from the *crh-1* gene and expression of the resulting phosphorylated CREB encoding protein was unaffected. Using two independent alleles, we found that mean lifespan was extended in circ-*crh-1* mutants. Gene expression alterations were also identified using RNA-Seq. Moving forward, intronic RCM deletion using CRISPR should be a widely applicable method to identify lifespan-regulating circRNAs in *C. elegans*.

Introduction, Results and Discussion

CircRNAs are a recently appreciated class of RNAs generated by backsplicing (Li et al., 2018). Most characterized circRNAs are produced from exons of protein-coding genes (Zhang et al., 2014). CircRNAs lack free ends, resulting in greater resistance to exoribonuclease digestion compared to their linear RNA counterparts (Jeck et al., 2013). Interestingly, circRNAs are found to accumulate in the brains of fruit flies, mice, and rat during aging (Gruner et al., 2016; Jeck et al., 2013; Zhou et al., 2018). Previously, we demonstrated that the majority of circRNAs expressed in *C. elegans* also accumulate during aging and that several age-accumulated circRNAs happened to be generated from genes with established roles in lifespan regulation, including *crh-1* (Cortes-Lopez et al., 2018). The *crh*-1 gene codes for an ortholog of the cAMP Response Element-Binding Protein (CREB) known to be involved in lifespan regulation (Chen et al., 2016; Lakhina et al., 2015). We previously reported that the two abundant circRNAs generated from the *crh-1* gene greatly increase in abundance during aging (i.e. *cel_circ_0000438* and *cel_circ_0000439*) (Cortes-Lopez et al., 2018). These circRNAs differ only in 6 nucleotides as a result of an alternative splice acceptor site, and are collectively referred to from here on as circ-*crh-1* (**Figure 8A**).

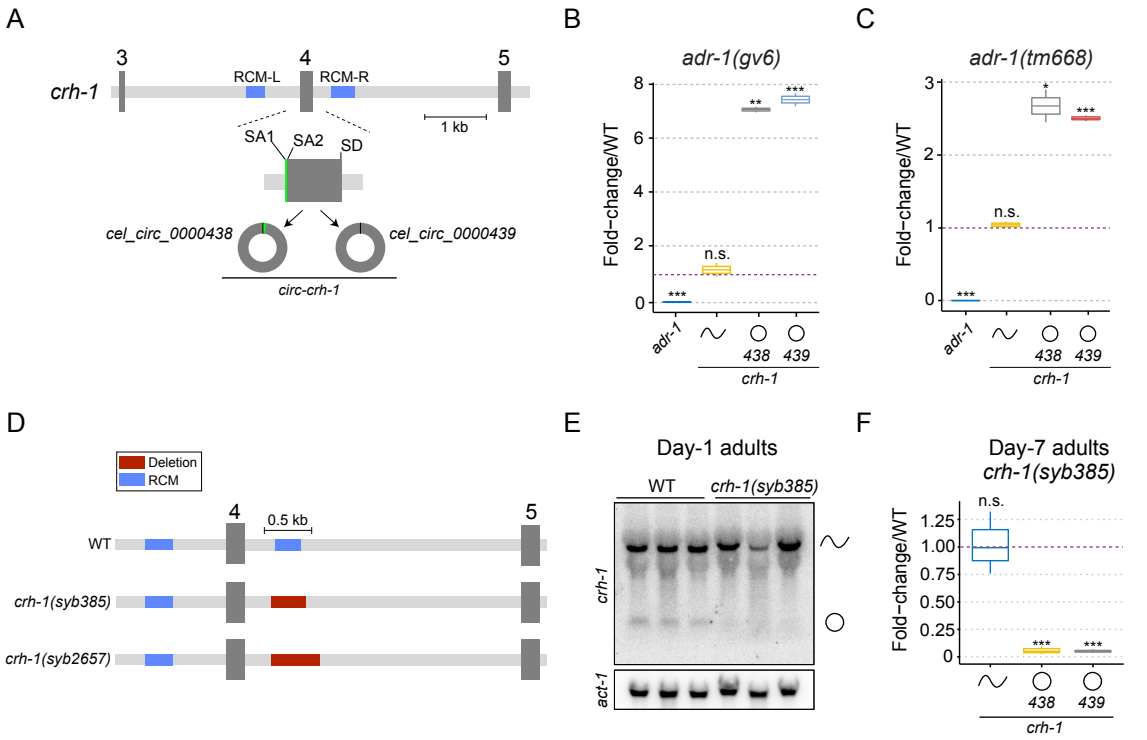

Figure 8. circ-*crh-1* regulation by ADR-1 and generation of CRISPR/Cas9 deletion alleles. **(A)** Schematic showing exon 3 to exon 5 of *crh-1* gene (chrIII:11685086-11691812). Two circRNAs are generated by backsplicing of exon 4, using two alternative splice acceptors (SA) and one shared splice donor (SD). Reverse complementary motifs (RCM-L and RCM-R) predicted to facilitate backsplicing of *crh-1* circRNAs are shown as blue rectangles. **(B-C)** Mutations in *adr-1* result in increased expression of circ-*crh-1* but not linear *crh-1* in day-1 adult animals, as determined by RT-qPCR. Linear *adr-1* transcripts are not expressed in *adr-1*(*gv6*) or *adr-1*(*tm668*) mutant alleles as expected. n=2 independent biological samples. **(D)** Schematic of *crh-1* from RCM-L to exon 5 (chrIII:11687255-11691508). Intronic deletions targeting the downstream RCM-R region were introduced by CRISPR/Cas9 and are presented as red rectangles. **(E)** Northern analysis of day-1 adult whole worms using dsDNA probe

complementary to *crh-1* exon 4. Signal from *crh-1* circRNAs are absent in *crh-1(syb385)* mutant animals compared to wild-type. **(F)** RT-qPCR expression analysis of linear and circular *crh-1* transcripts in day-7 *crh-1(syb385)* adult whole worms compared to wild-type animals. Both circRNAs are significantly reduced compared to wild-type, whereas the *crh-1* linear RNA is unchanged. n=3 independent biological samples. For RT-qPCR expression analyses, data was normalized to *cdc42* mRNA and is represented as mean ± SEM; n.s., not significant; *, $P<0.05$; **, $P<0.01$; ***, $P<0.001$. Strains used in this study are found in Supplementary Table S1. RT-qPCR and Northern blot primers can be found in Supplementary Table S2.

For certain circRNAs, RCMs within flanking introns facilitate backsplicing ostensibly by bringing the splice donor and acceptor sites into closer proximity (Jeck et al., 2013). The two *crh-1* circRNAs generated from exon 4 of the *crh-1* gene are flanked by long introns that contain sequences complementary to one another (RCM-L and RCM-R) (**Figure 8A**, **Figure S8A**). ADAR is a double-stranded RNA binding protein that when knocked down increases expression of some circRNAs in mammalian cells (Ivanov et al., 2015; Rybak-Wolf et al., 2015). We investigated *crh-1* expression in two independent ADAR mutant alleles, *adr-1(gv6)* and *adr-1(tm668)* (Hundley et al., 2008; Tonkin et al., 2002). RT-qPCR analysis of whole worms showed that circ-*crh-1* expression was significantly increased in both *adr-1* mutants, whereas linear *crh-1* mRNA was unchanged (**Figure 8B-C**). Interestingly, expression of circ-*crh-1* were greater in null *adr-1(gv6)* mutants compared to *adr-1(tm668)* mutants (~7 vs 2.5 fold), *adr-1*(*gv6*) mutants lack both double-stranded RNA-binding domains (dsRBD), whereas *adr-1*(*tm668*) lacks only one dsRBD (Tonkin et al., 2002). This suggests that the remaining dsRBD in *adr-1*(*tm668*) mutants might act to negatively regulate circ-*crh-1* expression with reduced effect. Taken together, this data suggests that ADR-1 regulates circ-*crh-1* through binding to its flanking intronic RCMs.

Generating circRNA loss-of-function organisms is challenging because circRNAs are derived from protein-coding genes, and thus attempts to disrupt circRNA expression can interfere with the biogenesis of protein-coding transcripts. Recently, CRISPR/Cas9 was used to delete RCMs in the introns

flanking mouse circ*Kcnt2* which abolished the circRNA and did not affect the linear RNA (Liu et al., 2020). We similarly used CRISPR/Cas9 to generate a 377 bp deletion overlapping the RCM-R region to generate the *crh-1(syb385)* mutant strain (**Figure 8D**). To confirm loss of circ-*crh-1*, we performed Northern blot analysis and found circ-*crh-1* to be undetectable, whereas linear *crh-1* expression persisted (**Figure 8E**). By RT-qPCR analysis, the circRNA signals were barely detectable in the *crh-1(syb385*) mutants in both 1 and 7 day old adults (**Figure 8F** and **Figure S8B**). Importantly, we found that expression of linear *crh-1* was not significantly affected (**Figure 8F** and **Figure S8B**). Next, we generated a second allele, *crh-1(syb2657)*, which was designed to delete a slightly larger portion of the intronic region surrounding the RCM-R (**Figure 8D**), and confirmed by RT-qPCR that only the circle and not mRNA from the *crh-1* gene was altered (**Figure S8C-D**). In either circRNA mutant, expression of phosphorylated CRH-1 protein (p-CREB) was unaltered compared to wild-type and as expected, p-CREB was undetectable in null *crh-1(n3315)* and *crh-1(tz2)* gene mutants (**Figure S8E-F**). Taken together, these results demonstrate the first successful circRNA mutant generated in *C. elegans*.

To directly test whether circ-*crh-1* plays a role in aging, we performed lifespan experiments at 20ºC for both *crh-1(syb385)* and *crh-1(syb2657)* mutant animals. Even though hundreds of circRNAs dramatically increase in expression during aging (Cortes-Lopez et al., 2018; Gruner et al., 2016; Westholm et al., 2014; Xu et al., 2018; Zhou et al., 2018), the removal of just circ-*crh-1* led to a significantly longer mean lifespan compared to wild-type (*syb385*, 11.5%

extension, *P*<0.0001; *syb2657*, 9.8% extension, *P*<0.001) (**Figure 9A**, **Supplementary Table S3**). Expression of circ-*crh-1* by *rab-3,* a neural-specific promoter, was able to partially rescue the lifespan phenotype observed in *crh-1(syb385)* worms (**Figure 9B** and **Supplementary Table S3**). Partial rescue by *rab-3* might reflect a requirement of circ-*crh-1* in multiple tissues, nonetheless these results indicate that circ-*crh-1* expression in neurons is an important determinant of *C. elegans* lifespan.

To identify gene expression changes that might provide clues for the molecular basis for the extended mean lifespan phenotype, we performed RNA-seq on 1 day old adults from wild-type, *crh-1(syb385)* or *crh-1*(*syb2657*) genetic backgrounds (**Supplementary Table S4**). We identified hundreds of differentially expressed genes (DEGs) for either circRNA mutant when compared to wild-type animals (**Figure 9C** and **Supplementary Table S5**). To identify gene candidates robustly affected by circ-*crh-1* loss we examined those which overlapped in both comparisons. In total, 52 genes were upregulated and 6 genes were downregulated in both datasets (**Figure 9C**). Interestingly, among the shared upregulated genes, functional clustering revealed a significant enrichment for *clec* genes, which are associated with innate immune function in *C. elegans*

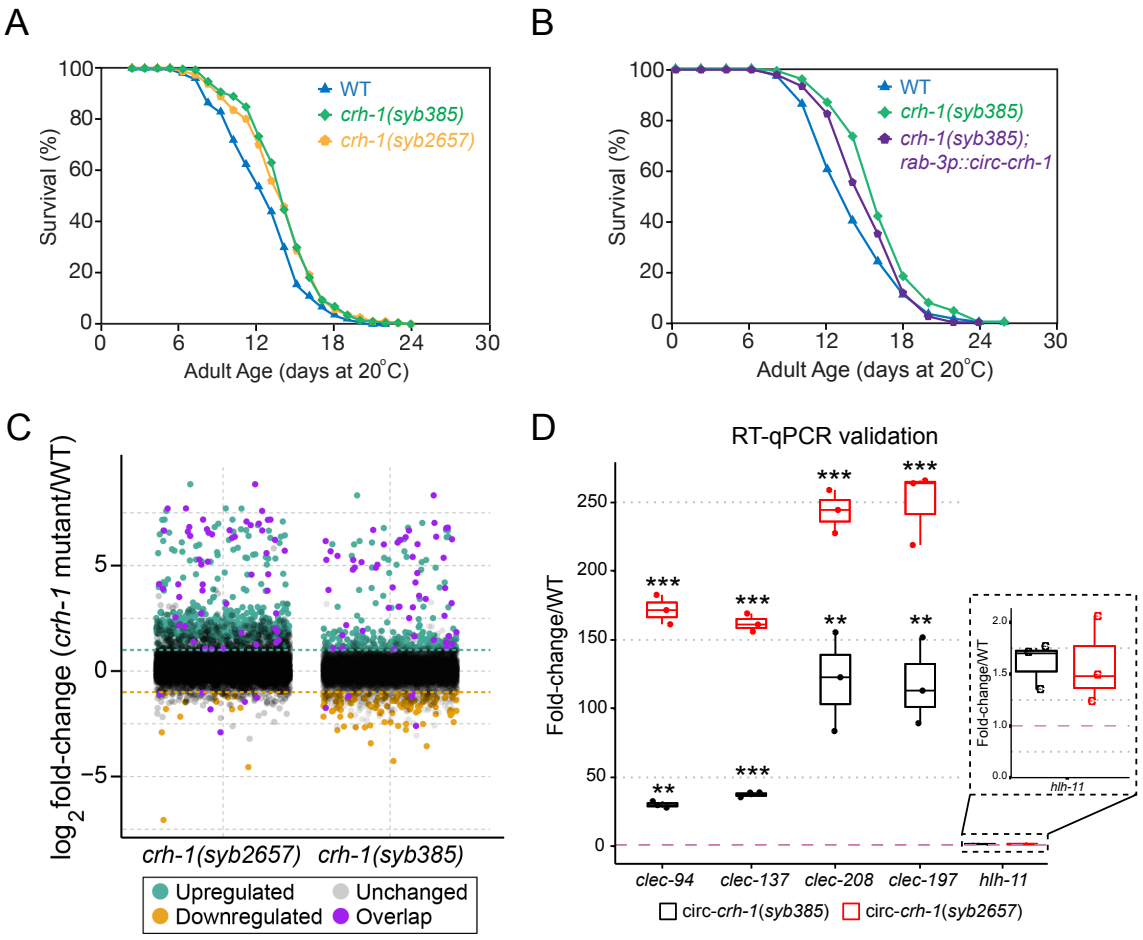

Figure 9. Loss of circ-*crh1* extends *C. elegans* lifespan and alters the transcriptome. (A) Loss of *crh-1* circRNAs extend mean lifespan but not maximum lifespan. Lifespan curves for *crh-1(syb385)* mutants (11.5% increase vs wild-type, *P*<0.0001, Mantel-Cox log-rank test) and *crh-1(syb2657)* mutants compared to wild-type (9.6% increase vs wild-type, *P*<0.001, Mantel-Cox log-rank test). n=3 independent lifespan assays were performed with n>150 animals for each assay and genotype in the absence of FUdR (see Supporting Information). **(B)** Lifespan curves for worms overexpressing the circ-*crh-1* in *rab-3*-expressing neurons compared to wild-type and *crh-1(syb385)* mutants. There is a non-significant difference in mean lifespan between wild-type and *crh-*

1(syb385); rab-3p::circ-crh-1 animals (*P*=0.013) Mantel-Cox log-rank test), as well as between *crh-1(syb385)* and *crh-1(syb385); rab-3p::circ-crh-1* animals (*P*=0.05) Mantel-Cox log-rank test). n=2 independent lifespan assays were performed with n>100 animals for each assay and genotype in the absence of FUdR (see Supporting information). See Supplementary Table S3 for lifespan statistics. **(C)** Scatter plot of mRNA expression changes in *crh-1(syb385)* or *crh-1(syb2657)* vs wild-type day 1 adult animals. Significantly downregulated and upregulated genes (log_2FC>1 and adj. *P*<0.05) are shown as orange and green dots, respectively. Genes that were up or downregulated in both *crh-1* mutant animals are shown as purple dots. **(D)** RT-qPCR expression analysis of 5 genes which were upregulated in both *crh-1* mutant animals relative to wild-type from RNA-seq data shown in panel c. n=3 independent biological samples. Data are represented as mean ± SEM; n.s., not significant; **, *P*<0.01; ***, *P*<0.001. Expression was normalized to *cdc-42* mRNA.

(reviewed in (Pees et al., 2016)). In addition, we observed that *hlh-11*, a conserved transcription factor, was upregulated in both *crh-1(syb385)* and *crh-1*(*syb2657*) mutants. We successfully validated expression trends for 4/4 of the *clec* genes but not *hlh-11* by RT-qPCR using independently prepared samples (**Figure 9D**). Together, these results indicate that circ-*crh-1* have a widespread effect on *C. elegans* transcriptome and might play a role in innate immunity.

CircRNAs generally increase during aging, which has been attributed to their high degree of stability, especially in post-mitotic tissues such as neurons (Knupp and Miura, 2018). We have speculated previously that the age-accumulation of circRNAs could be detrimental to cellular function due to the progressive nature of the age-accumulation (Knupp and Miura, 2018). Given the large number of circRNAs increased with aging, perhaps such a detrimental effect is independent of the specific identity of the individual circRNAs. Despite our hypothesis that circRNA accumulation could decrease lifespan, it nonetheless was quite surprising to find that loss of a single circRNA can increase mean lifespan. Which of the other hundreds of age-accumulated circRNAs might impact lifespan? Having established a CRISPR method to abolish circRNAs in *C. elegans*, and given its utility for aging research in general, a deep investigation into determining which other circRNAs regulate lifespan seems warranted.

Some age-accumulated circRNAs might have beneficial roles in aging cells. Recently, circSfl transgenic overexpression was found to extend lifespan in *Drosophila* (Weigelt et al., 2020). siRNA knockdown of circSfl was unsuccessful,

and genetic manipulations performed to reduce the circRNA also impacted linear mRNA isoforms. This highlights the difficulties in generating circRNA loss of function mutants to study their impact on aging. *In vivo* siRNA knockdown has been successfully implemented for certain circRNAs in *Drosophila* (Pamudurti et al., 2020), but some circRNAs simply cannot be specifically targeted due to sequence limitations of the back-spliced junction region. *C. elegans* have generally shorter introns than *Drosophila* and mammalian model systems. This might make them more amenable to efficient CRISPR manipulation of RCMs; however, it remains to be seen whether many *C. elegans* circRNAs can be specifically reduced or abolished using the RCM deletion methodology.

METHODS

Full description of methods can be found in the Supporting Material. Briefly, *C. elegans* were cultivated on the surface of NGM agar seeded with the *Escherichia coli* strain OP50, and grown in 20°C incubators using standard protocols. CRISPR deletion mutants were generated by Suny Biotech. Lifespan analysis was carried with synchronized adult N2 or outcrossed mutant worms with or without transgenes at 20°C. Lifespan curves were analyzed using OASIS2 (Han et al., 2016). For RNA analysis experiments, worms were cultivated on plates containing 5-fluorodeoxyuridine (FUdR). Raw RNA-Seq reads are deposited at GEO (link to be provided). RNA-Seq alignment was performed using HISAT2

(Kim et al., 2019) and differential expression was performed using DESeq2 (Love et al., 2014).

ACKNOWLEDGEMENTS

We thank members of the van der Linden and Miura labs for useful discussions and feedback on the manuscript. This work was supported by the NIH National Institute on Aging [grant: R21 AG058955]. The Cellular and Molecular Imaging (CMI) Core facility at the University of Nevada, supported by a grant from the NIH National Institutes of General Medical Sciences [grant: P30 GM103650]. DK was supported by the National Science Foundation Graduate Research Fellowship Program.

CONFLICT OF INTEREST

The authors declare no competing interests.

AUTHOR CONTRIBUTIONS

DK, BGJ, PM and AVDL designed the study, DK, BGJ, JMB and JJG performed the experiments. DK, BGJ, PM and AVDL analyzed the data. DK, BGJ, PM and AVDL wrote the manuscript. AVDL and PM supervised the study.

SUPPORTING INFORMATION

1. Supplementary Methods

2. Supplementary Figure S1

3. Supplementary Tables S1-S5

DATA AVAILABILITY STATEMENT

The data that supports the findings of this study are available in the Supporting Material of this article. The RNA-Seq data is deposited at the Gene Expression Omnibus (GEO) under GSE174408.

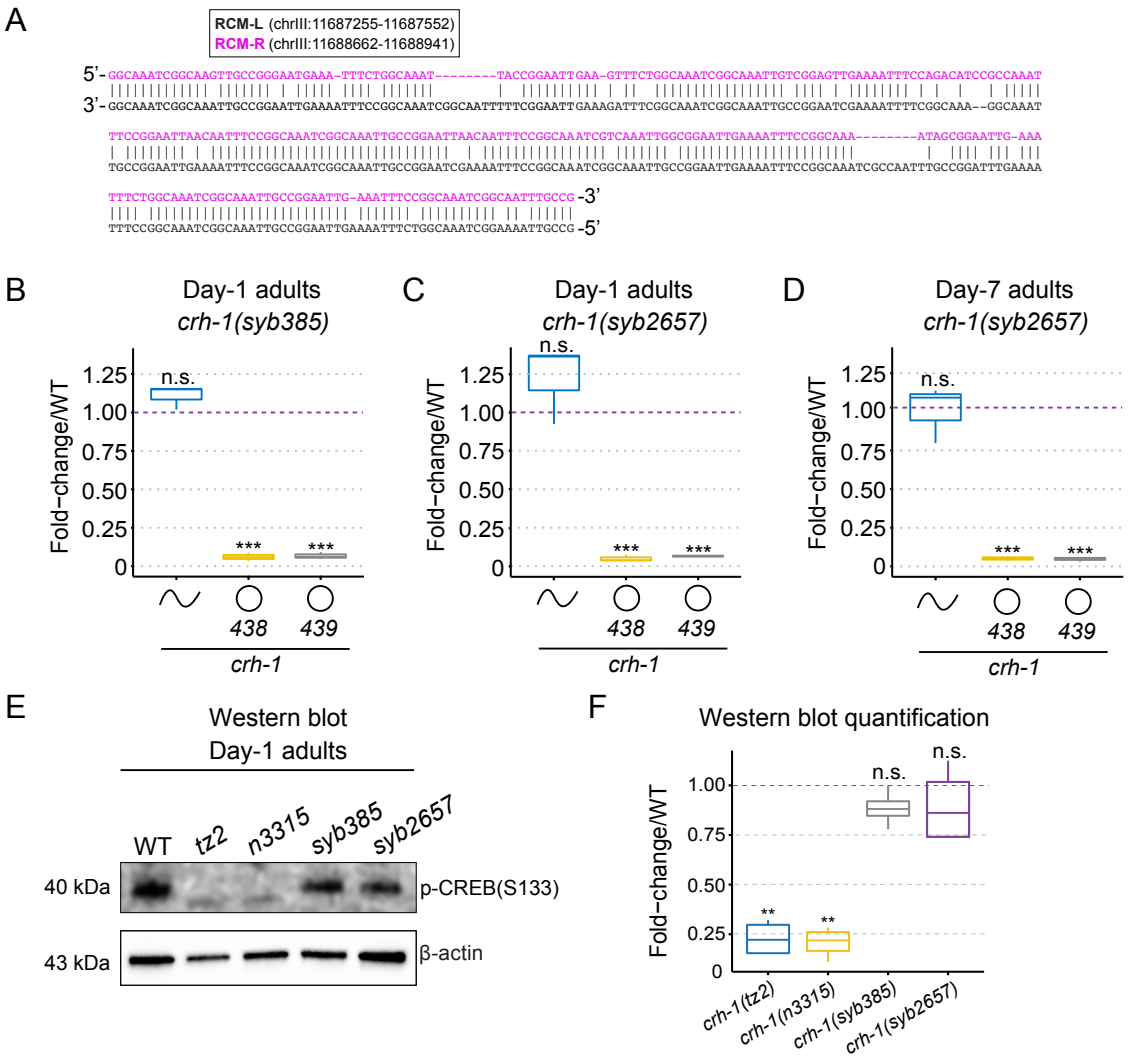

Supplementary Figure 8. circ-*crh-1* expression is ablated in two RCM-R deletion alleles, whereas p-CREB expression is unchanged. (A) Sequence alignment of RCM-L and RCM-R flanking exon 4 of the *crh-1* gene. **(B)** RT-qPCR expression analysis of linear and circular *crh-1* transcripts in day-7 *crh-1(syb385)* adult whole worms compared to wild-type animals. Both circRNAs are significantly reduced compared to wild-type, whereas the *crh-1* linear RNA is unchanged. n=2 independent biological samples. The same RT-qPCR expression analyses were repeated for *crh-1*(*syb2657*) mutant animals at day-1

(C) and day-7 **(D)**. For RT-qPCR expression analyses, data was normalized to *cdc-42* and is represented as mean ± SEM; n.s., not significant; *, *P*<0.05; **, *P*<0.01; ***, *P*<0.001. **(E)** Phosphorylated CRH-1 protein levels are normal in *crh-1* circRNA mutants (*syb385*, *syb2657*), but absent in *crh-1* null or loss-of-function mutants (*tz2*, *n3315*) compared to wild-type. A representative Western blot is shown. Signal indicates p-CRH-1 using antibody against mammalian p-CREB (Ser 133) (top panel). b-actin loading control is shown below. **(F)** Quantification of p-CREB expression in 1-day old adult animals. Data is normalized to wild-type and represented as the mean ± SEM. n=4 independent biological replicates.

General Discussion

CircRNAs were generally regarded as rare RNA species, even transcriptional noise. It was not until 2012 that total RNA-seq discovered how pervasive circRNAs actually are (Salzman et al., 2012). In the years following, circRNAs were identified in every multi-cellular organism examined (Jeck et al., 2013; Memczak et al., 2013; Wang et al., 2014). Numerous groups have examined the expression patterns of circRNAs in vertebrate tissues and in every instance found that circRNAs were enriched in the brain (Mahmoudi and Cairns, 2019; Rybak-Wolf et al., 2015; Szabo et al., 2015; You et al., 2015). Moreover, it has been well established that circRNAs are upregulated during neural differentiation and synapse maturation (Hollensen et al., 2020; Rybak-Wolf et al., 2015; You et al., 2015). Yet, it was completely unknown what factors might underlie the relatively high abundance of circRNAs in the brain. My dissertation work sought to reduce this knowledge gap.

My work presented in Chapter 2 identified NOVA2 as an *in vivo* regulator of circRNA biogenesis not only in the developing mammalian brain, but also in neurons. Loss of NOVA2 results in downregulation of circRNAs, suggesting it is a positive regulator of backsplicing. In agreement with this hypothesis, overexpression of NOVA2 *in vitro* significantly increased expression from an endogenous NOVA2-regulated circRNA, circ*Efnb2*. In the developing mouse cortex, at timepoints overlapping with neural differentiation, *Nova2* protein expression consistently increases (Saito et al., 2019). Thus, NOVA2 might at

least in part, underlie the propensity of circRNA expression in the mammalian brain. Interestingly, we found that NOVA2-regulation appears to be neuron cell-type specific (**Figure S4**). If this observation holds, then NOVA2 is also the first RBP identified to regulate circRNA expression uniquely in different neuron cell types. We approach conclusions regarding NOVA2 cell-type specific regulation with caution because we recognize that our findings might be limited by RNA-sequencing read depth. Greater read coverage at the backsplice junction (BSJ) would generate more statistical power to detect a greater number of NOVA2-regulated circRNAs in both neuron cell-types, resulting in a more robust conclusion. To enrich for circRNAs prior to RNA-seq, established enrichment strategies such as RNase-R (Jeck et al., 2013) or RPAD (Panda et al., 2017) could be applied. Use of additional RNA-seq platforms such as Oxford Nanopore long-read sequencing would also enable the discovery of additional circRNA isoforms that might be NOVA2-regulated, such as circRNAs which include retained introns. Long-read sequencing has recently been leveraged for such analyses in various human tissues (Xin et al., 2021). However, it has not been used to characterize alternative backsplicing in sorted neuron populations. Thus, results from these experiments would extend not only our findings from Chapter 2 but also be broadly beneficial to the circRNA field.

We demonstrated that intronic motifs flanking *circEfnb2* are important for its regulation by NOVA2 *in vitro*. One limitation of this analysis stems from a feature common to many circRNAs, such that *circEfnb2* is flanked by very long introns (**Figure 6A**). This led to our decision to clone truncated introns which

encompassed NOVA2 binding sites identified in NOVA2-CLIP datasets. Given that plasmid-based minigenes cannot always include the full genomic sequence of interest, to what extent are they useful to inform which motifs are important for RBP-mediated backsplicing regulation? To address this question, CRISPR-Cas9 could be targeted to binding motifs identified in Chapter 2 as important for NOVA2-regulation of *circEfnb2*. Perhaps in a system that more accurately recapitulates an *in vivo* system, such as mouse embryonic stem cells which can be differentiated into neurons. The results would be generally useful for labs investigating the *cis*-elements and *trans*-factors controlling circRNA regulation.

One unanswered question from Chapter 2 is the precise mechanism by which NOVA2 regulates backsplicing. Our artificial backsplicing minigene assays established that NOVA2 binding at both flanking introns promotes backsplicing relative to linear splicing (**Figure 7D**). Similar results have been observed for circRNAs regulated by QKI (Conn et al., 2015). QKI has been previously shown to form dimers with itself (Teplova et al., 2013), insinuating that QKI might dimerize across a circularizing locus similar to RCMs and bring participating splice sites into close proximity. Similarly, NOVA KH domains have also been found to dimerize, *in vitro* (Teplova et al., 2011). Thus, NOVA2 proteins might bind both flanking introns of a circularizing locus to facilitate backsplicing (**Figure 10**).

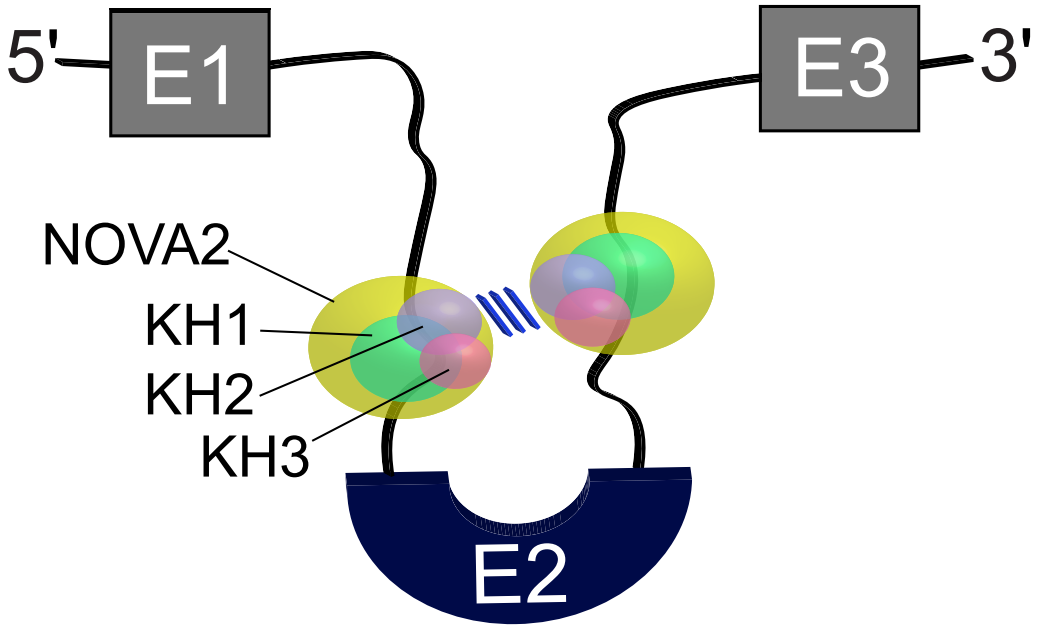

Figure 10. Model of NOVA2 dimerization to promote backsplicing. (A) Model of NOVA2 binding within introns flanking a circularizing locus (blue) to promote backsplicing through dimerization of at least two NOVA2 molecules. Interaction between NOVA2 molecules are shown as angled blue lines. NOVA2 KH1, KH2, and KH3 domains are colored green, purple, and magenta, respectively.

How can we investigate this hypothesis? In previous work, it was shown that introduction of RCMs into the flanking introns of non-circularizing loci could promote backsplicing (Zhang et al., 2014). A similar approach could be used to test the NOVA2 dimerization hypothesis. Construction of an artificial minigene, similar to ours (**Figure 7A**) that does not produce a circRNA followed by insertion of NOVA2 binding sites in both flanking introns would be a first step. If a circRNA is produced this suggests that NOVA2 is sufficient to promote backsplicing in general. Assuming that individual NOVA2 proteins interact across a circularizing locus to mediate backsplicing, mutations introduced independently at either NOVA2 intronic binding site upstream or downstream of the circularizing exon should significantly reduce or abolish circRNA expression. Whether or not this occurs, it is still likely that additional mechanisms are at play. This is because many NOVA2-regulated circRNAs *in vivo* were not flanked by intronic NOVA2-CLIP peaks. *In vivo*, backsplicing regulation by NOVA2 is undoubtedly in competition with other splicing factors. To determine additional regulators of neuron-expressed circRNAs and *in vivo* competitors of NOVA2, additional cKO mutants of various RBPs in mouse cortical neurons could be generated or obtained. Overlap between NOVA2-regulated circRNAs and circRNAs regulated in additional cKO mice would provide at least some context to the regulatory landscape.

What biological processes do NOVA2-regulated circRNAs participate in? Or circRNAs in general? The latter has been a long-standing question still without a well-defined answer. The problem is two-fold. First, it is difficult to

choose an individual circRNA for study. For instance, i*n silico* predictions based on primary sequence are unlikely to be fruitful unless there is significant enrichment for RBP binding motifs or miRNA seed regions. Even in these cases, circRNAs share common sequence with protein-coding exons, thus identical motifs are present in the likely more abundant linear transcript making it hard to delineate a distinct role for the circRNA. If a circRNA is highly expressed, perhaps exceeding expression of the protein-coding transcript, then further investigation might be warranted, especially if its expression changes dramatically between experimental conditions. Subcellular localization might be another useful criterion for selecting candidates. Cellular fractionation experiments have identified subsets of circRNAs enriched at synapses relative to their linear counterpart suggesting a role in synaptic transmission (Rybak-Wolf et al., 2015; You et al., 2015). Exon-intron circRNAs which regulate gene expression, seem to exhibit nuclear localization and are associated with RNA pol II and U1 snRNA (Li et al., 2015). RNA pol II pulldown followed by RNA-seq might illuminate additional regulatory circRNAs. Once a list of candidate circRNAs are generated, one approaches the second roadblock, *in vivo* targeting.

Targeting circRNAs *in vivo* with shRNAs or creating CRISPR mutant lines is an especially non-trivial task. In only two instances to date have shRNAs efficiently reduced circRNA expression in mammalian tissues (Liu et al., 2017; Shan et al., 2017). This strategy often requires the design of several shRNAs specific to the BSJ to ensure efficient knockdown of the circRNA and not mRNA

which shares common sequence. This is in addition to limiting any other potential off-targets. In both studies that successfully knocked down mammalian circRNAs *in vivo*, BSJ-targeting shRNAs were expressed via AAVs. Although AAVs are proven, powerful tools for manipulating gene expression in multiple tissues, including the CNS (Haery et al., 2019), other factors such as AAV titer, dosage, and delivery (which can be timely and expensive to determine) can impact AAV efficiency. Hence, while shown to be successful in some cases, AAV-mediated knockdown can be a laborious method to assess circRNA function *in vivo*. In contrast, CRISPR-Cas9 might be a more attractive approach to widely probe circRNAs functions.

Similar to shRNAs, CRISPR has already been used to determine the *in vivo* function for three circRNAs expressed in mammals (Piwecka et al., 2017; Xia et al., 2018; Zhu et al., 2019), including one in the brain (Piwecka et al., 2017). Unlike viral delivery of siRNAs or shRNAs, CRISPR-Cas9 offers stable reduction of circRNA expression. In addition, conditional circRNA knockouts in various cell-types such as neurons, could be more readily achieved. For example, supposing a candidate circRNA is flanked by intronic RCMs that mediates its expression, loxP sites could be introduced immediately upstream and downstream of the target RCM. Progeny with loxP insertions could then be crossed with a mouse expressing Cre recombinase under a cell-specific promoter, resulting in Cre-mediated excision of the RCM motif. One important limitation regarding CRISPR-generated circRNA mutants is the dependence on complementary *cis*-elements in introns flanking the circularizing locus. Although

not a requirement *per se*, no other *cis*-elements have been identified that broadly favor backsplicing independently of linear-splicing. Thus, these circRNAs will likely be investigated first.

In Chapter 3 we addressed a major knowledge gap with regard to circRNA aging research. In the past seven years several groups including our own have reported on the age-accumulation of circRNAs in both vertebrate (Gruner et al., 2016; Xu et al., 2018; Zhou et al., 2018) and invertebrate (Cortes-Lopez et al., 2018; Westholm et al., 2014) systems. Notably, age-accumulation appears to be a hallmark of aging brains in *Drosophila*, mice, rats and macaque (Gruner et al., 2016; Westholm et al., 2014; Xu et al., 2018; Zhou et al., 2018). In *C. elegans*, which albeit lacks a defined brain, we observed the strongest age-accumulation trend to date (Cortes-Lopez et al., 2018). The age-accumulation of circRNAs could be tied to the post-mitotic nature of neurons (*see section*: circRNAs are upregulated during neural differentiation and accumulate during aging), and might also be coupled to increased alternative splicing observed in the brain with aging. Whichever the case might be, what affect age-related circRNAs have with regard to longevity was unknown. Fundamentally, are circRNAs detrimental or protective in an aging organism? Our loss-of-function analyses indicate that *crh-1* circRNAs are detrimental to *C. elegans* longevity, as their ablation results in a significant increase in mean lifespan (**Figure 9A**). These results are in contrast to a previous report in *Drosophila*, where circSfl was concluded to extend fly lifespan (Weigelt et al., 2020). However, lifespan extension in this case cannot be solely attributed to loss of the circRNA, as CRISPR-Cas9 mutations to interrupt

circSfl backsplicing included deletions of exonic sequence present in the linearly spliced protein coding transcript, which also has a role in lifespan (Weigelt et al., 2020). As we did not observe significant changes in either linear *crh-1* expression (**Figure 8F** and **Figure S8C**) or activated CREB protein levels (**Figure S8F-G**) in our circ-*crh-1* mutants, our work is the first to demonstrate a function for circRNAs in lifespan independent of the linear host-gene.

Conclusions made regarding the role of circSfl in *Drosophila* lifespan were complicated due to difficulties in achieving adequate knockdown of circSfl via siRNAs (Weigelt et al., 2020). Attempts to circumvent the use of siRNAs by CRISPR gene-editing were also ineffective as they interrupted linear splicing. This inability to solely target circSfl by CRISPR is likely due a lack of known sequence elements that promote circSfl backsplicing. As discussed previously many *Drosophila* expressed circRNAs lack RCMs in their flanking introns (Westholm et al., 2014) and thus highlights a major limitation for its use as a model to assess circRNA function by genetic loss-of-function approaches in general. In contrast, circRNAs expressed in *C. elegans* are typically flanked by intronic RCMs, which can be targeted by CRISPR for circRNA loss-of-function analyses. Moreover, techniques such as co-CRISPR (Kim et al., 2014), (simultaneous editing of the target locus and a secondary locus which results in a visible phenotype) can also greatly facilitate the selection of edited progeny. Potential off-targeting by gene-editing can also be rapidly mitigated in worms by outcrossing due to their short generation times. Thus compared to *Drosophila*, *C.*

elegans appears to be a better model system to study the function of individual circRNAs.

Along these lines, *C. elegans* also has numerous advantages relative to other model organisms such as mice, with regard to lifespan in particular that we considered. For instance, compared to mice, worms are relatively low-cost, easy to maintain, and have a short generation time and lifespan. The latter two points alone were instrumental in our ability to repeatedly reproduce lifespan phenotypes in two independent *crh-1* mutant lines and perform subsequent rescue experiments during the review process in a timely fashion. A similar analysis in mice would take years to accomplish. Yet despite these many great features that aided in our ability to identify functional, age-related circRNAs in *C. elegans*, some relevant limitations remain.

For instance, the majority of biochemical experiments performed using *C. elegans* utilize protein lysates or nucleic acid extractions from whole worm extracts. This, coupled with the lack of cell lines originating from *C. elegans* results in a limited understanding of any tissue-specific processes or expression patterns. Along these lines, we performed total RNA-seq analysis using adult whole worms to elucidate the mechanism by which *crh-1* circRNAs extend lifespan. We identified hundreds of differentially expressed genes. Understanding which cell-types contribute most to the observed gene expression changes would greatly aid in our identification of biological processes that might explain lifespan extension. Previous work indicates that CRH protein is expressed in neurons and intestinal cells (Chen et al., 2016), suggesting that the most transcription (and

therefore, backsplicing) of the *crh-1* gene occurs in those tissues. We analyzed total RNA-seq data generated from isolated worm cell types (Kaletsky et al., 2018) and found that *cel_circ_0000439* was indeed expressed in both neurons and intestines (data not shown). However, due to the challenges associated with isolating specific cell types from worms, we are not easily able to confirm these findings by more quantitative methods such as RT-qPCR. Cellular fractionation experiments are also challenging in worms and would help determine if *crh-1* circRNAs localize to the nucleus versus cytoplasm. If *crh-1* circRNAs exhibited nuclear localization it might suggest that they regulate gene transcription.

It has not been evaluated to what extent circRNA loci in *C. elegans* overlap with circRNAs expressed in mouse or humans. Such an analysis would be advantageous in selecting additional circRNAs with potential function in higher species such as mice or humans. While *C. elegans* is not ideal for determining the biochemical mechanism underlying a given circRNA phenotype, it is a powerful tool for first assessing which circRNA are most likely functional. These circRNAs could be further investigated in other model organisms more amenable to biochemical techniques. Together, our work demonstrates that *C. elegans* is a premier model to expand the number of functionally characterized circRNAs.

References

Abdelmohsen, K., Panda, A.C., De, S., Grammatikakis, I., Kim, J., Ding, J., Noh, J.H., Kim, K.M., Mattison, J.A., de Cabo, R.*, et al.* (2015). Circular RNAs in monkey muscle: age-dependent changes. Aging (Albany NY) *7*, 903-910.

Abdelmohsen, K., Panda, A.C., Munk, R., Grammatikakis, I., Dudekula, D.B., De, S., Kim, J., Noh, J.H., Kim, K.M., Martindale, J.L.*, et al.* (2017). Identification of HuR target circular RNAs uncovers suppression of PABPN1 translation by CircPABPN1. RNA Biol *14*, 361-369.

Ashwal-Fluss, R., Meyer, M., Pamudurti, N.R., Ivanov, A., Bartok, O., Hanan, M., Evantal, N., Memczak, S., Rajewsky, N., and Kadener, S. (2014). circRNA biogenesis competes with pre-mRNA splicing. Mol Cell *56*, 55-66.

Bachmayr-Heyda, A., Reiner, A.T., Auer, K., Sukhbaatar, N., Aust, S., Bachleitner-Hofmann, T., Mesteri, I., Grunt, T.W., Zeillinger, R., and Pils, D. (2015). Correlation of circular RNA abundance with proliferation--exemplified with colorectal and ovarian cancer, idiopathic lung fibrosis, and normal human tissues. Sci Rep *5*, 8057.

Barbosa-Morais, N.L., Irimia, M., Pan, Q., Xiong, H.Y., Gueroussov, S., Lee, L.J., Slobodeniuc, V., Kutter, C., Watt, S., Colak, R.*, et al.* (2012). The evolutionary landscape of alternative splicing in vertebrate species. Science *338*, 1587-1593.

Barrett, S.P., and Salzman, J. (2016). Circular RNAs: analysis, expression and potential functions. Development *143*, 1838-1847.

Buckanovich, R.J., and Darnell, R.B. (1997). The neuronal RNA binding protein Nova-1 recognizes specific RNA targets in vitro and in vivo. Mol Cell Biol *17*, 3194-3201.

Buckanovich, R.J., Posner, J.B., and Darnell, R.B. (1993). Nova, the paraneoplastic Ri antigen, is homologous to an RNA-binding protein and is specifically expressed in the developing motor system. Neuron *11*, 657-672.

Buckanovich, R.J., Yang, Y.Y., and Darnell, R.B. (1996). The onconeural antigen Nova-1 is a neuron-specific RNA-binding protein, the activity of which is inhibited by paraneoplastic antibodies. J Neurosci *16*, 1114-1122.

Cao, D. (2021). Reverse complementary matches simultaneously promote both back-splicing and exon-skipping. BMC Genomics *22*, 586.

Capel, B., Swain, A., Nicolis, S., Hacker, A., Walter, M., Koopman, P., Goodfellow, P., and Lovell-Badge, R. (1993). Circular transcripts of the testis-determining gene Sry in adult mouse testis. Cell *73*, 1019-1030.

Chen, L., Wang, C., Sun, H., Wang, J., Liang, Y., Wang, Y., and Wong, G. (2021). The bioinformatics toolbox for circRNA discovery and analysis. Brief Bioinform *22*, 1706-1728.

Chen, Y.C., Chen, H.J., Tseng, W.C., Hsu, J.M., Huang, T.T., Chen, C.H., and Pan, C.L. (2016). A C. elegans Thermosensory Circuit Regulates Longevity through crh-1/CREB-Dependent flp-6 Neuropeptide Signaling. Dev Cell *39*, 209-223.

Cheng, J., Metge, F., and Dieterich, C. (2016). Specific identification and quantification of circular RNAs from sequencing data. Bioinformatics *32*, 1094-1096.

Cocquerelle, C., Daubersies, P., Majerus, M.A., Kerckaert, J.P., and Bailleul, B. (1992). Splicing with inverted order of exons occurs proximal to large introns. EMBO J *11*, 1095-1098.

Conn, S.J., Pillman, K.A., Toubia, J., Conn, V.M., Salmanidis, M., Phillips, C.A., Roslan, S., Schreiber, A.W., Gregory, P.A., and Goodall, G.J. (2015). The RNA binding protein quaking regulates formation of circRNAs. Cell *160*, 1125-1134.

Consortium, C.e.S. (1998). Genome sequence of the nematode C. elegans: a platform for investigating biology. Science *282*, 2012-2018.

Cortes-Lopez, M., Gruner, M.R., Cooper, D.A., Gruner, H.N., Voda, A.I., van der Linden, A.M., and Miura, P. (2018). Global accumulation of circRNAs during aging in Caenorhabditis elegans. BMC Genomics *19*, 8.

Denzel, M.S., Lapierre, L.R., and Mack, H.I.D. (2019). Emerging topics in C. elegans aging research: Transcriptional regulation, stress response and epigenetics. Mech Ageing Dev *177*, 4-21.

Dillman, A.A., Hauser, D.N., Gibbs, J.R., Nalls, M.A., McCoy, M.K., Rudenko, I.N., Galter, D., and Cookson, M.R. (2013). mRNA expression, splicing and editing in the embryonic and adult mouse cerebral cortex. Nat Neurosci *16*, 499-506.

Dredge, B.K., and Darnell, R.B. (2003). Nova regulates GABA(A) receptor gamma2 alternative splicing via a distal downstream UCAU-rich intronic splicing enhancer. Mol Cell Biol *23*, 4687-4700.

Dredge, B.K., Stefani, G., Engelhard, C.C., and Darnell, R.B. (2005). Nova autoregulation reveals dual functions in neuronal splicing. EMBO J *24*, 1608-1620.

Du, W.W., Yang, W., Chen, Y., Wu, Z.K., Foster, F.S., Yang, Z., Li, X., and Yang, B.B. (2017). Foxo3 circular RNA promotes cardiac senescence by modulating multiple factors associated with stress and senescence responses. Eur Heart J *38*, 1402-1412.

Du, W.W., Yang, W., Liu, E., Yang, Z., Dhaliwal, P., and Yang, B.B. (2016). Foxo3 circular RNA retards cell cycle progression via forming ternary complexes with p21 and CDK2. Nucleic Acids Res *44*, 2846-2858.

Dube, U., Del-Aguila, J.L., Li, Z., Budde, J.P., Jiang, S., Hsu, S., Ibanez, L., Fernandez, M.V., Farias, F., Norton, J.*, et al.* (2019). An atlas of cortical circular RNA expression in Alzheimer disease brains demonstrates clinical and pathological associations. Nat Neurosci *22*, 1903-1912.

Dubin, R.A., Kazmi, M.A., and Ostrer, H. (1995). Inverted repeats are necessary for circularization of the mouse testis Sry transcript. Gene *167*, 245-248.

Ebbesen, K.K., Hansen, T.B., and Kjems, J. (2017). Insights into circular RNA biology. RNA Biol *14*, 1035-1045.

Enuka, Y., Lauriola, M., Feldman, M.E., Sas-Chen, A., Ulitsky, I., and Yarden, Y. (2016). Circular RNAs are long-lived and display only minimal early alterations in response to a growth factor. Nucleic Acids Res *44*, 1370-1383.

Errichelli, L., Dini Modigliani, S., Laneve, P., Colantoni, A., Legnini, I., Capauto, D., Rosa, A., De Santis, R., Scarfo, R., Peruzzi, G.*, et al.* (2017). FUS affects circular RNA expression in murine embryonic stem cell-derived motor neurons. Nat Commun *8*, 14741.

Gao, Y., Wang, J., Zheng, Y., Zhang, J., Chen, S., and Zhao, F. (2016). Comprehensive identification of internal structure and alternative splicing events in circular RNAs. Nat Commun *7*, 12060.

Gao, Y., Zhang, J., and Zhao, F. (2018). Circular RNA identification based on multiple seed matching. Brief Bioinform *19*, 803-810.

Gehman, L.T., Stoilov, P., Maguire, J., Damianov, A., Lin, C.H., Shiue, L., Ares, M., Jr., Mody, I., and Black, D.L. (2011). The splicing regulator Rbfox1 (A2BP1) controls neuronal excitation in the mammalian brain. Nat Genet *43*, 706-711.

Groen, E.J., Fumoto, K., Blokhuis, A.M., Engelen-Lee, J., Zhou, Y., van den Heuvel, D.M., Koppers, M., van Diggelen, F., van Heest, J., Demmers, J.A.*, et al.* (2013). ALS-associated mutations in FUS disrupt the axonal distribution and function of SMN. Hum Mol Genet *22*, 3690-3704.

Gruner, H., Cortes-Lopez, M., Cooper, D.A., Bauer, M., and Miura, P. (2016). CircRNA accumulation in the aging mouse brain. Sci Rep *6*, 38907.

Guo, J.U., Agarwal, V., Guo, H., and Bartel, D.P. (2014). Expanded identification and characterization of mammalian circular RNAs. Genome Biol *15*, 409.

Haery, L., Deverman, B.E., Matho, K.S., Cetin, A., Woodard, K., Cepko, C., Guerin, K.I., Rego, M.A., Ersing, I., Bachle, S.M.*, et al.* (2019). Adeno-Associated Virus Technologies and Methods for Targeted Neuronal Manipulation. Front Neuroanat *13*, 93.

Hall, H., Medina, P., Cooper, D.A., Escobedo, S.E., Rounds, J., Brennan, K.J., Vincent, C., Miura, P., Doerge, R., and Weake, V.M. (2017). Transcriptome profiling of aging Drosophila photoreceptors reveals gene expression trends that correlate with visual senescence. BMC Genomics *18*, 894.

Han, S.K., Lee, D., Lee, H., Kim, D., Son, H.G., Yang, J.S., Lee, S.V., and Kim, S. (2016). OASIS 2: online application for survival analysis 2 with features for the analysis of maximal lifespan and healthspan in aging research. Oncotarget *7*, 56147-56152.

Hansen, T.B., Jensen, T.I., Clausen, B.H., Bramsen, J.B., Finsen, B., Damgaard, C.K., and Kjems, J. (2013). Natural RNA circles function as efficient microRNA sponges. Nature *495*, 384-388.

Hansen, T.B., Wiklund, E.D., Bramsen, J.B., Villadsen, S.B., Statham, A.L., Clark, S.J., and Kjems, J. (2011). miRNA-dependent gene silencing involving Ago2-mediated cleavage of a circular antisense RNA. EMBO J *30*, 4414-4422.

Harashima, A., Guettouche, T., and Barber, G.N. (2010). Phosphorylation of the NFAR proteins by the dsRNA-dependent protein kinase PKR constitutes a

novel mechanism of translational regulation and cellular defense. Genes Dev *24*, 2640-2653.

Harries, L.W., Hernandez, D., Henley, W., Wood, A.R., Holly, A.C., Bradley-Smith, R.M., Yaghootkar, H., Dutta, A., Murray, A., Frayling, T.M.*, et al.* (2011). Human aging is characterized by focused changes in gene expression and deregulation of alternative splicing. Aging Cell *10*, 868-878.

Heinzen, E.L., Yoon, W., Tate, S.K., Sen, A., Wood, N.W., Sisodiya, S.M., and Goldstein, D.B. (2007). Nova2 interacts with a cis-acting polymorphism to influence the proportions of drug-responsive splice variants of SCN1A. Am J Hum Genet *80*, 876-883.

Holdt, L.M., Sass, K., Gabel, G., Bergert, H., Thiery, J., and Teupser, D. (2011). Expression of Chr9p21 genes CDKN2B (p15(INK4b)), CDKN2A (p16(INK4a), p14(ARF)) and MTAP in human atherosclerotic plaque. Atherosclerosis *214*, 264-270.

Holdt, L.M., Stahringer, A., Sass, K., Pichler, G., Kulak, N.A., Wilfert, W., Kohlmaier, A., Herbst, A., Northoff, B.H., Nicolaou, A.*, et al.* (2016). Circular non-coding RNA ANRIL modulates ribosomal RNA maturation and atherosclerosis in humans. Nat Commun *7*, 12429.

Hollensen, A.K., Thomsen, H.S., Lloret-Llinares, M., Kamstrup, A.B., Jensen, J.M., Luckmann, M., Birkmose, N., Palmfeldt, J., Jensen, T.H., Hansen, T.B.*, et al.* (2020). circZNF827 nucleates a transcription inhibitory complex to balance neuronal differentiation. Elife *9*.

Huang, A., Zheng, H., Wu, Z., Chen, M., and Huang, Y. (2020). Circular RNA-protein interactions: functions, mechanisms, and identification. Theranostics *10*, 3503-3517.

Huang, G., Zhu, H., Shi, Y., Wu, W., Cai, H., and Chen, X. (2015). cir-ITCH plays an inhibitory role in colorectal cancer by regulating the Wnt/beta-catenin pathway. PLoS One *10*, e0131225.

Huang, R., Zhang, Y., Han, B., Bai, Y., Zhou, R., Gan, G., Chao, J., Hu, G., and Yao, H. (2017). Circular RNA HIPK2 regulates astrocyte activation via cooperation of autophagy and ER stress by targeting MIR124-2HG. Autophagy *13*, 1722-1741.

Hundley, H.A., Krauchuk, A.A., and Bass, B.L. (2008). C. elegans and H. sapiens mRNAs with edited 3' UTRs are present on polysomes. RNA *14*, 2050-2060.

Ivanov, A., Memczak, S., Wyler, E., Torti, F., Porath, H.T., Orejuela, M.R., Piechotta, M., Levanon, E.Y., Landthaler, M., Dieterich, C.*, et al.* (2015). Analysis of intron sequences reveals hallmarks of circular RNA biogenesis in animals. Cell Rep *10*, 170-177.

Jeck, W.R., Sorrentino, J.A., Wang, K., Slevin, M.K., Burd, C.E., Liu, J., Marzluff, W.F., and Sharpless, N.E. (2013). Circular RNAs are abundant, conserved, and associated with ALU repeats. RNA *19*, 141-157.

Jensen, K.B., Dredge, B.K., Stefani, G., Zhong, R., Buckanovich, R.J., Okano, H.J., Yang, Y.Y., and Darnell, R.B. (2000a). Nova-1 regulates neuron-

specific alternative splicing and is essential for neuronal viability. Neuron *25*, 359-371.

Jensen, K.B., Musunuru, K., Lewis, H.A., Burley, S.K., and Darnell, R.B. (2000b). The tetranucleotide UCAY directs the specific recognition of RNA by the Nova K-homology 3 domain. Proc Natl Acad Sci U S A *97*, 5740-5745.

Ji, P., Wu, W., Chen, S., Zheng, Y., Zhou, L., Zhang, J., Cheng, H., Yan, J., Zhang, S., Yang, P.*, et al.* (2019). Expanded Expression Landscape and Prioritization of Circular RNAs in Mammals. Cell Rep *26*, 3444-3460 e3445.

Kaletsky, R., Yao, V., Williams, A., Runnels, A.M., Tadych, A., Zhou, S., Troyanskaya, O.G., and Murphy, C.T. (2018). Transcriptome analysis of adult Caenorhabditis elegans cells reveals tissue-specific gene and isoform expression. PLoS Genet *14*, e1007559.

Kelemen, O., Convertini, P., Zhang, Z., Wen, Y., Shen, M., Falaleeva, M., and Stamm, S. (2013). Function of alternative splicing. Gene *514*, 1-30.

Kim, D., Langmead, B., and Salzberg, S.L. (2015). HISAT: a fast spliced aligner with low memory requirements. Nat Methods *12*, 357-360.

Kim, D., Paggi, J.M., Park, C., Bennett, C., and Salzberg, S.L. (2019). Graph-based genome alignment and genotyping with HISAT2 and HISAT-genotype. Nat Biotechnol *37*, 907-915.

Kim, H., Ishidate, T., Ghanta, K.S., Seth, M., Conte, D., Jr., Shirayama, M., and Mello, C.C. (2014). A co-CRISPR strategy for efficient genome editing in Caenorhabditis elegans. Genetics *197*, 1069-1080.

Kim, U., Wang, Y., Sanford, T., Zeng, Y., and Nishikura, K. (1994). Molecular cloning of cDNA for double-stranded RNA adenosine deaminase, a candidate enzyme for nuclear RNA editing. Proc Natl Acad Sci U S A *91*, 11457-11461.

Kleaveland, B., Shi, C.Y., Stefano, J., and Bartel, D.P. (2018). A Network of Noncoding Regulatory RNAs Acts in the Mammalian Brain. Cell *174*, 350-362 e317.

Knupp, D., Cooper, D.A., Saito, Y., Darnell, R.B., and Miura, P. (2021). NOVA2 regulates neural circRNA biogenesis. Nucleic Acids Res *49*, 6849-6862.

Knupp, D., and Miura, P. (2018). CircRNA accumulation: A new hallmark of aging? Mech Ageing Dev *173*, 71-79.

Kramer, M.C., Liang, D., Tatomer, D.C., Gold, B., March, Z.M., Cherry, S., and Wilusz, J.E. (2015). Combinatorial control of Drosophila circular RNA expression by intronic repeats, hnRNPs, and SR proteins. Genes Dev *29*, 2168-2182.

Kwiatkowski, T.J., Jr., Bosco, D.A., Leclerc, A.L., Tamrazian, E., Vanderburg, C.R., Russ, C., Davis, A., Gilchrist, J., Kasarskis, E.J., Munsat, T.*, et al.* (2009). Mutations in the FUS/TLS gene on chromosome 16 cause familial amyotrophic lateral sclerosis. Science *323*, 1205-1208.

Lakhina, V., Arey, R.N., Kaletsky, R., Kauffman, A., Stein, G., Keyes, W., Xu, D., and Murphy, C.T. (2015). Genome-wide functional analysis of CREB/long-term memory-dependent transcription reveals distinct basal and memory gene expression programs. Neuron *85*, 330-345.

Langmead, B., and Salzberg, S.L. (2012). Fast gapped-read alignment with Bowtie 2. Nat Methods *9*, 357-359.

Leggere, J.C., Saito, Y., Darnell, R.B., Tessier-Lavigne, M., Junge, H.J., and Chen, Z. (2016). NOVA regulates Dcc alternative splicing during neuronal migration and axon guidance in the spinal cord. Elife *5*, e14264.

Legnini, I., Di Timoteo, G., Rossi, F., Morlando, M., Briganti, F., Sthandier, O., Fatica, A., Santini, T., Andronache, A., Wade, M.*, et al.* (2017). Circ-ZNF609 Is a Circular RNA that Can Be Translated and Functions in Myogenesis. Mol Cell *66*, 22-37 e29.

Lenzi, J., De Santis, R., de Turris, V., Morlando, M., Laneve, P., Calvo, A., Caliendo, V., Chio, A., Rosa, A., and Bozzoni, I. (2015). ALS mutant FUS proteins are recruited into stress granules in induced pluripotent stem cell-derived motoneurons. Dis Model Mech *8*, 755-766.

Lewis, H.A., Musunuru, K., Jensen, K.B., Edo, C., Chen, H., Darnell, R.B., and Burley, S.K. (2000). Sequence-specific RNA binding by a Nova KH domain: implications for paraneoplastic disease and the fragile X syndrome. Cell *100*, 323-332.

Li, X., Liu, C.X., Xue, W., Zhang, Y., Jiang, S., Yin, Q.F., Wei, J., Yao, R.W., Yang, L., and Chen, L.L. (2017a). Coordinated circRNA Biogenesis and Function with NF90/NF110 in Viral Infection. Mol Cell *67*, 214-227 e217.

Li, X., Liu, S., Zhang, L., Issaian, A., Hill, R.C., Espinosa, S., Shi, S., Cui, Y., Kappel, K., Das, R.*, et al.* (2019). A unified mechanism for intron and exon definition and back-splicing. Nature *573*, 375-380.

Li, X., Yang, L., and Chen, L.L. (2018). The Biogenesis, Functions, and Challenges of Circular RNAs. Mol Cell *71*, 428-442.

Li, Y., Zheng, F., Xiao, X., Xie, F., Tao, D., Huang, C., Liu, D., Wang, M., Wang, L., Zeng, F.*, et al.* (2017b). CircHIPK3 sponges miR-558 to suppress heparanase expression in bladder cancer cells. EMBO Rep *18*, 1646-1659.

Li, Z., Huang, C., Bao, C., Chen, L., Lin, M., Wang, X., Zhong, G., Yu, B., Hu, W., Dai, L.*, et al.* (2015). Exon-intron circular RNAs regulate transcription in the nucleus. Nat Struct Mol Biol *22*, 256-264.

Liang, D., Tatomer, D.C., Luo, Z., Wu, H., Yang, L., Chen, L.L., Cherry, S., and Wilusz, J.E. (2017). The Output of Protein-Coding Genes Shifts to Circular RNAs When the Pre-mRNA Processing Machinery Is Limiting. Mol Cell *68*, 940-954 e943.

Liang, D., and Wilusz, J.E. (2014). Short intronic repeat sequences facilitate circular RNA production. Genes Dev *28*, 2233-2247.

Liao, Y., Smyth, G.K., and Shi, W. (2014). featureCounts: an efficient general purpose program for assigning sequence reads to genomic features. Bioinformatics *30*, 923-930.

Licatalosi, D.D., and Darnell, R.B. (2006). Splicing regulation in neurologic disease. Neuron *52*, 93-101.

Liu, B., Ye, B., Zhu, X., Yang, L., Li, H., Liu, N., Zhu, P., Lu, T., He, L., Tian, Y.*, et al.* (2020). An inducible circular RNA circKcnt2 inhibits ILC3 activation to facilitate colitis resolution. Nat Commun *11*, 4076.

Liu, C., Yao, M.D., Li, C.P., Shan, K., Yang, H., Wang, J.J., Liu, B., Li, X.M., Yao, J., Jiang, Q.*, et al.* (2017). Silencing Of Circular RNA-ZNF609 Ameliorates Vascular Endothelial Dysfunction. Theranostics *7*, 2863-2877.

Liu, C.X., Li, X., Nan, F., Jiang, S., Gao, X., Guo, S.K., Xue, W., Cui, Y., Dong, K., Ding, H.*, et al.* (2019). Structure and Degradation of Circular RNAs Regulate PKR Activation in Innate Immunity. Cell *177*, 865-880 e821.

Liu, D., Conn, V., Goodall, G.J., and Conn, S.J. (2018). A Highly Efficient Strategy for Overexpressing circRNAs. Methods Mol Biol *1724*, 97-105.

Love, M.I., Huber, W., and Anders, S. (2014). Moderated estimation of fold change and dispersion for RNA-seq data with DESeq2. Genome Biol *15*, 550.

Luque, F.A., Furneaux, H.M., Ferziger, R., Rosenblum, M.K., Wray, S.H., Schold, S.C., Jr., Glantz, M.J., Jaeckle, K.A., Biran, H., Lesser, M.*, et al.* (1991). Anti-Ri: an antibody associated with paraneoplastic opsoclonus and breast cancer. Ann Neurol *29*, 241-251.

Mahmoudi, E., and Cairns, M.J. (2019). Circular RNAs are temporospatially regulated throughout development and ageing in the rat. Sci Rep *9*, 2564.

Matera, A.G., and Wang, Z. (2014). A day in the life of the spliceosome. Nat Rev Mol Cell Biol *15*, 108-121.

Mazin, P., Xiong, J., Liu, X., Yan, Z., Zhang, X., Li, M., He, L., Somel, M., Yuan, Y., Phoebe Chen, Y.P.*, et al.* (2013). Widespread splicing changes in human brain development and aging. Mol Syst Biol *9*, 633.

Memczak, S., Jens, M., Elefsinioti, A., Torti, F., Krueger, J., Rybak, A., Maier, L., Mackowiak, S.D., Gregersen, L.H., Munschauer, M.*, et al.* (2013). Circular RNAs are a large class of animal RNAs with regulatory potency. Nature *495*, 333-338.

Merkin, J., Russell, C., Chen, P., and Burge, C.B. (2012). Evolutionary dynamics of gene and isoform regulation in Mammalian tissues. Science *338*, 1593-1599.

Molyneaux, B.J., Goff, L.A., Brettler, A.C., Chen, H.H., Hrvatin, S., Rinn, J.L., and Arlotta, P. (2015). DeCoN: genome-wide analysis of in vivo transcriptional dynamics during pyramidal neuron fate selection in neocortex. Neuron *85*, 275-288.

Nallagatla, S.R., Toroney, R., and Bevilacqua, P.C. (2011). Regulation of innate immunity through RNA structure and the protein kinase PKR. Curr Opin Struct Biol *21*, 119-127.

Niethamer, T.K., and Bush, J.O. (2019). Getting direction(s): The Eph/ephrin signaling system in cell positioning. Dev Biol *447*, 42-57.

Nigro, J.M., Cho, K.R., Fearon, E.R., Kern, S.E., Ruppert, J.M., Oliner, J.D., Kinzler, K.W., and Vogelstein, B. (1991). Scrambled exons. Cell *64*, 607-613.

O'Connell, M.A., Krause, S., Higuchi, M., Hsuan, J.J., Totty, N.F., Jenny, A., and Keller, W. (1995). Cloning of cDNAs encoding mammalian double-stranded RNA-specific adenosine deaminase. Mol Cell Biol *15*, 1389-1397.

Pamudurti, N.R., Bartok, O., Jens, M., Ashwal-Fluss, R., Stottmeister, C., Ruhe, L., Hanan, M., Wyler, E., Perez-Hernandez, D., Ramberger, E.*, et al.* (2017). Translation of CircRNAs. Mol Cell *66*, 9-21 e27.

Pamudurti, N.R., Patop, I.L., Krishnamoorthy, A., Ashwal-Fluss, R., Bartok, O., and Kadener, S. (2020). An in vivo strategy for knockdown of circular RNAs. Cell Discov *6*, 52.

Pan, Q., Shai, O., Lee, L.J., Frey, B.J., and Blencowe, B.J. (2008). Deep surveying of alternative splicing complexity in the human transcriptome by high-throughput sequencing. Nat Genet *40*, 1413-1415.

Panda, A.C., De, S., Grammatikakis, I., Munk, R., Yang, X., Piao, Y., Dudekula, D.B., Abdelmohsen, K., and Gorospe, M. (2017). High-purity circular RNA isolation method (RPAD) reveals vast collection of intronic circRNAs. Nucleic Acids Res *45*, e116.

Pees, B., Yang, W., Zarate-Potes, A., Schulenburg, H., and Dierking, K. (2016). High Innate Immune Specificity through Diversified C-Type Lectin-Like Domain Proteins in Invertebrates. J Innate Immun *8*, 129-142.

Pfeifer, I., Elsby, R., Fernandez, M., Faria, P.A., Nussenzveig, D.R., Lossos, I.S., Fontoura, B.M., Martin, W.D., and Barber, G.N. (2008). NFAR-1 and -2 modulate translation and are required for efficient host defense. Proc Natl Acad Sci U S A *105*, 4173-4178.

Piwecka, M., Glazar, P., Hernandez-Miranda, L.R., Memczak, S., Wolf, S.A., Rybak-Wolf, A., Filipchyk, A., Klironomos, F., Cerda Jara, C.A., Fenske, P.*, et al.* (2017). Loss of a mammalian circular RNA locus causes miRNA deregulation and affects brain function. Science *357*.

Qu, K., Garamszegi, S., Wu, F., Thorvaldsdottir, H., Liefeld, T., Ocana, M., Borges-Rivera, D., Pochet, N., Robinson, J.T., Demchak, B.*, et al.* (2016). Integrative genomic analysis by interoperation of bioinformatics tools in GenomeSpace. Nat Methods *13*, 245-247.

Rodriguez, S.A., Grochova, D., McKenna, T., Borate, B., Trivedi, N.S., Erdos, M.R., and Eriksson, M. (2016). Global genome splicing analysis reveals an increased number of alternatively spliced genes with aging. Aging Cell *15*, 267-278.

Ruggiu, M., Herbst, R., Kim, N., Jevsek, M., Fak, J.J., Mann, M.A., Fischbach, G., Burden, S.J., and Darnell, R.B. (2009). Rescuing Z+ agrin splicing in Nova null mice restores synapse formation and unmasks a physiologic defect in motor neuron firing. Proc Natl Acad Sci U S A *106*, 3513-3518.

Rybak-Wolf, A., Stottmeister, C., Glazar, P., Jens, M., Pino, N., Giusti, S., Hanan, M., Behm, M., Bartok, O., Ashwal-Fluss, R.*, et al.* (2015). Circular RNAs in the Mammalian Brain Are Highly Abundant, Conserved, and Dynamically Expressed. Mol Cell *58*, 870-885.

Saito, Y., Miranda-Rottmann, S., Ruggiu, M., Park, C.Y., Fak, J.J., Zhong, R., Duncan, J.S., Fabella, B.A., Junge, H.J., Chen, Z.*, et al.* (2016). NOVA2-mediated RNA regulation is required for axonal pathfinding during development. Elife *5*.

Saito, Y., Yuan, Y., Zucker-Scharff, I., Fak, J.J., Jereb, S., Tajima, Y., Licatalosi, D.D., and Darnell, R.B. (2019). Differential NOVA2-Mediated Splicing in Excitatory and Inhibitory Neurons Regulates Cortical Development and Cerebellar Function. Neuron *101*, 707-720 e705.

Salzman, J., Chen, R.E., Olsen, M.N., Wang, P.L., and Brown, P.O. (2013). Cell-type specific features of circular RNA expression. PLoS Genet *9*, e1003777.

Salzman, J., Gawad, C., Wang, P.L., Lacayo, N., and Brown, P.O. (2012). Circular RNAs are the predominant transcript isoform from hundreds of human genes in diverse cell types. PLoS One *7*, e30733.

Sekar, S., Cuyugan, L., Adkins, J., Geiger, P., and Liang, W.S. (2018). Circular RNA expression and regulatory network prediction in posterior cingulate astrocytes in elderly subjects. BMC Genomics *19*, 340.

Shan, K., Liu, C., Liu, B.H., Chen, X., Dong, R., Liu, X., Zhang, Y.Y., Liu, B., Zhang, S.J., Wang, J.J*., et al.* (2017). Circular Noncoding RNA HIPK3 Mediates Retinal Vascular Dysfunction in Diabetes Mellitus. Circulation *136*, 1629-1642.

Shen, S., Park, J.W., Lu, Z.X., Lin, L., Henry, M.D., Wu, Y.N., Zhou, Q., and Xing, Y. (2014). rMATS: robust and flexible detection of differential alternative splicing from replicate RNA-Seq data. Proc Natl Acad Sci U S A *111*, E5593-5601.

Shibayama, M., Ohno, S., Osaka, T., Sakamoto, R., Tokunaga, A., Nakatake, Y., Sato, M., and Yoshida, N. (2009). Polypyrimidine tract-binding protein is essential for early mouse development and embryonic stem cell proliferation. FEBS J *276*, 6658-6668.

Sijen, T., and Plasterk, R.H. (2003). Transposon silencing in the Caenorhabditis elegans germ line by natural RNAi. Nature *426*, 310-314.

Song, X., Zhang, N., Han, P., Moon, B.S., Lai, R.K., Wang, K., and Lu, W. (2016). Circular RNA profile in gliomas revealed by identification tool UROBORUS. Nucleic Acids Res *44*, e87.

Starke, S., Jost, I., Rossbach, O., Schneider, T., Schreiner, S., Hung, L.H., and Bindereif, A. (2015). Exon circularization requires canonical splice signals. Cell Rep *10*, 103-111.

Stein, L.D., Bao, Z., Blasiar, D., Blumenthal, T., Brent, M.R., Chen, N., Chinwalla, A., Clarke, L., Clee, C., Coghlan, A*., et al.* (2003). The genome sequence of Caenorhabditis briggsae: a platform for comparative genomics. PLoS Biol *1*, E45.

Stoll, L., Sobel, J., Rodriguez-Trejo, A., Guay, C., Lee, K., Veno, M.T., Kjems, J., Laybutt, D.R., and Regazzi, R. (2018). Circular RNAs as novel regulators of beta-cell functions in normal and disease conditions. Mol Metab *9*, 69-83.

Suenkel, C., Cavalli, D., Massalini, S., Calegari, F., and Rajewsky, N. (2020). A Highly Conserved Circular RNA Is Required to Keep Neural Cells in a Progenitor State in the Mammalian Brain. Cell Rep *30*, 2170-2179 e2175.

Sulston, J.E., and Horvitz, H.R. (1977). Post-embryonic cell lineages of the nematode, Caenorhabditis elegans. Dev Biol *56*, 110-156.

Sun, S., Ling, S.C., Qiu, J., Albuquerque, C.P., Zhou, Y., Tokunaga, S., Li, H., Qiu, H., Bui, A., Yeo, G.W.*, et al.* (2015). ALS-causative mutations in FUS/TLS confer gain and loss of function by altered association with SMN and U1-snRNP. Nat Commun *6*, 6171.

Szabo, L., Morey, R., Palpant, N.J., Wang, P.L., Afari, N., Jiang, C., Parast, M.M., Murry, C.E., Laurent, L.C., and Salzman, J. (2015). Statistically based splicing detection reveals neural enrichment and tissue-specific induction of circular RNA during human fetal development. Genome Biol *16*, 126.

Teplova, M., Hafner, M., Teplov, D., Essig, K., Tuschl, T., and Patel, D.J. (2013). Structure-function studies of STAR family Quaking proteins bound to their in vivo RNA target sites. Genes Dev *27*, 928-940.

Teplova, M., Malinina, L., Darnell, J.C., Song, J., Lu, M., Abagyan, R., Musunuru, K., Teplov, A., Burley, S.K., Darnell, R.B.*, et al.* (2011). Protein-RNA and protein-protein recognition by dual KH1/2 domains of the neuronal splicing factor Nova-1. Structure *19*, 930-944.

Tonkin, L.A., Saccomanno, L., Morse, D.P., Brodigan, T., Krause, M., and Bass, B.L. (2002). RNA editing by ADARs is important for normal behavior in Caenorhabditis elegans. EMBO J *21*, 6025-6035.

Vance, C., Rogelj, B., Hortobagyi, T., De Vos, K.J., Nishimura, A.L., Sreedharan, J., Hu, X., Smith, B., Ruddy, D., Wright, P.*, et al.* (2009). Mutations in FUS, an RNA processing protein, cause familial amyotrophic lateral sclerosis type 6. Science *323*, 1208-1211.

Veno, M.T., Hansen, T.B., Veno, S.T., Clausen, B.H., Grebing, M., Finsen, B., Holm, I.E., and Kjems, J. (2015). Spatio-temporal regulation of circular RNA expression during porcine embryonic brain development. Genome Biol *16*, 245.

Vo, J.N., Cieslik, M., Zhang, Y., Shukla, S., Xiao, L., Zhang, Y., Wu, Y.M., Dhanasekaran, S.M., Engelke, C.G., Cao, X.*, et al.* (2019). The Landscape of Circular RNA in Cancer. Cell *176*, 869-881 e813.

Vuong, C.K., Black, D.L., and Zheng, S. (2016). The neurogenetics of alternative splicing. Nat Rev Neurosci *17*, 265-281.

Wang, E.T., Sandberg, R., Luo, S., Khrebtukova, I., Zhang, L., Mayr, C., Kingsmore, S.F., Schroth, G.P., and Burge, C.B. (2008). Alternative isoform regulation in human tissue transcriptomes. Nature *456*, 470-476.

Wang, P.L., Bao, Y., Yee, M.C., Barrett, S.P., Hogan, G.J., Olsen, M.N., Dinneny, J.R., Brown, P.O., and Salzman, J. (2014). Circular RNA is expressed across the eukaryotic tree of life. PLoS One *9*, e90859.

Weigelt, C.M., Sehgal, R., Tain, L.S., Cheng, J., Esser, J., Pahl, A., Dieterich, C., Gronke, S., and Partridge, L. (2020). An Insulin-Sensitive Circular RNA that Regulates Lifespan in Drosophila. Mol Cell *79*, 268-279 e265.

Westholm, J.O., Miura, P., Olson, S., Shenker, S., Joseph, B., Sanfilippo, P., Celniker, S.E., Graveley, B.R., and Lai, E.C. (2014). Genome-wide analysis of drosophila circular RNAs reveals their structural and sequence properties and age-dependent neural accumulation. Cell Rep *9*, 1966-1980.

Wickham, H. (2016). ggplot2: Elegant Graphics for Data Analysis (Springer-Verlag New York).

Will, C.L., and Luhrmann, R. (2011). Spliceosome structure and function. Cold Spring Harb Perspect Biol *3*.

Xia, P., Wang, S., Ye, B., Du, Y., Li, C., Xiong, Z., Qu, Y., and Fan, Z. (2018). A Circular RNA Protects Dormant Hematopoietic Stem Cells from DNA Sensor cGAS-Mediated Exhaustion. Immunity *48*, 688-701 e687.

Xin, R., Gao, Y., Gao, Y., Wang, R., Kadash-Edmondson, K.E., Liu, B., Wang, Y., Lin, L., and Xing, Y. (2021). isoCirc catalogs full-length circular RNA isoforms in human transcriptomes. Nat Commun *12*, 266.

Xu, K., Chen, D., Wang, Z., Ma, J., Zhou, J., Chen, N., Lv, L., Zheng, Y., Hu, X., Zhang, Y.*, et al.* (2018). Annotation and functional clustering of circRNA expression in rhesus macaque brain during aging. Cell Discov *4*, 48.

Yang, Y., Fan, X., Mao, M., Song, X., Wu, P., Zhang, Y., Jin, Y., Yang, Y., Chen, L.L., Wang, Y.*, et al.* (2017). Extensive translation of circular RNAs driven by N(6)-methyladenosine. Cell Res *27*, 626-641.

Yang, Y.Y., Yin, G.L., and Darnell, R.B. (1998). The neuronal RNA-binding protein Nova-2 is implicated as the autoantigen targeted in POMA patients with dementia. Proc Natl Acad Sci U S A *95*, 13254-13259.

Yano, M., Hayakawa-Yano, Y., Mele, A., and Darnell, R.B. (2010). Nova2 regulates neuronal migration through an RNA switch in disabled-1 signaling. Neuron *66*, 848-858.

You, X., Vlatkovic, I., Babic, A., Will, T., Epstein, I., Tushev, G., Akbalik, G., Wang, M., Glock, C., Quedenau, C.*, et al.* (2015). Neural circular RNAs are derived from synaptic genes and regulated by development and plasticity. Nat Neurosci *18*, 603-610.

Yu, C.Y., Li, T.C., Wu, Y.Y., Yeh, C.H., Chiang, W., Chuang, C.Y., and Kuo, H.C. (2017). The circular RNA circBIRC6 participates in the molecular circuitry controlling human pluripotency. Nat Commun *8*, 1149.

Zhang, C., and Darnell, R.B. (2011). Mapping in vivo protein-RNA interactions at single-nucleotide resolution from HITS-CLIP data. Nat Biotechnol *29*, 607-614.

Zhang, X.O., Wang, H.B., Zhang, Y., Lu, X., Chen, L.L., and Yang, L. (2014). Complementary sequence-mediated exon circularization. Cell *159*, 134-147.

Zhang, Y., Xue, W., Li, X., Zhang, J., Chen, S., Zhang, J.L., Yang, L., and Chen, L.L. (2016). The Biogenesis of Nascent Circular RNAs. Cell Rep *15*, 611-624.

Zheng, Q., Bao, C., Guo, W., Li, S., Chen, J., Chen, B., Luo, Y., Lyu, D., Li, Y., Shi, G.*, et al.* (2016). Circular RNA profiling reveals an abundant circHIPK3 that regulates cell growth by sponging multiple miRNAs. Nat Commun *7*, 11215.

Zheng, X., and Bevilacqua, P.C. (2004). Activation of the protein kinase PKR by short double-stranded RNAs with single-stranded tails. RNA *10*, 1934-1945.

Zhou, T., Xie, X., Li, M., Shi, J., Zhou, J.J., Knox, K.S., Wang, T., Chen, Q., and Gu, W. (2018). Rat BodyMap transcriptomes reveal unique circular RNA

features across tissue types and developmental stages. RNA *24*, 1443-1456.

Zhu, P., Zhu, X., Wu, J., He, L., Lu, T., Wang, Y., Liu, B., Ye, B., Sun, L., Fan, D.*, et al.* (2019). IL-13 secreted by ILC2s promotes the self-renewal of intestinal stem cells through circular RNA circPan3. Nat Immunol *20*, 183-194.

Zimmerman, A.J., Hafez, A.K., Amoah, S.K., Rodriguez, B.A., Dell'Orco, M., Lozano, E., Hartley, B.J., Alural, B., Lalonde, J., Chander, P.*, et al.* (2020). A psychiatric disease-related circular RNA controls synaptic gene expression and cognition. Mol Psychiatry.

Appendix I

Published online 22 June 2021 *Nucleic Acids Research, 2021, Vol. 49, No. 12* ***6849–6862***
https://doi.org/10.1093/nar/gkab523

NOVA2 regulates neural circRNA biogenesis

David Knupp[1], Daphne A. Cooper[1], Yuhki Saito[2], Robert B. Darnell[2] and Pedro Miura[1,*]

[1]Department of Biology, University of Nevada, Reno, Reno, NV 89557, USA and [2]Laboratory of Molecular Neuro-oncology and Howard Hughes Medical Institute, The Rockefeller University, New York, NY 10065, USA

Received May 22, 2020; Revised May 03, 2021; Editorial Decision June 02, 2021; Accepted June 09, 2021

ABSTRACT

Circular RNAs (circRNAs) are highly expressed in the brain and their expression increases during neuronal differentiation. The factors regulating circRNAs in the developing mouse brain are unknown. NOVA1 and NOVA2 are neural-enriched RNA-binding proteins with well-characterized roles in alternative splicing. Profiling of circRNAs from RNA-seq data revealed that global circRNA levels were reduced in embryonic cortex of *Nova2* but not *Nova1* knockout mice. Analysis of isolated inhibitory and excitatory cortical neurons lacking NOVA2 revealed an even more dramatic reduction of circRNAs and establishes a widespread role for NOVA2 in enhancing circRNA biogenesis. To investigate the *cis*-elements controlling NOVA2-regulation of circRNA biogenesis, we generated a backsplicing reporter based on the *Efnb2* gene. We found that NOVA2-mediated backsplicing of circ*Efnb2* was impaired when YCAY clusters located in flanking introns were mutagenized. CLIP (cross-linking and immunoprecipitation) and additional reporter analyses demonstrated the importance of NOVA2 binding sites located in both flanking introns of circRNA loci. NOVA2 is the first RNA-binding protein identified to globally promote circRNA biogenesis in the developing brain.

INTRODUCTION

Alternative splicing (AS) affects ∼95% of human multi-exon genes (1). Through AS, hundreds of thousands of RNA isoforms with distinct structural properties, localization patterns, and translation efficiencies can be expressed as protein isoforms with diverse functions (2). In the mammalian nervous system, AS is especially pervasive and highly conserved (3,4). During brain development, AS is responsible for establishing neuron-specific splicing patterns at defined stages, and developmentally regulated alternative exons have essential roles in synapse formation, neuronal migration and axon guidance (5–8). Stage-specific AS patterns during development are controlled by RNA binding proteins (RBPs) enriched or specifically expressed in neurons and are critical for proper development as their dysregulation underlies many neurological disorders (9–13).

Circular RNAs (circRNAs) are generated through backsplicing, a type of AS (14). During backsplicing, the downstream 5′ splice site (SS) covalently bonds the upstream 3′ SS of a circularizing exon creating a closed loop 'circle' that is resistant to exoribonuclease digestion (14). Most characterized circRNAs are derived from annotated exons of protein-coding genes, and many are independently regulated from their host genes and exhibit unique expression patterns over various time-points (15). Thus far, ascribed circRNA functions include sequestration of microRNAs, translation of small peptides, modulation of the immune response, and transportation and scaffolding of RBPs (16–26). CircRNAs are enriched in brain tissues on a genome-wide level (27–30) and are dramatically upregulated during neural differentiation and maturation (15,29,30). CircRNAs are also found to accumulate during aging and this trend appears to be specific to brain tissues and neurons (31–33). The functional significance of brain-expressed circRNAs is emerging, with only a handful of circRNAs found to have roles in the nervous system (34–36).

Several RBPs have been identified to regulate circRNA biogenesis, including Muscleblind, Quaking (QKI), ADAR, FUS and several hnRNPs and SR proteins (37–41). However, investigation of circRNA regulation by RBPs from *in vivo* brain or neuron datasets is lacking. There are several well-characterized splicing factors with roles in the nervous system including RBFOX1/2/3, PTPBP1/2, nrSR100/Srrm4, Hu proteins and NOVA1/2 (8). Deletion or dysregulation of any of these splicing factors results in serious and often lethal neurological defects (8). Among the best characterized neural-enriched splicing factors are the NOVA proteins, which were originally discovered as autoantigens in patients with paraneoplastic opsoclonus-myoclonus ataxia, a neurological condition characterized by motor and cognitive defects (42–44). NOVA1 and NOVA2 are paralogues that bind clusters of YCAY motifs to regulate AS (45–47). Knockout (KO) of either paralogue in mice results in early lethality. This has been attributed to death of motor neurons in the case of NOVA1 deficiency, and aberrant migration of cortical and Purkinje neurons in the case of NOVA2 (13,48–50). Although both proteins

*To whom correspondence should be addressed. Tel: +1 775 682 7004; Fax: +1 775 784 1302; Email: pmiura@unr.edu

recognize the same RNA binding motif, their expression is largely reciprocal. For instance, immunohistochemical and *in situ* hybridization data indicate NOVA2 is lowly expressed in midbrain and spinal cord, whereas high expression is observed in the cortex and hippocampus. In contrast, NOVA1 is highly expressed in the midbrain and spinal cord and is relatively low expressed in the cortex (13,44). Furthermore, NOVA1 and NOVA2 appear to control different splicing regulatory networks in the developing cortex (13). More recently, conditional knockout (cKO) of NOVA2 in either excitatory (Emx1+) or inhibitory (Gad2+) neurons led to thousands of AS events that were largely unique to each cell-type (50). In addition, loss of NOVA2 in excitatory neurons resulted in disorganization of cortical and hippocampal laminar structures, whereas this was not observed in NOVA2-KO inhibitory neurons. These findings showcase the importance of examining AS outcomes among different neuron subtypes.

Here, we examined circRNA expression in RNA-Seq data from mouse cortex samples lacking NOVA1 or NOVA2. We found that the absence of NOVA2 caused a reduction in global circRNA levels. In sorted excitatory and inhibitory neurons, NOVA2 loss was found to dramatically reduce circRNA expression. These changes in circRNA levels were largely independent from transcriptional changes or changes in linear alternative splicing. Using CLIP data and backsplicing reporter analysis, we found that NOVA2 binding sites in the introns flanking circRNA exons are important for NOVA-2 mediated circRNA biogenesis.

MATERIALS AND METHODS

Accession numbers

Wild-Type (WT), *Nova1-KO* and *Nova2-KO* whole cortex RNA-seq data were obtained from Gene Expression Omnibus (GEO) under accession number GSE69711. Fluorescence-activated cell sorted (FACS) sorted *Nova2*-KO neuron RNA-seq datasets were obtained from GEO under accession number GSE103316. For individual Sequence Read Archive (SRA) accession numbers see Supplementary File S1.

Mouse tissue preparation, RNA extraction, RNaseR Treatment and RT-qPCR

All procedures in mice were performed in compliance with protocols approved by the Institutional Animal Care and Use Committee (IACUC) of the Rockefeller University or the University of Nevada, Reno. Mouse tissue samples were pulverized using a mortar and pestle on dry ice, and RNA was extracted using Trizol (ThermoFisher Scientific). For harvesting cultured cells PBS washes were performed followed by Trizol extraction. For RNase R treatment, 100μg total RNA from cortex or cultured HEK293 cells was treated with or without 1 μl of RNaseR [20 U/μl] (Lucigen), plus 1.9 μl RNaseOUT [40 U/μl] (ThermoFisher Scientific) and 1 μl Turbo-DNase [2 U/μl] (Invitrogen) in a 60 μl reaction volume for 30 min at 37°C. RNase R reactions were terminated and RNA was purified as previously described (51). Equal amounts of RNase R or mock treated RNA served as input for cDNA preparation. PolyA+ RNA and polyA− RNA was obtained using previously described methods (51). Briefly, the NucleoTrap mRNA column-based kit (Machery-Nagel) was used according to the manufacturers protocol. RNA present in the flow-through (not bound to oligo(dT) beads) was precipitated to isolate the polyA− fraction. For RT-qPCR experiments, Turbo-DNase (Invitrogen) treated RNA was reverse transcribed using random hexamers (Invitrogen) and Maxima reverse transcriptase (ThermoFisher Scientific) according to the manufacturer's specifications. RT-qPCR was performed on a BioRad CFX96 real time PCR machine using SYBR select mastermix for CFX (Applied Biosystems). The delta delta Ct method was used for quantification. Target gene expression for both circRNA and host-mRNA expression was normalized to *Gapdh*. Experiments were performed using biological triplicates. Student's *t*-test (two-tailed and unpaired) was used to test for statistical significance.

Cell culture

HEK293 cells (ATCC) were cultured in DMEM (ThermoFisher Scientific) with 10% FBS (Atlanta Biologicals). HEK293 cells were transfected with NOVA2 expression plasmid or empty vector control (Gifts from Dr Zhe Chen at University of Minnesota) in addition to the circ*Efnb2* or circ*Mini* backsplicing reporters, using PEI transfection reagent (Polysciences), and reduced serum medium Opti-MEM (ThermoFisher Scientific). The cells were cultured for 24 h prior to RNA extraction.

Northern blotting

RNA samples were denatured by mixing with 3 volumes NorthernMax Formaldehyde loading dye (ThermoFisher Scientific) and ethidium bromide (10 μg/ml) for 15 min at 65°C. Denatured samples were loaded onto a 1% MOPS gel with 1× Denaturing Gel Buffer (ThermoFisher Scientific) and ran at 102V for 60 min. RNA samples were transferred to a Cytiva Whatman Nytran SuperCharge membrane (ThermoFisher Scientific) for 1.5 h using a Whatman TurboBlotter transfer system (ThermoFisher Scientific) and NorthernMax Transfer Buffer. Samples were then UV cross-linked with a Stratagene linker to the nylon membrane prior to probe hybridization. Double-stranded DNA probes were prepared by end-point PCR and labeled with dCTP [α-32P] (PerkinElmer) using the Cytvia Amersham Megaprimer labeling kit (Thermo Fisher Scientific) according to manufacturer's instructions. Blots were hybridized overnight in ULTRAhyb™ Ultrasensitive Hybridization buffer (ThermoFisher Scientific) at 42°C. Following hybridization, blots were washed at room temperature 2 × 5 min in a low-stringency buffer followed by 2 × 15 min in a high-stringency buffer at 42°C. Blots were then exposed for 4–5 days to a GE Storage Phosphor screen (Millipore Sigma) before imaging on a Typhoon™ FLA 7000 imager (GE). Probe sequences are listed in Supplementary File S9.

RNA-Seq analysis for circRNA prediction, mapping and differential expression

For *de novo* identification of circRNAs, raw FASTQ files were aligned to the mm9 genome using HISAT2 v2.1.0 (52) (parameters: –no-mixed –no-discordant). Unmapped reads were aligned using BWA v0.7.8-r455 mem and CIRI2 v2.0.4 (53) was used to obtain a set of predicted circRNA loci using default parameters. For alignment to circRNA junction spanning FASTA sequence templates of 220 nt we used Bowtie2 v2.2.5 (54) (parameters: -score-min = C,-15,0). After mapping, Picard (http://broadinstitute.github.io/picard) (parameters: MarkDuplicates ASSUME_SORTED = true REMOVE_DUPLICATES = true) was used to remove duplicate reads. To quantify the number of mapped reads for each junction we used featureCounts v1.5.0 (55) (parameters: -C -t circle_junction). mm9 circRNA coordinates were converted to mm10 genome-build using UCSC liftover tool. All supplementary data tables are reported in mm10 coordinates.

For each dataset (*Nova1*-KO versus WT, *Nova2*-KO versus WT, *Nova2*-cKO$^{tdTomato;Emx1\text{-}Cre}$ versus WT, *Nova2*-cKO$^{tdTomato;Gad2\text{-}Cre}$ versus WT) a cutoff of six reads across the six libraries for each condition (3 biological replicates per condition) was set. To account for difference in library depth among samples, scaling by circRNA Counts Per Million of reads (CPM) in each library was performed. Fold-change CPM values were generated between KO and WT conditions. A cutoff of 2.0-fold-change difference and significance threshold of $P < 0.05$ via t-test was used across the normalized CPM values to identify differentially expressed circRNAs. Correction for multiple hypothesis testing was not performed.

The CircTest pipeline was performed to quantify host gene independent circRNA expression patterns. DCC/CircTest v0.4.7 was used to quantify host gene read counts. In accordance with DCC pipeline (56), FASTQ files were mapped with STAR 2.6.0b using the recommended parameters and aligned to the GRCm38 genome. The circRNA and linear RNA counts obtained from DCC were used as input for the Circ.test module (parameters: Nreplcates = 3 filter.sample = 4 filter.count = 3 percentage = 0.1 circle_description = c(1:3)). To define a circRNA as host gene independently expressed, we used the default parameter, adj. $P < 0.05$ (Benjamini–Hochberg correction). ggplot2 (57) R packages and custom scripts were used to generate all plots.

Mapping and quantification of linear RNA expression

Reads were aligned to the NCBI37 reference genome using HISAT2 v2.1.0 (GENCODE annotations M1 release, NCBIM37, Ensembl 65). FeatureCounts v1.5.0 (parameters -t exon -g gene_id) was used to obtain a counts table as input for differential expression analysis. For differential expression analysis, DESeq2 v1.26.0 was performed using Benjamini-Hochberg correction and apeglm Bayesian shrinkage estimators with a 2.0-fold-change and adj. $P < 0.05$ required to consider a linear RNA as differentially expressed. For alternative splicing analysis, the rMATS pipeline (58) was used to calculate significant exon skipping events in *Nova2*-cKO$^{tdTomato;Emx1\text{-}Cre}$ versus WT and *Nova2*-cKO$^{tdTomato;Gad2\text{-}Cre}$ versus WT datasets. FASTQ files were mapped using STAR 2.6.0b using default parameters (parameters: –chimSegmentMin 2 –outFilterMismatchNmax 3 –alignEndsType EndToEnd –runThreadN 4 –outSAMstrandField intronMotif –outSAMtype BAM SortedByCoordinate –alignSJDBoverhang 6 –alignIntronMax 30000) and aligned to the GRCm38/mm10 genome (GENCODE annotations vM22 release). rMATs-v.3.2.5 was used to discover significant alternative splice events under the default parameters. For post processing, we filtered the output file, SE.MATS.ReadsOnTargetAndJunctionCounts.txt to contain skipping events with FDR <0.01. Mapped circRNA BED files were converted to mm10 coordinates using UCSC genome browser liftover tool. Then bedtools suite was used to find overlap with significant exon skipping events. Overlaps were manually checked using Integrative Genomics Viewer (IGV) (59).

NOVA2-CLIP analysis

cTag-CLIP data from excitatory (Emx1+) and inhibitory (Gad2+) neurons (50) were used to examine overlap with NOVA2-regulated circRNAs. Emx1+ and Gad2+ circRNAs that were NOVA2-regulated in both the CIRI2 and DCC/CircTest analyses were chosen for comparison against non-differentially expressed circRNAs (FC < 1 and $P > 0.50$) identified by CIRI2 (minimum average 3 BSJ counts per condition). First, we extracted intron coordinates from the UCSC table browser. Next, Bedtools suite was used to extract upstream and downstream introns flanking the circRNA loci. Finally, Bedtools suite was used to identify the presence or absence of intronic NOVA2-CLIP peaks (upstream/downstream or both flanking introns).

Backsplicing reporter assays

All plasmids are available upon request. The pUC19 plasmid backbone was used to generate circ*Efnb2* and circ*Mini* backsplicing reporters with modifications. Briefly, the CMV enhancer/promoter region was amplified from the pcDNA3.0 backbone using Phusion High-Fidelity Polymerase (NEB) and subcloned into the pUC19 vector upstream of the circ*Efnb2* or circ*Mini* backsplicing cassettes. In addition, BGH and rB-Globin poly(A) sequences were subcloned downstream of the backsplicing cassettes using synthetic gene fragments (gBlocks, IDT) for transcription termination. All fragments used to generate the backbone vector and subsequent backsplicing cassettes were cloned using the NEB Hifi assembly kit (NEB) following the manufacturers protocols.

For circ*Efnb2* reporter three genomic fragments were amplified by PCR using Phusion High-Fidelity Polymerase. The three genomic fragments (mm10 coordinates) are as follows: (i) truncated upstream *Efnb2* exon1 (81 bp) plus downstream flanking intron (134 bp) (chr8:8660350–8660564); (ii) circularizing *Efnb2* exon 2 (284 bp) plus partial upstream (448 bp) and downstream (475 bp) flanking introns (chr8:8638731–8639937) and (iii) truncated *Efnb2* exon 3 (72 bp) plus partial intronic upstream sequence (197

bp) (chr8:8623169–8623437); (chr8:8660350–8660564). Initial transfection experiments with circ*Efnb2*-WT demonstrated two unintended backspliced products originating from the AmpR cassette and non-coding sequence immediately downstream of the CMV promoter when examined by RT-PCR. As a result, we introduced two silent mutations into the AmpR coding sequence and deleted 115 bp of non-essential sequence between the CMV promoter and circ*Efnb2* cassette. Follow-up experiments showed all unintended backspliced products were abolished. Mutations located in the circ*Efnb2* introns were introduced by PCR amplification of the pWT backbone using Phusion High-Fidelity polymerase and ligation with gBlock donor DNA carrying point mutations targeting YCAY motifs. Mutations were confirmed by Sanger sequencing.

To generate the artificial circMini-WT vector, two gBlocks consisting of full-length GFP coding sequence, partial human *ZKSCAN1* intron sequence and partial *Mboat2* intron sequence were cloned into the modified pUC19 vector described above. We used the Berkeley Drosophila Genome Project splice prediction tool (https://www.fruitfly.org/seq_tools/splice.html) with default settings to guide GFP and intron sequence modifications that would improve splicing efficiency and prevent unintended splice products from being generated. In addition, existing YCAY motifs were mutated to prevent NOVA2 binding. Artificial 10x YCAY sequence was produced via gBlocks and were cloned 50 bp upstream (pMini-Up), 49 bp downstream (pMini-Down) or in both locations (pMini-Both) in relation to the circRNA loci.

RESULTS

Global circRNA levels are reduced in *Nova2*-KO whole cortex

To investigate potential factors that might contribute to regulation of circRNAs in the murine brain, we analyzed paired-end total RNA-seq data from embryonic *Nova1-KO* and *Nova2*-KO mouse cortex samples for changes in circRNA expression (13) (Supplementary File S1). These RNA-seq libraries were generated using random hexamer-based priming as opposed to oligo(dT) priming for cDNA synthesis, thus enabling detection of circRNAs which are not-polyadenylated. CircRNAs were identified by back-splice junction (BSJ) reads using the CIRI2 algorithm (Figure 1A). We set a minimum expression threshold of six BSJ reads across the six libraries (minimum average of 1 read per biological replicate) for each dataset, resulting in 1565 and 3708 exonic circRNAs identified for the *Nova1* and *Nova2* datasets, respectively (Supplementary Files S2 and S3). BSJ read counts were normalized to library size to obtain Counts Per Million mapped reads (CPM). Global circRNA CPM values were found to be significantly reduced in *Nova2*-KO samples compared to controls ($P < 2.48 \times 10^{-11}$, Wilcoxon-rank sum test with continuity correction) (Figure 1B). In contrast, global circRNA levels were not altered in *Nova1*-KO mice compared to controls (Figure 1B).

In order to capture expression of individual circRNAs in *Nova2*-KO cortex we generated volcano plots using *P*-value and fold-change, as previously reported (32). We observed a slight trend for downregulation in *Nova2*-KO mouse cortex compared to WT samples. From the volcano plot, it is evident that more circRNAs were downregulated than upregulated in the KO condition ($P < 0.05$, $\text{Log}_2\text{FC} > 1$) (Figure 1C). In contrast, the *Nova1*-KO dataset lacked any biased expression trend (Supplementary Figure S1A). The reduced circRNA levels in *Nova2*-KO samples could have been a consequence of reduced transcriptional activity from the host genes that the circRNAs are derived from. Thus, we performed differential expression analysis for the mRNAs generated from the host genes of the regulated circRNAs (Supplementary Figure S1B). Alignment was performed using HISAT2 (60), and DESeq2 (52) was used to perform differential expression analysis of mRNAs. No significant changes in host gene mRNA expression were detected. In addition, density plots were generated to contrast total read counts from circRNAs versus their linear RNA counterparts from the same host gene. Read counts were obtained using DCC (see Materials and Methods) (56). We observed a clear downward shift along the y-axis, reflecting reduced circRNA expression, while linear RNA expression along the x-axis centered near zero indicating only minor expression changes (Figure 1D). Together, these data suggest that NOVA2-mediated regulation of circRNA biogenesis is largely independent of host gene transcription changes.

In order to provide experimental support for the circRNA expression trends, we performed RT-qPCR confirmation for 10 circRNAs that were either reduced (seven loci) or increased (three loci) in the *Nova2*-KO condition (Figure 1E). For circRNA quantification, outward facing primers that only detect the circularized exons were used (Figure 1F). For quantification of the cognate mRNA, we employed primer sets with one primer located in an exon that is circularized and the other is located in the flanking upstream or downstream exon (Figure 1F and Supplementary File S9). Overall, we observed a good correlation between RNA-seq expression trends and our RT-qPCR results, confirming expression trends for 9/10 circRNAs and 8/10 host gene linear RNAs. In addition, we validated the circularity of these targets with RNase R, a 3′ to 5′ exoribonuclease that degrades linear RNAs while circRNAs are relatively more resistant (61). We found all 10 to be resistant to RNase R treatment, whereas the linear control transcript *Psmd4* was degraded (Supplementary Figure S1C). These experiments indicate that our sequencing analysis pipeline can detect bonafide circRNA expression changes.

Loss of NOVA2 dramatically reduces global circRNA levels in isolated neuron subpopulations

NOVA2 expression is mostly limited to neurons (44). In contrast, circRNAs are expressed in various brain cell-types such as astrocytes, neurons, glia and oligodendrocytes (29,62). We reasoned that our analysis in whole cortex might obscure the specific regulation of circRNAs in neurons by NOVA2. Thus, we analyzed circRNAs in NOVA2 deficient neuron subpopulation datasets. Total RNA-seq data from fluorescence-activated cell sorted (FACS) embryonic inhibitory and excitatory cortical neurons deficient in NOVA2 (50) were analyzed using the CIRI2 pipeline. We identified 4123 and 2440 exonic circRNAs in Gad2+ and Emx1+ datasets, respectively, that passed our minimum BSJ read threshold (Supplementary Files S4 and S5). Global cir-

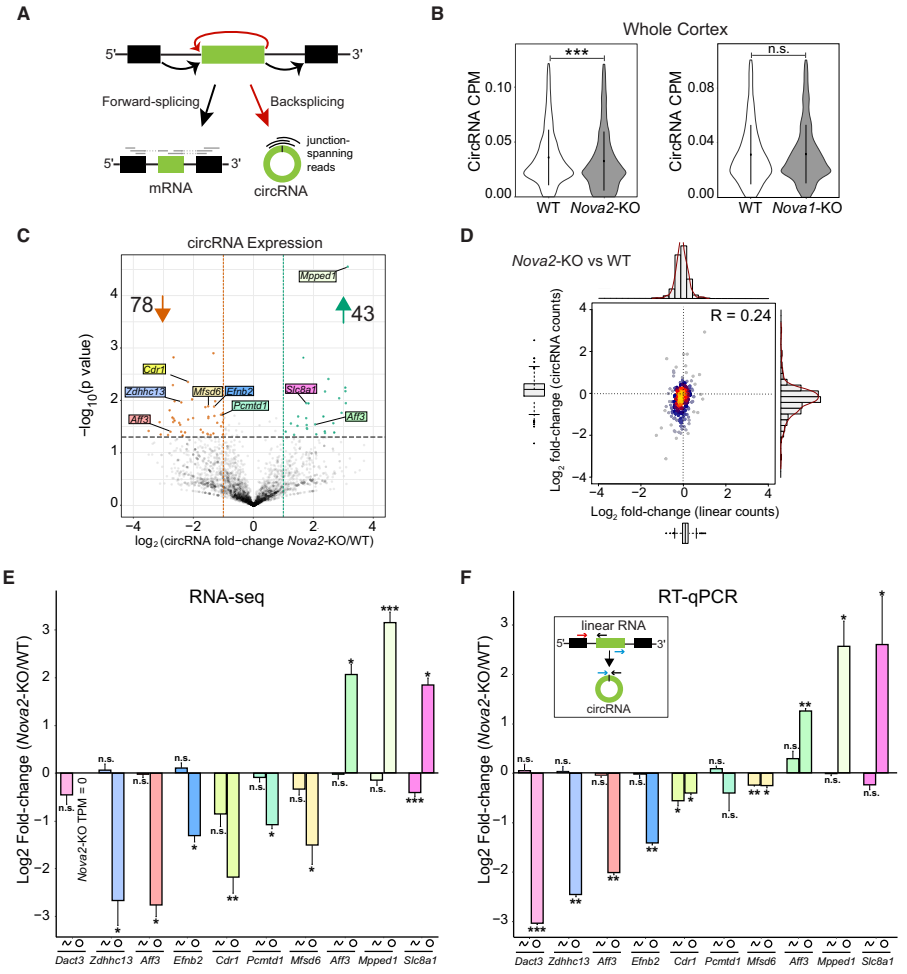

Figure 1. NOVA2 regulation of circRNA biogenesis in mouse cortex. (**A**) Schematic of forward-spliced and backspliced read alignments for detection of linear RNA and circRNA expression, respectively. The circularizing exon is shown in green. (**B**) CircRNA CPM is significantly reduced in *Nova2*-KO (*left*) but not *Nova1*-KO (*right*) whole cortex. Significance reflects non-parametrical Wilcoxon rank-sum test with continuity correction. $n = 3$ biological replicates for each condition. (**C**) Volcano plot of circRNAs in *Nova2*-KO versus WT showing circRNAs downregulated (orange dots) and upregulated (green dots) in the knockout condition ($\log_2$FC > 1, $P < 0.05$). (**D**) High density scatterplot of 311 circRNAs (minimum three BSJ read counts in four out of six replicates). Y-axis reflects $\log_2$ fold-change of circRNA counts. X-axis reflects $\log_2$ fold-change of linear counts from host genes. (**E**) RNA-seq quantification of 10 circRNAs (7 downregulated, three upregulated) in *Nova2*-KO versus WT and their corresponding host gene mRNA expression. (**F**) RT-qPCR quantification of the same 10 regulated circRNAs and their host gene mRNAs normalized to *Gapdh*. Inset diagram depicts primer locations used for circRNA and host gene linear mRNA quantification. $^{*}P < 0.05$; $^{**}P < 0.01$; $^{***}P < 0.001$; n.s., not significant. Student's *t*-test was used for statistical significance (two-tailed, unpaired). CPM, Counts Per Million. See also Supplementary Figures S1 and S3.

cRNA levels were significantly decreased in both *Nova2*-KO datasets ($P < 2.2 \times 10^{-16}$, Wilcoxon-rank sum test with continuity correction) (Figure 2A, B; inset violin plots). Similar to results from whole cortex, linear expression from the host gene of the differentially expressed circRNAs did not show any significant changes (Supplementary Figure S2A, B). Volcano plots demonstrated a striking downregulation trend for hundreds of circRNAs in both inhibitory and excitatory neurons in the absence of NOVA2, with only a handful of upregulated circRNAs (Figure 2A, B). At least 9-fold more circRNAs were downregulated in either dataset compared to the number of circRNAs upregulated. Reduced circRNA expression in the knockouts remained when the analysis was performed with increased minimum thresholds of 10, 20, and 30 backspliced reads per condition (Supplementary Figure S3A–C). Our results indicate that NOVA2 generally promotes circRNA biogenesis in cortical neurons.

We next analyzed the same datasets using DCC/CircTest, an independent circRNA analysis pipeline (56). DCC computes forward and backspliced read counts, whereas the CircTest module calculates the ratio of BSJ reads to linear, forward spliced reads and robustly tests for their independence. Applying a stringent filtering method (minimum 3 BSJ counts in 4 out of 6 biological replicates), we identified 519 and 750 circRNAs from excitatory and inhibitory cortical neuron populations, respectively (Supplementary File S6). In agreement with our CIRI2 analysis (Figure 2A, B), in the absence of NOVA2, we found a significant reduction of circRNA expression when normalized to the linear reads arising from the same host-gene ($P < 2.2 \times 10^{-16}$, Wilcoxon-rank sum test with continuity correction; Figure 2C). Density plots showed a pronounced reduction in circRNA expression in both *Nova2*-KO neuron populations (vertical axis, Figure 2D, E). In contrast, linear RNAs from the same host gene showed only a minor shift to the right along the x-axis. Overall, we observed a weak correlation (Emx1+; $R = 0.36$ and Gad2+; $R = 0.23$) between circular and linear expression changes. We found that 456/519 Emx1+ expressed circRNAs (87%) and 495/750 of Gad2+ circRNAs (66%) passed CircTest significance testing for independence of circRNA and linear RNA expression (Supplementary File S6). Taken together, these results demonstrate that NOVA2-regulation of backsplicing is independent of linear host gene expression.

NOVA2-regulated circRNAs and exon skipping events show little overlap

There are some reported instances of circRNA loci overlapping with exon skipping events (reviewed in (63)). We thus determined to what degree NOVA2 regulated exon skipping events (SE) overlapped with NOVA2 regulated circRNAs. We applied replicate Multivariate Analysis of Transcript Splicing (rMATS) (58) to probe for statistically significant SE events in the excitatory and inhibitory neuron datasets (Supplementary File S7). Returning to our CIRI2 generated list of differentially expressed circRNAs, we found that in excitatory neurons, only 3/24 upregulated circRNAs and 10/265 downregulated circRNAs overlapped with at least one significant SE event. Likewise, in inhibitory neurons only 1/16 upregulated circRNAs and 7/209 downregulated circRNAs overlapped with at least one significant SE event. Of note, all the circRNAs that overlapped with at least one SE event were multi-exonic, and in all instances only some of the exons within the circRNA loci were skipped. i.e. none of the regulated skipping events skipped an entire NOVA2-regulated circRNA. Given these results, we conclude that NOVA2-regulation of circRNAs is unrelated to NOVA2-mediated exon skipping.

NOVA2-regulated circRNAs display cell-type specific regulation

We examined the overlap of NOVA2-regulated circRNAs between excitatory and inhibitory cell populations. We found that 247/293 and 120/225 of the NOVA2-regulated circRNAs in excitatory and inhibitory neurons, respectively, were expressed in both neuronal subtypes. Despite this broad overlap, we found that the identity of NOVA2-regulated circRNAs were largely distinct between the two cell-types (Supplementary Figure S4). Only 18 circRNAs were found to be NOVA2-regulated in both excitatory and inhibitory neurons. This is in line with what was previously found with the same datasets for linear alternative splicing (50). Thus, it appears that NOVA2 circRNA regulation exhibits neuronal sub-type specificity.

Circ*Efnb2* is an abundant, conserved circRNA regulated by NOVA2

Having uncovered a genome-wide role for NOVA2 in circRNA regulation, we next turned to a single circRNA locus for investigation into the mechanism. To choose a candidate for further study, we identified the circRNAs found to be differentially expressed in both pipelines (CIRI2 or CircTest) and found 74 in the Emx1 dataset and 36 in the Gad2 dataset (Supplementary File S8). Of these, only 7 circRNAs (all reduced in the *Nova2*-KO condition) were common to both Emx1 and Gad2 datasets (Supplementary File S8). This included circ*0015034* (referred to from here on as circ*Efnb2*) (Figure 3A). Circ*Efnb2* is a 284 nt long circRNA generated from the second exon of the *Efnb2* gene. *Efnb2* encodes ephrin-B2, a transmembrane ligand which mediates cell-to-cell communication via contact with adjacent Eph receptor (64). The same locus also produces a circRNA in humans (circBaseID; hsa_circ_0029247) with identical primary sequence. Finally, circ*Efnb2* is abundant, ranking in the top 15% of high confidence circRNAs with respect to circRNA to mRNA ratio (Figure 3B).

To confirm the circularity of circ*Efnb2*, we performed northern analysis of mouse cortex samples. We observed clear bands of the expected sizes for both the linear and circular products. Treatment with RNase R enriched circ*Efnb2* and depleted the linear transcript, confirming the circular and linear nature of the two major bands (Figure 3C). In addition, we captured polyA+ RNA from mouse cortex samples using oligo(dT) beads, as well as unbound RNAs (polyA- fraction) for Northern blot analysis. As expected, the polyA+ fraction enriched for polyadenylated, linear *Efnb2* mRNA and depleted the polyA tail-lacking circRNA (Figure 3D).

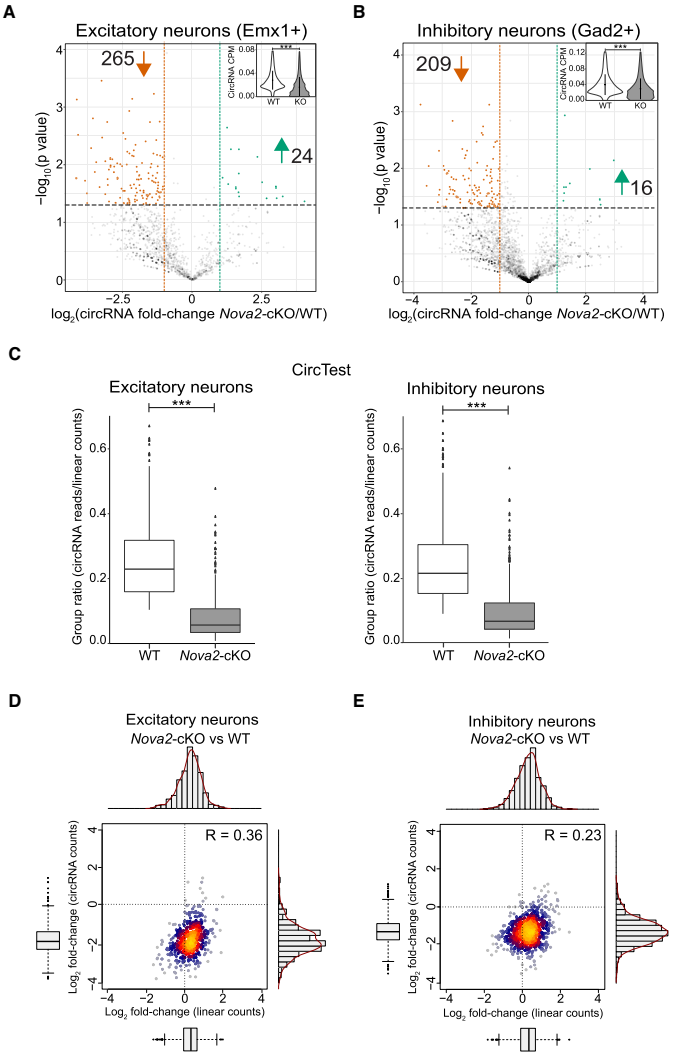

Figure 2. NOVA2 regulation of circRNA biogenesis in cortical excitatory and inhibitory neurons. (**A**) Volcano plot of circRNAs detected using CIRI2 in excitatory cortical neurons (Emx1) and (**B**) inhibitory cortical neurons (Gad2) deficient in NOVA2. In both datasets, more circRNAs were significantly downregulated compared to upregulated in *Nova2*-cKO cells relative to WT ($log_2FC>1$, $P < 0.05$). Inset violin plots show significant reduction in total circRNA CPM. Statistical analyses were carried out as in Figure 1B. (**C**) CircTest group ratio is significantly reduced in *Nova2-c*KO condition. Significance reflects non-parametrical Wilcoxon rank-sum test with continuity correction. $n = 3$ biological replicates for each condition. Group ratio is defined as the number of BSJ reads divided by the number linear-spliced reads (y-axis). (**D**) High density scatterplot of 456 DCC/CircTest identified high confidence circRNAs (minimum three BSJ read counts in four out of six biological replicates) from excitatory neurons deficient in NOVA2. Y-axis reflects log_2 fold-change of circRNA counts. X-axis reflects log_2 fold-change of linear counts from host genes. Pearson correlation coefficient is shown in the upper right corner, indicating weak correlation between circRNA and linear RNA counts in *Nova2*-null excitatory neurons. (**E**) Same analysis repeated for *Nova2*-cKO inhibitory neurons with 495 high confidence circRNAs represented. $^{***}P < 0.001$. CPM, Counts Per Million. See also Supplementary Figures S2–S4.

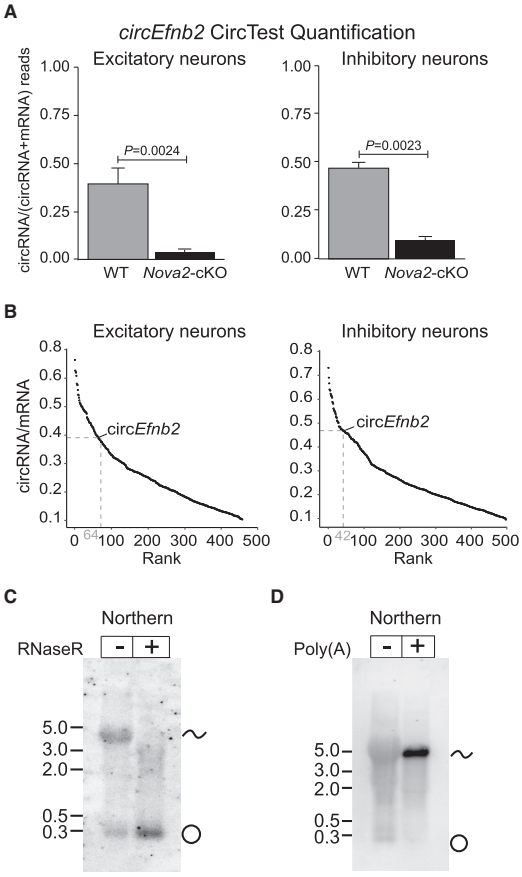

Figure 3. Circ*Efnb2* is an abundant circRNA regulated by NOVA2. (**A**) CircRNA to mRNA ratio plot generated by CircTest. Ratio of circular junction read counts from circ*Efnb2* to average total counts at exon borders are shown. *P*-values were generated from CircTest module. (**B**) CircRNA/mRNA expression rank of *circEfnb2* in embryonic excitatory (64th) or inhibitory (42nd) neuron datasets (top 15%; both datasets). (**C**) Northern blot using probe overlapping circularized exon of *Efnb2* detects bands corresponding to the circRNA and mRNA from embryonic whole cortex RNA with or without RNase R treatment. (**D**) Northern blot performed for poly(A)- and poly(A)+ samples. RNA samples for Northern were obtained from E18 whole cortex.

Generation of a circEfnb2 backsplicing reporter

NOVA2 has a well-characterized YCAY binding motif (65). In order to determine which binding sites help facilitate NOVA2 regulation of *circEfnb2* we constructed a backsplicing reporter. To guide the design of the backsplicing reporter, we analyzed CLIP tags identified in NOVA2 cTag-CLIP Emx1 and Gad2 neuron datasets (50) (Figure 4A). Due to the extended lengths of the 5′ and 3′ flanking introns (20.9kb and 15.5kb, respectively), the circularizing exon combined with its full-length flanking introns is not amenable to plasmid subcloning and transfection. We thus opted to subclone truncated upstream and downstream flanking intronic regions that included major NOVA2-CLIP peaks (Figure 4A; 'fragment 2'). In addition, we included partial sequences from exons 1 and 3 and ∼150 bp of intron sequence to retain linear splicing from the reporter (Figure 4A; 'fragment 1 and 3'). Fragment 3 also included prominent NOVA2-CLIP peaks. In the intronic sequences, we noted the presence of multiple YCAY motifs that were not associated with CLIP tags.

Consistent with previous NOVA2 splicing reporter studies, we examined regulation of circ*Efnb2* in HEK293 cells which express very low levels of *Nova2* (Supplementary Fig-

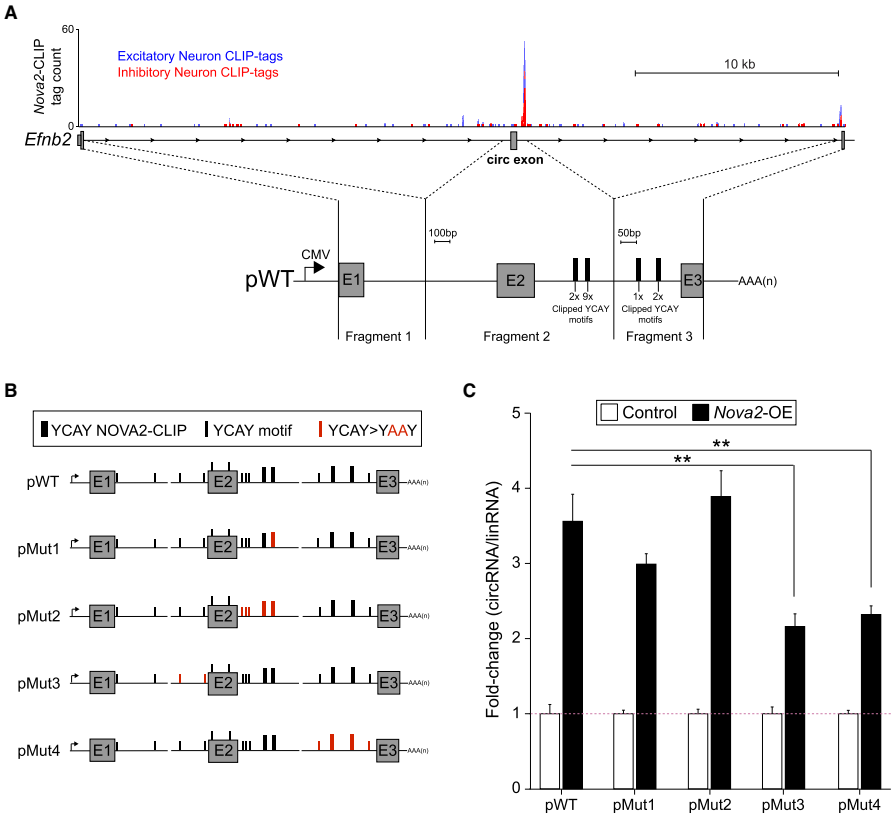

Figure 4. Role of intronic NOVA2 binding sites in Circ-*Efnb2* backsplicing. (**A**) Schematic of *Efnb2* locus shown in antisense (mm10, chr8:8623077–8660773). NOVA2 cTag-CLIP tags from excitatory cortical neurons (blue) or inhibitory neurons (red) visualized using UCSC genome browser. Three genomic fragments used to construct the backsplicing reporter (pWT) are shown below, and the number of individual YCAY motifs present within each NOVA2-CLIP peak (thick black bar) are reported. Note, *Efnb2* Exon 1 (E1) and Exon 3 (E3) in the pWT backsplicing reporter are truncated, whereas circularizing Exon 2 (E2) is full length. (**B**) Reporter schematics for circEfnb2. NOVA2-CLIP peaks are represented by thick black bars as in panel A. YCAY motifs not associated with NOVA2-CLIP peaks are represented as thin black bars. Mutated YCAY motifs or CLIP peaks are shown in red. (**C**) RT-qPCR of circ*Efnb2* expression from reporters co-transfected with NOVA2 expression plasmid (*Nova2*-OE) or empty expression vector in HEK293 cells. For expression data, target genes were normalized to linear-spliced transcript (lin*Efnb2*) generated by the reporter. $n = 3$ biological replicates. Error bars are represented as mean ± SEM. $^{**}P < 0.01$ (Student's *t*-test, two-tailed and unpaired). See also Supplementary Figure S5.

ure S5A) (13,66–69). Initial analysis of the RNAs generated from the reporter revealed the spurious usage of cryptic splice acceptor and donor sites in the plasmid backbone, which were subsequently mutated (see Materials and Methods). With the corrected plasmid we performed transient transfections and confirmed the expression and circularity of the reporter generated circRNA by RT-PCR (Supplementary Figure S5B). In addition, we validated the expression and circularity of the reporter circRNA by RNase R treatment followed by Northern blot (Supplementary Figure S5C), and quantified RNase R resistance by RT-qPCR (Supplementary Figure S5D).

We examined the response of our *Efnb2* backsplicing reporter (pWT, Figure 4B) to NOVA2 overexpression. Co-transfection of the reporter with NOVA2 led to a ∼3.5-fold increase in backsplicing relative to linear splicing (Figure 4C). Co-transfection of another neural-enriched splicing factor, HuD, did not alter backsplicing of circ*Efnb2* (Supplementary Figure S5E), providing evidence of NOVA2 regulatory specificity. Together, these data demonstrate that the

Efnb2 backsplicing reporter recapitulates NOVA2 regulation of *Efnb2* circRNA biogenesis.

NOVA2 regulates backsplicing of circEfnb2 via intronic YCAY motifs

To understand how NOVA2 might regulate circ*Efnb2* backsplicing, we introduced point mutations at putative NOVA2 binding sites (Figure 4B). Within our reporter, there were four NOVA2 CLIP peaks, all found within intronic regions. Two peaks were located just downstream of exon 2 (E2), and the other two were located just upstream of exon 3 (E3) (Figure 4A). To assess the relevance of YCAY motifs, we mutated them to YAAY, since the CA dinucleotide is essential for NOVA2 recognition (70). For RT-qPCR quantification, we normalized circRNA expression to linear-spliced transcript expression in order to observe any relative changes in backsplicing. Circular and linear products normalized to *Gapdh* are shown in Supplementary Figure S5F. First, we targeted the CLIP peak consisting of 9 YCAY motifs (Figure 4A,B). Surprisingly, we did not observe a significant difference from pWT (Figure 4C, pMut1). Next, we mutated the adjacent CLIP peak (2x YCAY), along with three additional YCAY motifs not identified by CLIP (pMut2). However, we still did not observe a reduction in NOVA2-mediated backsplicing of circ*Efnb2* (Figure 4C).

We proceeded to mutate two non-clipped YCAY motifs immediately upstream of exon 2 (pMut3). Even though these motifs lacked NOVA2-CLIP support, mutating them caused a significant reduction in NOVA2-regulated backsplicing (Figure 4C). Finally, we turned our attention to the intronic region just upstream of exon 3 and mutated both remaining CLIP peaks as well as two adjacent YCAY motifs not identified by CLIP (pMut4). In this case, we also found significant reduction in NOVA2-mediated backsplicing compared to the WT reporter (Figure 4C). Together these data suggest that NOVA2 intronic binding on either side of the *Efnb2* circRNA locus impacts its regulation.

NOVA2 binding sites in circRNA flanking introns promote backsplicing

Given these reporter analysis results, we next turned to genome-wide cTag-CLIP data to investigate whether NOVA2 binding to both flanking introns is a general feature of NOVA2-regulated circRNA loci. For this analysis, we used the subset of high confidence, NOVA2-regulated circRNAs from the excitatory and inhibitory datasets (36 circRNAs for inhibitory neurons and 74 for excitatory neurons). For a non-regulated control comparison group, we used circRNAs unchanged by NOVA2 loss ($P > 0.50$, FC < 1) (Supplementary File S8). We hypothesized that this robust subset would provide the best chance to identify relevant NOVA2 positional binding information. Using NOVA2-CLIP data obtained from each sorted neuron dataset we checked for the presence of CLIP peaks in the upstream and downstream introns flanking each circRNA. We discovered that in excitatory neurons, NOVA2 bound both flanking introns of a regulated circRNA at a significantly higher frequency than non-differentially expressed controls ($P = 0.02$, Pearson's Chi-squared test with Yates' continuity correction) (Supplementary Figure S6A). In contrast, the presence of CLIP sites in just one intron (either upstream or downstream) was not significantly different between regulated circRNAs and controls. This suggests that NOVA2 intronic binding on both sides of a circRNA locus plays a role in backsplicing regulation. However, when we investigated inhibitory neurons, which had a lower sample size of regulated circRNAs, statistical significance for the same trend was not observed (Supplementary Figure S6B).

The *Efnb2* backsplicing reporter analysis and CLIP analysis suggested that NOVA2 binding in the introns upstream and downstream of a circularizing locus promote NOVA2 regulated circRNA biogenesis. To further investigate the generality of this observation, we generated an artificial backsplicing minigene reporter, pMini, which was devoid of *Efnb2* sequences. This plasmid contains full length GFP coding sequence in the same vector backbone as our circ*Efnb2* reporter. GFP was fragmented into three artificial exons flanked by intronic sequences consisting of human *ZKSCAN1* reverse complementary matches (RCMs) to facilitate enhanced circRNA expression (Figure 5A). Existing YCAY motifs that might impact circRNA regulation were mutagenized. We confirmed that all of our pMini variants produced a single circRNA products by RT-PCR in control or NOVA2 overexpression conditions using outward facing primers (Supplementary Figure S7A). We also confirmed the expression of the 497 nt circRNA product by Northern blot and RT-qPCR (Figure 5B, C), under RNase R or mock treatment conditions. As expected, RNaseR degraded the plasmid generated linear transcript (Figure 5B, C).

In the WT reporter that lacks any YCAY motifs (pMini-WT) we did not observe a significant increase in backsplicing in response to NOVA2 overexpression (Figure 5D). We next introduced YCAY repeats into various intronic locations on the reporter. We introduced a 10x YCAY repeat into pMini-WT ∼50 bp upstream of the circRNA exon (pMini-Up) or ∼50 bp downstream of the circRNA exon (pMini-Down), and in both locations (pMini-Both). For RT-qPCR quantification, we normalized circRNA expression to linear-spliced transcript expression. Circular and linear products normalized to *Gapdh* are shown in Supplementary Figure S7B. Similar to pWT, introduction of YCAY repeats into the upstream intron only did not increase the circular/linear RNA ratio (pMini-Up, Figure 5D). A similar result was observed when YCAY repeats were inserted into the downstream intron only (pMini-Down, Figure 5D). Finally, we tested the impact of placing NOVA2 binding sites both upstream and downstream of the circularizing exon (pMini-Both). Remarkably, we found that for this reporter, NOVA2 co-transfection led to a nearly 3-fold increase in circular/linear RNA ratio (Figure 5D). Thus, similar to our circ*Efnb2* reporter, and in accordance with CLIP data from excitatory neurons, our results show that the presence of NOVA2 binding sites in both introns impacts backsplicing.

DISCUSSION

Here, we identify NOVA2 as a regulator of circRNA biogenesis in neurons. We found that within the mouse embryonic cortex, loss of NOVA2 globally reduced circRNA ex-

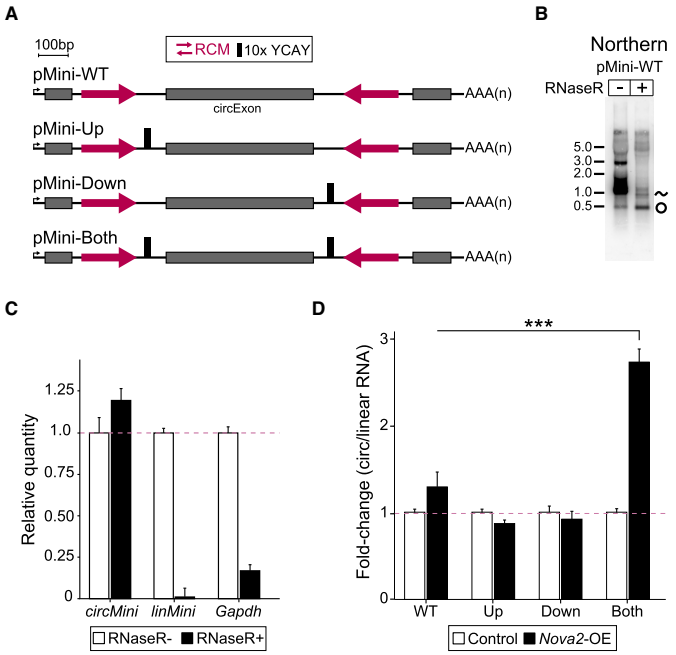

Figure 5. NOVA2 binding sites in both flanking introns mediate NOVA2 backsplicing. (**A**) Schematics of artificial backsplicing reporters. Exonic sequences (gray) were derived from GFP open reading frame. Reverse complementary matches (RCMs) are shown as red opposing arrows. A repeat region of 10 tandem YCAY motifs (thick black bar) was inserted into the intronic locations shown. (**B**) Northern blot using probe overlapping circularized exon of pMini reporter to detect circRNA and mRNA from transfected HEK293 cells. RNA was treated with RNase R to deplete linear transcript and enrich for circ*Mini*. (**C**) RT-qPCR expression analysis of RNase R treated RNA shown in panel B. Expression is relative to the mock RNase R condition. (**D**) RT-qPCR analysis of circ*Mini* transcript derived from pMini reporter constructs in HEK293 cells cotransfected with NOVA2 expressing plasmid (*Nova2*-OE) or empty vector control. For expression data, circ*Mini* is normalized to the linear-spliced transcript (lin*Mini*) generated by the reporter. $n = 3$ biological replicates. Error bars are represented as mean ± SEM. $^{***}P < 0.001$, Student's *t*-test, two-tailed and unpaired. See also Supplementary Figures S6 and S7.

pression, and that this reduction was largely independent from mRNA expression changes of the host gene. This effect of global circRNA reduction upon NOVA2 loss was even more pronounced when a sorted neuron population was analyzed. We found that NOVA2-regulated circRNAs within each cell-type were largely distinct, despite overlapping expression patterns. To investigate the *cis*-elements involved in circRNA regulation by NOVA2, we focused on a conserved and abundant circRNA from the *Efnb2* gene. Using backsplicing reporter analysis we demonstrated that intronic YCAY sequences both upstream and downstream of the circRNA locus were important for NOVA2-regulation. CLIP analysis in excitatory neurons provided support for this finding.

CircRNAs are typically expressed at a low level compared to their linear counterparts. For most accepted analysis pipelines, only BSJ reads are used for quantification, making differential expression analysis problematic. Thus, we applied multiple validated pipelines to quantify circRNA expression genome-wide (53,56), and performed extensive validation of differential expression trends using RT-qPCR (Figure 1E,F). Investigating the sorted neuron datasets more closely, we found that NOVA2 appeared to regulate circRNAs in a cell-type specific manner (Supplementary Figure S4A), similar to what has been previously shown for linear alternative splicing (50). Additional genome-wide analyses using library preparation methods that enhance read depth specifically for circRNAs are warranted to provide more conclusive support for this finding. On a similar front, our global analysis of how NOVA2 CLIP peaks correlated with NOVA2 regulated circRNAs could be improved by having more accurate circRNA expression quantification. There was a very low number of high-confidence NOVA2-regulated circRNAs in the Gad2 dataset (only 36)– it is possible that with greater read depth we would identify more regulated circRNAs and obtain better insight into the genome-wide features of circRNA regulation by NOVA2.

We chose circ*Efnb2*, a single-exon circRNA conserved from mouse to human, to investigate what *cis*-elements control NOVA2-regulation of circRNAs biogenesis. Using backsplicing reporter analysis we found that YCAY motifs on either side of the circularizing locus were important for regulating circ*Efnb2* (Figure 4C). One of the important motifs identified was located in the intronic region preceding the 3′ splice-acceptor of the exon downstream of the circRNA locus. This suggests that NOVA2 binding in this region far downstream from the circRNA promotes backsplicing. A caveat of this interpretation is that several kb of the intron could not be included in our backsplicing reporter (Figure 4A). We discovered that two YCAY motifs upstream of circ*Efnb2* were important for regulation of backsplicing, even though they lacked NOVA2-CLIP support (Figure 4C). This was somewhat surprising and suggests that the CLIP datasets might have limited utility in predicting binding sites important for backsplicing. On the other hand, this result could reflect an inherent limitation of cell culture systems for recapitulating neuronal circRNA regulation patterns. Performing mutagenesis of the intronic YCAY motifs at the endogenous *Efnb2* locus in ES-derived neurons or in mice with CRISPR genome-editing could provide more conclusive support.

To investigate NOVA2 regulation more generally, we constructed an artificial backsplicing vector, pMini, which was devoid of NOVA2 binding sites (Figure 5A). We introduced YCAY clusters into intronic regions upstream and downstream of the circularizing exon based on findings from the circ*Efnb2* reporter. We found that NOVA2-induced backsplicing in the pMini reporter required the presence of YCAY clusters in both flanking introns. This result is analogous to what was previously observed for the RBP *quaking* (QKI) (37,38). In that study, QKI-regulated backsplicing from a reporter was found to be dependent on QKI binding sites in both upstream and downstream introns (38). QKI has been shown to self-dimerize (71), thus it was hypothesized that QKI dimerization could be involved in the backsplicing mechanism. Interestingly, NOVA proteins can also self-dimerize (72), thus similar backsplicing regulatory mechanisms might be at play for both QKI and NOVA2.

Nova2-KO mice display a host of degenerative brain phenotypes which have been attributed to deregulation of linear alternative splicing (13,49,50). Hundreds of circRNAs were found here to be differentially regulated by *Nova2*. Could reduced levels of circRNAs such as circ*Efnb2* contribute to the neurodevelopmental defects of *Nova2*-KO mice? There are many possible ways NOVA2-regulated circRNAs could impact neural development, given the different ways circRNAs impact gene regulation. For example, some circRNAs travel to synapses and act as scaffolds for various RBPs, whereas others regulate the transcriptional activity of genes in the nucleus (30,73,74). Some circRNAs have been recently associated with neurological defects in mice (34) and humans (36,75). Despite technical challenges, several recent studies have demonstrated the feasibility of both targeting circRNAs using RNAi (36,76) and deleting intronic RCMs using CRISPR to reduce or eliminate circRNA expression (74). Moving forward, it will be interesting to assess the role of NOVA2-regulated circRNAs such as circ*Efnb2* in neural development using such approaches.

DATA AVAILABILITY

CIRI2 is an open source, freely available tool for access at Source Forge (https://sourceforge.net/projects/ciri/files/CIRI2/).

HISAT2 is an open source, freely available tool for access at Johns Hopkins University (https://ccb.jhu.edu/software/hisat2/manual.shtml).

STAR is an open source, freely available tool in the GitHub repository (https://github.com/alexdobin/STAR).

DCC/CircTest is an open source, freely available tool in the GitHub repository (https://github.com/dieterich-lab/DCC) and (https://github.com/dieterich-lab/CircTest).

rMATS is an open source, freely available tool at Source Forge (http://rnaseq-mats.sourceforge.net).

SUPPLEMENTARY DATA

Supplementary Data are available at NAR Online.

ACKNOWLEDGEMENTS

We thank Dr Zhe Chen (University of Minnesota) for sharing plasmids. We thank Nora Perrone-Bizzozero (University of New Mexico) for sharing the HuD plasmid. We thank A. van der Linden, Z. Chen, Z. Zhang and B. Bae for helpful feedback and discussion on the manuscript.

FUNDING

National Institute on Aging [R15 AG052931]; National Institute of General Medical Sciences [R35 GM138319]; D.K. is supported by the National Science Foundation Graduate Research Fellowship Program; Core facilities at the University of Nevada, Reno campus were supported by NIGMS [COBRE P30 GM103650]. Funding for open access charge: National Institute of General Medical Sciences [R35 GM138319].

Conflict of interest statement. None declared.

REFERENCES

1. Pan,Q., Shai,O., Lee,L.J., Frey,B.J. and Blencowe,B.J. (2008) Deep surveying of alternative splicing complexity in the human transcriptome by high-throughput sequencing. *Nat. Genet.*, **40**, 1413–1415.
2. Kelemen,O., Convertini,P., Zhang,Z., Wen,Y., Shen,M., Falaleeva,M. and Stamm,S. (2013) Function of alternative splicing. *Gene*, **514**, 1–30.
3. Barbosa-Morais,N.L., Irimia,M., Pan,Q., Xiong,H.Y., Gueroussov,S., Lee,L.J., Slobodeniuc,V., Kutter,C., Watt,S., Colak,R. *et al.* (2012) The evolutionary landscape of alternative splicing in vertebrate species. *Science*, **338**, 1587–1593.
4. Merkin,J., Russell,C., Chen,P. and Burge,C.B. (2012) Evolutionary dynamics of gene and isoform regulation in mammalian tissues. *Science*, **338**, 1593–1599.
5. Dillman,A.A., Hauser,D.N., Gibbs,J.R., Nalls,M.A., Mccoy,M.K., Rudenko,I.N., Galter,D. and Cookson,M.R. (2013) mRNA expression, splicing and editing in the embryonic and adult mouse cerebral cortex. *Nat. Neurosci.*, **16**, 499–506.
6. Mazin,P., Xiong,J., Liu,X., Yan,Z., Zhang,X., Li,M., He,L., Somel,M., Yuan,Y., Phoebe Chen,Y.P. *et al.* (2013) Widespread splicing changes in human brain development and aging. *Mol. Syst. Biol.*, **9**, 633.

7. Molyneaux,B.J., Goff,L.A., Brettler,A.C., Chen,H.H., Hrvatin,S., Rinn,J.L. and Arlotta,P. (2015) Decon: genome-wide analysis of in vivo transcriptional dynamics during pyramidal neuron fate selection in neocortex. *Neuron*, **85**, 275–288.
8. Vuong,C.K., Black,D.L. and Zheng,S. (2016) The neurogenetics of alternative splicing. *Nat. Rev. Neurosci.*, **17**, 265–281.
9. Shibayama,M., Ohno,S., Osaka,T., Sakamoto,R., Tokunaga,A., Nakatake,Y., Sato,M. and Yoshida,N. (2009) Polypyrimidine tract-binding protein is essential for early mouse development and embryonic stem cell proliferation. *FEBS J.*, **276**, 6658–6668.
10. Licatalosi,D.D. and Darnell,R.B. (2006) Splicing regulation in neurologic disease. *Neuron*, **52**, 93–101.
11. Gehman,L.T., Stoilov,P., Maguire,J., Damianov,A., Lin,C.H., Shiue,L., Ares,M. Jr, Mody,I. and Black,D.L. (2011) The splicing regulator Rbfox1 (A2BP1) controls neuronal excitation in the mammalian brain. *Nat. Genet.*, **43**, 706–711.
12. Ruggiu,M., Herbst,R., Kim,N., Jevsek,M., Fak,J.J., Mann,M.A., Fischbach,G., Burden,S.J. and Darnell,R.B. (2009) Rescuing Z+ agrin splicing in nova null mice restores synapse formation and unmasks a physiologic defect in motor neuron firing. *Proc. Natl. Acad. Sci. U.S.A.*, **106**, 3513–3518.
13. Saito,Y., Miranda-Rottmann,S., Ruggiu,M., Park,C.Y., Fak,J.J., Zhong,R., Duncan,J.S., Fabella,B.A., Junge,H.J., Chen,Z. *et al.* (2016) NOVA2-Mediated RNA regulation is required for axonal pathfinding during development. *Elife*, **5**, e14371.
14. Li,X., Yang,L. and Chen,L.L. (2018) The biogenesis, functions, and challenges of circular RNAs. *Mol. Cell*, **71**, 428–442.
15. Veno,M.T., Hansen,T.B., Veno,S.T., Clausen,B.H., Grebing,M., Finsen,B., Holm,I.E. and Kjems,J. (2015) Spatio-Temporal regulation of circular RNA expression during porcine embryonic brain development. *Genome Biol.*, **16**, 245.
16. Holdt,L.M., Stahringer,A., Sass,K., Pichler,G., Kulak,N.A., Wilfert,W., Kohlmaier,A., Herbst,A., Northoff,B.H., Nicolaou,A. *et al.* (2016) Circular non-coding RNA ANRIL modulates ribosomal RNA maturation and atherosclerosis in humans. *Nat. Commun.*, **7**, 12429.
17. Hansen,T.B., Jensen,T.I., Clausen,B.H., Bramsen,J.B., Finsen,B., Damgaard,C.K. and Kjems,J. (2013) Natural RNA circles function as efficient microrna sponges. *Nature*, **495**, 384–388.
18. Huang,G., Zhu,H., Shi,Y., Wu,W., Cai,H. and Chen,X. (2015) Cir-ITCH plays an inhibitory role in colorectal cancer by regulating the Wnt/Beta-Catenin pathway. *PLoS One*, **10**, E0131225.
19. Du,W.W., Yang,W., Liu,E., Yang,Z., Dhaliwal,P. and Yang,B.B. (2016) Foxo3 circular RNA retards cell cycle progression via forming ternary complexes with P21 And CDK2. *Nucleic Acids Res.*, **44**, 2846–2858.
20. Abdelmohsen,K., Panda,A.C., Munk,R., Grammatikakis,I., Dudekula,D.B., De,S., Kim,J., Noh,J.H., Kim,K.M., Martindale,J.L. *et al.* (2017) Identification of hur target circular RNAs uncovers suppression of PABPN1 translation by circpabpn1. *RNA Biol.*, **14**, 361–369.
21. Legnini,I., Di Timoteo,G., Rossi,F., Morlando,M., Briganti,F., Sthandier,O., Fatica,A., Santini,T., Andronache,A., Wade,M. *et al.* (2017) Circ-ZNF609 is a circular RNA that can be translated and functions in myogenesis. *Mol. Cell*, **66**, 22–37.
22. Li,X., Liu,C.X., Xue,W., Zhang,Y., Jiang,S., Yin,Q.F., Wei,J., Yao,R.W., Yang,L. and Chen,L.L. (2017) Coordinated circrna biogenesis and function with NF90/NF110 in viral infection. *Mol. Cell*, **67**, 214–227.
23. Li,Y., Zheng,F., Xiao,X., Xie,F., Tao,D., Huang,C., Liu,D., Wang,M., Wang,L., Zeng,F. *et al.* (2017) Circhipk3 sponges Mir-558 to suppress heparanase expression in bladder cancer cells. *EMBO Rep.*, **18**, 1646–1659.
24. Pamudurti,N.R., Bartok,O., Jens,M., Ashwal-Fluss,R., Stottmeister,C., Ruhe,L., Hanan,M., Wyler,E., Perez-Hernandez,D., Ramberger,E. *et al.* (2017) Translation of circrnas. *Mol. Cell*, **66**, 9–21.
25. Yang,Y., Fan,X., Mao,M., Song,X., Wu,P., Zhang,Y., Jin,Y., Yang,Y., Chen,L.L., Wang,Y. *et al.* (2017) Extensive translation of circular RNAs driven by N(6)-Methyladenosine. *Cell Res.*, **27**, 626–641.
26. Liu,C.X., Li,X., Nan,F., Jiang,S., Gao,X., Guo,S.K., Xue,W., Cui,Y., Dong,K., Ding,H. *et al.* (2019) Structure and degradation of circular RNAs regulate PKR activation in innate immunity. *Cell*, **177**, 865–880.
27. Memczak,S., Jens,M., Elefsinioti,A., Torti,F., Krueger,J., Rybak,A., Maier,L., Mackowiak,S.D., Gregersen,L.H., Munschauer,M. *et al.* (2013) Circular RNAs are a large class of animal RNAs with regulatory potency. *Nature*, **495**, 333–338.
28. Westholm,J.O., Miura,P., Olson,S., Shenker,S., Joseph,B., Sanfilippo,P., Celniker,S.E., Graveley,B.R. and Lai,E.C. (2014) Genome-wide analysis of drosophila circular RNAs reveals their structural and sequence properties and age-dependent neural accumulation. *Cell Rep.*, **9**, 1966–1980.
29. Rybak-Wolf,A., Stottmeister,C., Glazar,P., Jens,M., Pino,N., Giusti,S., Hanan,M., Behm,M., Bartok,O., Ashwal-Fluss,R. *et al.* (2015) Circular RNAs in the mammalian brain are highly abundant, conserved, and dynamically expressed. *Mol. Cell*, **58**, 870–885.
30. You,X., Vlatkovic,I., Babic,A., Will,T., Epstein,I., Tushev,G., Akbalik,G., Wang,M., Glock,C., Quedenau,C. *et al.* (2015) Neural circular RNAs are derived from synaptic genes and regulated by development and plasticity. *Nat. Neurosci.*, **18**, 603–610.
31. Hall,H., Medina,P., Cooper,D.A., Escobedo,S.E., Rounds,J., Brennan,K.J., Vincent,C., Miura,P., Doerge,R. and Weake,V.M. (2017) Transcriptome profiling of aging Drosophila photoreceptors reveals gene expression trends that correlate with visual senescence. *BMC Genomics*, **18**, 894.
32. Gruner,H., Cortes-Lopez,M., Cooper,D.A., Bauer,M. and Miura,P. (2016) circRNA accumulation in the aging mouse brain. *Sci. Rep.*, **6**, 38907.
33. Knupp,D. and Miura,P. (2018) circRNA accumulation: a new hallmark of aging? *Mech. Ageing Dev.*, **173**, 71–79.
34. Piwecka,M., Glazar,P., Hernandez-Miranda,L.R., Memczak,S., Wolf,S.A., Rybak-Wolf,A., Filipchyk,A., Klironomos,F., Cerda Jara,C.A., Fenske,P. *et al.* (2017) Loss of a mammalian circular RNA locus causes miRNA deregulation and affects brain function. *Science*, **357**, eaam8526.
35. Suenkel,C., Cavalli,D., Massalini,S., Calegari,F. and Rajewsky,N. (2020) A highly conserved circular RNA is required to keep neural cells in a progenitor state in the mammalian brain. *Cell Rep.*, **30**, 2170–2179.
36. Zimmerman,A.J., Hafez,A.K., Amoah,S.K., Rodriguez,B.A., Dell'Orco,M., Lozano,E., Hartley,B.J., Alural,B., Lalonde,J., Chander,P. *et al.* (2020) A psychiatric disease-related circular RNA controls synaptic gene expression and cognition. *Mol. Psychiatry*, **25**, 2712–2727.
37. Ashwal-Fluss,R., Meyer,M., Pamudurti,N.R., Ivanov,A., Bartok,O., Hanan,M., Evantal,N., Memczak,S., Rajewsky,N. and Kadener,S. (2014) circRNA biogenesis competes with pre-mRNA splicing. *Mol. Cell*, **56**, 55–66.
38. Conn,S.J., Pillman,K.A., Toubia,J., Conn,V.M., Salmanidis,M., Phillips,C.A., Roslan,S., Schreiber,A.W., Gregory,P.A. and Goodall,G.J. (2015) The RNA binding protein Quaking regulates formation of circRNAs. *Cell*, **160**, 1125–1134.
39. Ivanov,A., Memczak,S., Wyler,E., Torti,F., Porath,H.T., Orejuela,M.R., Piechotta,M., Levanon,E.Y., Landthaler,M., Dieterich,C. *et al.* (2015) Analysis of intron sequences reveals hallmarks of circular RNA biogenesis in animals. *Cell Rep.*, **10**, 170–177.
40. Kramer,M.C., Liang,D., Tatomer,D.C., Gold,B., March,Z.M., Cherry,S. and Wilusz,J.E. (2015) Combinatorial control of drosophila circular RNA expression by intronic repeats, hnRNPs, and SR proteins. *Genes Dev.*, **29**, 2168–2182.
41. Errichelli,L., Dini Modigliani,S., Laneve,P., Colantoni,A., Legnini,I., Capauto,D., Rosa,A., De Santis,R., Scarfo,R., Peruzzi,G. *et al.* (2017) FUS affects circular RNA expression in murine embryonic stem cell-derived motor neurons. *Nat. Commun.*, **8**, 14741.
42. Luque,F.A., Furneaux,H.M., Ferziger,R., Rosenblum,M.K., Wray,S.H., Schold,S.C. Jr, Glantz,M.J., Jaeckle,K.A., Biran,H., Lesser,M. *et al.* (1991) Anti-Ri: An antibody associated with paraneoplastic opsoclonus and breast cancer. *Ann. Neurol.*, **29**, 241–251.
43. Buckanovich,R.J., Posner,J.B. and Darnell,R.B. (1993) Nova, the paraneoplastic Ri antigen, is homologous to an RNA-binding protein and is specifically expressed in the developing motor system. *Neuron*, **11**, 657–672.
44. Yang,Y.Y., Yin,G.L. and Darnell,R.B. (1998) The neuronal RNA-binding protein Nova-2 is implicated as the autoantigen

targeted in POMA patients with dementia. *Proc. Natl. Acad. Sci. U.S.A.*, **95**, 13254–13259.
45. Buckanovich,R.J., Yang,Y.Y. and Darnell,R.B. (1996) The onconeural antigen Nova-1 is a neuron-specific RNA-Binding protein, the activity of which is inhibited by paraneoplastic antibodies. *J. Neurosci.*, **16**, 1114–1122.
46. Buckanovich,R.J. and Darnell,R.B. (1997) The neuronal RNA binding protein Nova-1 recognizes specific RNA targets in vitro and in vivo. *Mol. Cell. Biol.*, **17**, 3194–3201.
47. Lewis,H.A., Musunuru,K., Jensen,K.B., Edo,C., Chen,H., Darnell,R.B. and Burley,S.K. (2000) Sequence-specific RNA binding by a Nova KH domain: Implications for paraneoplastic disease and the fragile X syndrome. *Cell*, **100**, 323–332.
48. Jensen,K.B., Dredge,B.K., Stefani,G., Zhong,R., Buckanovich,R.J., Okano,H.J., Yang,Y.Y. and Darnell,R.B. (2000) Nova-1 regulates neuron-specific alternative splicing and is essential for neuronal viability. *Neuron*, **25**, 359–371.
49. Yano,M., Hayakawa-Yano,Y., Mele,A. and Darnell,R.B. (2010) Nova2 regulates neuronal migration through an RNA switch in disabled-1 signaling. *Neuron*, **66**, 848–858.
50. Saito,Y., Yuan,Y., Zucker-Scharff,I., Fak,J.J., Jereb,S., Tajima,Y., Licatalosi,D.D. and Darnell,R.B. (2019) Differential NOVA2-mediated splicing in excitatory and inhibitory neurons regulates cortical development and cerebellar function. *Neuron*, **101**, 707–720.
51. Cortes-Lopez,M., Gruner,M.R., Cooper,D.A., Gruner,H.N., Voda,A.I., Van Der Linden,A.M. and Miura,P. (2018) Global accumulation of circRNAs during aging in Caenorhabditis elegans. *BMC Genomics*, **19**, 8.
52. Love,M.I., Huber,W. and Anders,S. (2014) Moderated estimation of fold change and dispersion for RNA-Seq data with DESeq2. *Genome Biol.*, **15**, 550.
53. Gao,Y., Zhang,J. and Zhao,F. (2018) Circular RNA identification based on multiple seed matching. *Brief. Bioinform.*, **19**, 803–810.
54. Langmead,B. and Salzberg,S.L. (2012) Fast gapped-read alignment with Bowtie 2. *Nat. Methods*, **9**, 357–359.
55. Liao,Y., Smyth,G.K. and Shi,W. (2014) Featurecounts: an efficient general purpose program for assigning sequence reads to genomic features. *Bioinformatics*, **30**, 923–930.
56. Cheng,J., Metge,F. and Dieterich,C. (2016) Specific identification and quantification of circular RNAs from sequencing data. *Bioinformatics*, **32**, 1094–1096.
57. Wickham,H. (2016) In: *ggplot2: Elegant Graphics For Data Analysis*. Springer-Verlag, NY. https://ggplot2.tidyverse.org.
58. Shen,S., Park,J.W., Lu,Z.X., Lin,L., Henry,M.D., Wu,Y.N., Zhou,Q. and Xing,Y. (2014) rMATS: Robust and flexible detection of differential alternative splicing from replicate RNA-Seq data. *Proc. Natl. Acad. Sci. U.S.A.*, **111**, E5593–E5601.
59. Qu,K., Garamszegi,S., Wu,F., Thorvaldsdottir,H., Liefeld,T., Ocana,M., Borges-Rivera,D., Pochet,N., Robinson,J.T., Demchak,B. *et al.* (2016) Integrative genomic analysis by interoperation of bioinformatics tools in genomespace. *Nat. Methods*, **13**, 245–247.
60. Kim,D., Langmead,B. and Salzberg,S.L. (2015) HISAT: A fast spliced aligner with low memory requirements. *Nat. Methods*, **12**, 357–360.
61. Jeck,W.R., Sorrentino,J.A., Wang,K., Slevin,M.K., Burd,C.E., Liu,J., Marzluff,W.F. and Sharpless,N.E. (2013) Circular RNAs are abundant, conserved, and associated with ALU repeats. *RNA*, **19**, 141–157.
62. Sekar,S., Cuyugan,L., Adkins,J., Geiger,P. and Liang,W.S. (2018) Circular RNA expression and regulatory network prediction in posterior cingulate astrocytes in elderly subjects. *BMC Genomics*, **19**, 340.
63. Ebbesen,K.K., Hansen,T.B. and Kjems,J. (2017) Insights into circular RNA biology. *RNA Biol.*, **14**, 1035–1045.
64. Niethamer,T.K. and Bush,J.O. (2019) Getting Direction(s): the Eph/Ephrin signaling system in cell positioning. *Dev. Biol.*, **447**, 42–57.
65. Zhang,C. and Darnell,R.B. (2011) Mapping in vivo protein-RNA interactions at single-nucleotide resolution from HITS-CLIP data. *Nat. Biotechnol.*, **29**, 607–614.
66. Leggere,J.C., Saito,Y., Darnell,R.B., Tessier-Lavigne,M., Junge,H.J. and Chen,Z. (2016) NOVA regulates DCC alternative splicing during neuronal migration and axon guidance in the spinal cord. *Elife*, **5**, E14264.
67. Heinzen,E.L., Yoon,W., Tate,S.K., Sen,A., Wood,N.W., Sisodiya,S.M. and Goldstein,D.B. (2007) Nova2 interacts with a cis-acting polymorphism to influence the proportions of drug-responsive splice variants of SCN1A. *Am. J. Hum. Genet.*, **80**, 876–883.
68. Dredge,B.K. and Darnell,R.B. (2003) Nova regulates GABA(A) receptor Gamma2 alternative splicing via a distal downstream UCAU-rich intronic splicing enhancer. *Mol. Cell. Biol.*, **23**, 4687–4700.
69. Dredge,B.K., Stefani,G., Engelhard,C.C. and Darnell,R.B. (2005) Nova autoregulation reveals dual functions in neuronal splicing. *EMBO J.*, **24**, 1608–1620.
70. Jensen,K.B., Musunuru,K., Lewis,H.A., Burley,S.K. and Darnell,R.B. (2000) The tetranucleotide UCAY directs the specific recognition of RNA by the Nova K-homology 3 domain. *Proc. Natl. Acad. Sci. U.S.A.*, **97**, 5740–5745.
71. Teplova,M., Hafner,M., Teplov,D., Essig,K., Tuschl,T. and Patel,D.J. (2013) Structure-function studies of STAR family Quaking proteins bound to their in vivo RNA target sites. *Genes Dev.*, **27**, 928–940.
72. Teplova,M., Malinina,L., Darnell,J.C., Song,J., Lu,M., Abagyan,R., Musunuru,K., Teplov,A., Burley,S.K., Darnell,R.B. *et al.* (2011) Protein-RNA and protein-protein recognition by dual KH1/2 domains of the neuronal splicing factor Nova-1. *Structure*, **19**, 930–944.
73. Li,Z., Huang,C., Bao,C., Chen,L., Lin,M., Wang,X., Zhong,G., Yu,B., Hu,W., Dai,L. *et al.* (2015) Exon-intron circular RNAs regulate transcription in the nucleus. *Nat. Struct. Mol. Biol.*, **22**, 256–264.
74. Xia,P., Wang,S., Ye,B., Du,Y., Li,C., Xiong,Z., Qu,Y. and Fan,Z. (2018) A circular RNA protects dormant hematopoietic stem cells from DNA sensor cGAS-mediated exhaustion. *Immunity*, **48**, 688–701.
75. Dube,U., Del-Aguila,J.L., Li,Z., Budde,J.P., Jiang,S., Hsu,S., Ibanez,L., Fernandez,M.V., Farias,F., Norton,J. *et al.* (2019) An atlas of cortical circular RNA expression in Alzheimer disease brains demonstrates clinical and pathological associations. *Nat. Neurosci.*, **22**, 1903–1912.
76. Pamudurti,N.R., Patop,I.L., Krishnamoorthy,A., Ashwal-Fluss,R., Bartok,O. and Kadener,S. (2020) An in vivo strategy for knockdown of circular RNAs. *Cell Discov.*, **6**, 52.